Study of Optical Wireless Power Transmission to Moving Objects

DISSERTATION

Study of Optical Wireless Power Transmission to Moving Targets

移動体への光無線給電に関する研究

Graduate School of
Natural Science and Technology
Kanazawa University

Division of Electrical Engineering and Computer Science

Student ID: 1724042007
Name: Alexander William Setiawan Putra
Chief Advisor: Associate Professor Takeo Maruyama
Date of Submission: September 2020

ABSTRACT

Wireless Power Transmission (WPT) is a technique to transmit power from transmitter to receiver through medium wirelessly (without any cable) using electromagnetic wave. There are three methods of WPT: magnetic induction coupling WPT, microwave WPT and Optical WPT (OWPT). Among these WPT methods, OWPT has many advantages compared with the other methods. In OWPT, light sources such as laser and LED are used as the transmitter to convert electric power to optical power and solar cell is used as the receiver to convert back optical power into electric power that can be used as power supply for electronic devices. By taking advantage of small size and divergence angle of laser beam, OWPT can be used to transmit high power density to longer distance than the other WPT method. Based on theoretical analysis which had been done in this research, OWPT can be used to transmit power through air (atmosphere) with more than 30% system efficiency for 1 km distance between transmitter and receiver using infrared laser and Si solar cell. This high system efficiency for long distance transmission is not achievable by the other WPT methods. Small size of laser beam has also brought additional opportunity to OWPT system which is the possibility for OWPT to be used for supplying power to moving target because the laser beam can be easily steered to follow a moving target. The challenge that follows this opportunity is about how to recognize position of the receiver and steer the beam; hence, the beam will only hit the receiver. In this research, OWPT system using camera with color segmentation method and Galvano mirror to recognize the receiver (target) and steer the laser beam was designed and developed. 980 nm laser and Si solar cell were used as the transmitter and receiver, respectively. Using this method, OWPT to 1-dimensional moving target, multiple targets, 2-dimensional moving target and OWPT to moving target which was insensitive to the brightness of environment had been demonstrated. The system efficiency of this OWPT to moving target was calculated to be 3.8% for distance between transmitter and receiver was 60 cm, this efficiency was mainly limited by the efficiency of laser diode and solar cell which were only 20% and 22%, respectively. Hence, it is predicted that this system efficiency can be enhanced more by using more efficient laser diode and higher efficiency solar cell. Additionally, OWPT through water and hybrid power and data transmission had also been demonstrated.

ACKNOWLEDGEMENT

During my study in Kanazawa University for 3 years, I have encountered so many new challenges, priceless experiences and many new friends whom I hold dear in my heart and to whom I am indebted with. First and foremost, I want to express my gratitude to my advisor Associate Professor Takeo Maruyama who has taught me more than about how to be good researcher, many new life lessons and experiences inside and outside laboratory but also has become my mentor, my "second father" and my supporter during the ups and downs in these 3 years journey. I also would like to express my gratitude to Emeritus Professor Minoru Yamada, my advisor during my Master degree because without his guidance, I would never be able to start this journey and his support and encouragement throughout this journey.

I want to express my gratitude to my partners, my brothers-in-arms in this research group: Mr. Hendra Adinanta, Mr. Hirotaka Kato, Mr. Motoharu Tanizawa, Mr. Tatsuya Yoshida, Mr. Masataka Tsutsumi and Mr. Shota Sato for great discussions, wonderful teamwork and many new ideas. I would like to give thanks to other lab members who have become my special companions and colleagues during my research journey: Mr. Wildan Panji Tresna, Mr. Takuma Ichikawa, Mr. Hiroya Mitsuno, Mr. Kamishima Seiji, Mr. Masato Shimada, Mr. Dejima and Mr. Lu Sicheng.

I am lucky enough to have gone through many challenges during my study and my life in Kanazawa together with these exceptional brothers and with guidance from these two kind and beloved advisors. Too many beautiful memories we have created in this laboratory such as surviving the snowstorm in 2017 and 2018, climbing Mt. Hakusan and Mt. Fuji and struggle in middle of the Corona virus pandemic 2020. Without their companionship and support, I would not be able to survive these hardships.

Last but not least, I would like to give special thanks to my family in Indonesia for their constant love and encouragement, to Indonesian students society in Ishikawa (PPI-Ishikawa) and to my beloved partners-in-crime in my part time job at 第七餃子.

TABLE OF CONTENTS

LIST OF FIGURES

LIST OF TABLES

CHAPTER 1

INTRODUCTION

In this chapter, background of research, problems that wants to be solved in this research and objectives of research are explained. The unique characteristics of this research are also explained.

1.1 Trend of Development of Technology: From Wired to Wireless

All electronic devices need electrical power. As the power source in mobile devices such as handphone and unmanned automatic vehicle (UAV) for example drones and unmanned underwater vehicle (UUV), high capacity batteries are used. However, these batteries also have limited capacity. If the batteries run out of power, they need to be charged. Nowadays, charger with electric cable is used to charge the batteries. This wired power transmission has disadvantages because the mobility for device which is charged will be limited by the length of the cable. In the other words, it is impossible to use the device under charging for the distance longer than the length of the cable from the electric socket. For mobile devices, this condition will become problem. Moreover, the capacity of battery is proportional with its weight, hence, there is trade-off between the battery capacity and weight with the mobility of mobile devices and UAVs. [1-4]

The main purpose of the development of technology is in order to increase the quality of human's life. In nowadays society, the mobility of human is very high and fast. In this society,

there is a demand for technology which can support this fast and high mobility way of life. In order to answer this demand, there is a trend in the development of future technology to replace the wired connection into wireless connection which can provide service to this high mobility society. This "wired to wireless" trend of development of technology can be seen from the development of data communication technology. In the past data communication technology, wired cable is used to transmit data from one place to another. However, nowadays, the development of Wi-Fi and cellular communication has provided wireless data communication which can be used everywhere without any restriction. Based on this trend, wireless power transmission technology which can be used to transmit power for electronic device without any cable is also demanded.

1.2 Introduction of Wireless Power Transmission

Due to the demand of a system which can be used to power electronics devices up from long distance, wireless power transmission (WPT) system is developed. As the name suggests, in this system, electric cable is not used as the medium for power transmission. electromagnetic wave through an unconfined space is used as the medium for power transmission. The development of WPT system and its applications in human's daily life has brought many advantages such as possibility to produce smaller electronic devices without any batteries, due to non-existence of electric cord for charging, there is no hassle which increases the user friendliness of the electronic devices, increase durability and flexibility of the devices because there is no need to change battery and it increases mobility of the devices [1-4].

Basic WPT system can be seen from Figure 1.1. The main components of WPT system are transmitter which is used to transform electric power to electromagnetic wave, receiver which is used to transform electromagnetic waves to electric power that can be used to power electronics devices up and medium which is an unconfined space where the electromagnetic wave flows from transmitter to receiver.

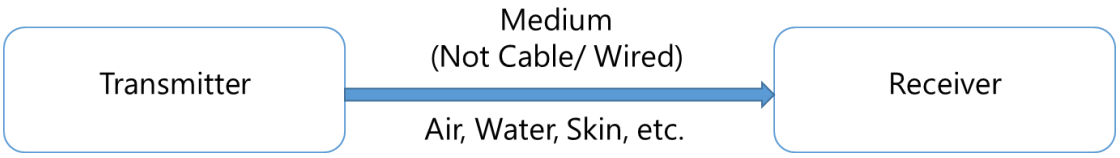

Figure 1. 1 Basic diagram of wireless power transmission (WPT) system.

The methods of WPT can be separated into two categories which are near field and far field WPT. The main example of near field WPT system in the induction coupling WPT. On the other hand, the best examples or far field WPT systems are microwave WPT and optical wireless power transmission (OWPT). Illustration of these three systems can be seen from Figure 1.2.

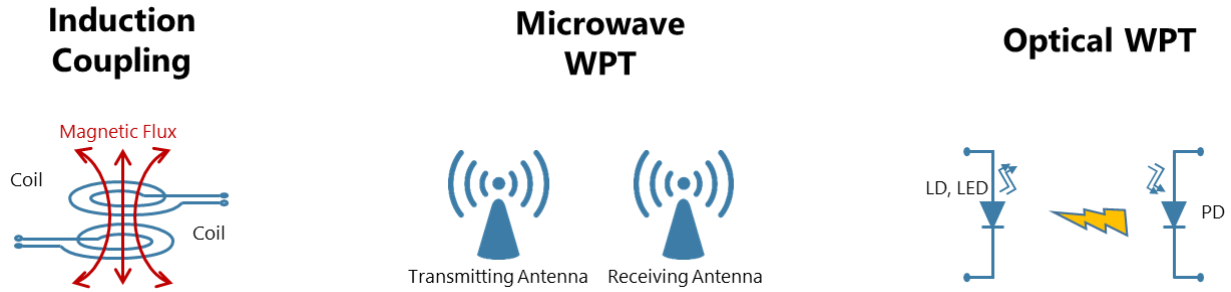

Figure 1. 2 Methods of wireless power transmission.

In induction coupling WPT system, coils are used as the transmitter and receiver. The history of the development of this technology can be traced back to Nikola Tesla in 19th Century. In 1891, Nikola Tesla demonstrated that electric power can be transmitted wirelessly through air using Tesla coil which is a pair of radio frequency power transformer that can be used to produce high voltage and high frequency alternating-current electricity [5-6]. This experiment is the demonstration of induction WPT system. Hence, induction coupling WPT system is the first WPT system which is demonstrated. Since that day, the development of induction coupling WPT system

has gone through many new innovations with the main motivation is to eliminate the need of charging the device by tethering it which electric socket.

In 2008, Wireless Power Consortium was established with the main purpose is to standardize induction coupling WPT technology, hence, it can be widely applied for many devices in the market. This standard is called "Qi" [7-8]. Hence, the induction coupling WPT system is popularly known as Qi wireless charging. Nowadays, this wireless charging technology is implemented in almost all new electronic devices such as smartwatches, smartphone, and other electronic devices. The main advantage of this technology is high power transmission efficiency, however, the distance between coils for transmitter and receiver has to be very near which limited the mobility of the devices under charging. This Qi wireless charging has become a new standard for new mobile devices and it is predicted that in 2020, more than 15 billion of electronic devices will have this Qi wireless charging capability [2,9].

In microwave WPT system, a pair of antennas is used as the transmitter and receiver. On the other hand, in OWPT system, light sources such as laser and LED are used as the transmitter and solar cell is used as the transmitter. The main advantages of microwave and OWPT system are the possibility to transmit power for long distance between transmitter and receiver and the ease of steering the microwave and laser beam, hence, it can be used to trace and follow moving target and can be used to charge a moving device. However, the maximum power transmission efficiencies of the system are lower than induction coupling WPT system.

The other difference between induction coupling WPT, microwave WPT and OWPT is the electromagnetic wave frequency that is used for power transmission. The electromagnetic spectrum of frequency regions and their respective WPT technology can be seen from Figure 1.3. induction coupling WPT uses low electromagnetic wave frequency with several kHz to MHz frequency, microwave WPT uses microwave frequency band with several GHz frequency and OWPT uses light frequency which is higher than THz. The differences among these three methods of WPT are summarized in Table 1.1. Among these three methods of WPT, due to small size and small diffraction angle of laser, OWPT can be used for transmitting power to longer distance

between transmitter and receiver than other WPT technologies. Laser or light source which is used in OWPT can also be steered easily compared with microwave in microwave WPT.

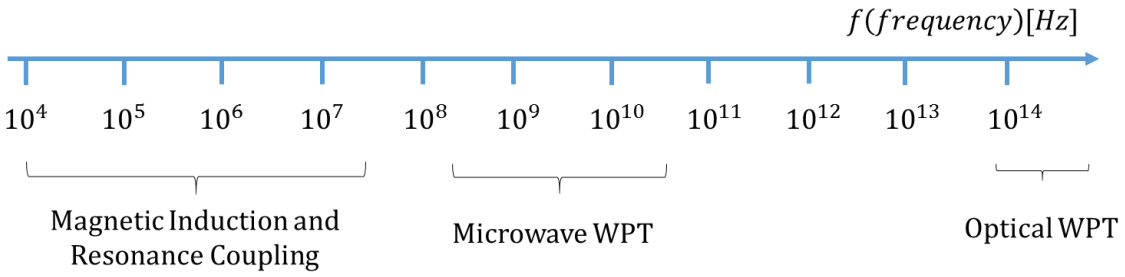

Figure 1. 3 Wireless power transmission method and its respective frequency band.

Table 1. 1 Differences between wireless power transmission methods.

	Magnetic Coupling	Microwave	Optical
Ease to steer the beam	Low	High	High
Mobility of target	Low	High	High
Operational distance	Short	Long	Long
Operational frequency	10 kHz - 1 MHz (Induction Coupling) 1 MHz - 100 MHz (Resonance Coupling)	1 GHz – 30 GHz	>100 THz
Back-to-back efficiency	~90%	~70%	~50%
RF interference	No	Yes	No

1.3 The Importance of Beam Steering and Target Recognition

As explained in Section 1.2, OWPT has advantage in terms of ease for steering the beam by taking advantage of small size of beam. This advantage gives possibility to OWPT to be used to transmit power to moving target and object. However, it is important to steer the beam, hence, the beam will only illuminate the target. In this case, special target recognition method is needed. There are many methods for target recognition and beam steering methods which are proposed and can be used in OWPT system. Retrodirective mirrors, four elements photodiode and retroreflective array which are put at the receiver are three of the examples of technique to recognize the target which is solar cell. The other technique is using camera and image recognition software. By using this method, the OWPT system can be simplified. The details of beam steering and target recognition method will be discussed in Chapter 5.

1.4 Research Objectives

The objectives of this research are:

i. To study and theoretically analyze the system efficiency of OWPT system, to compare it with the other WPT system and theoretically analyze and propose possible applications of OWPT system.

ii. To create and develop OWPT system to moving target using Galvano mirror to steer the beam and camera to recognize the target which can be used at all environmental condition.

iii. To develop hybrid free space optical wireless communication and OWPT system.

1.5 Significance of Research

The main contributions of this research can be divided into two general significances. The first contribution is to explore the possibility of application of OWPT system by theoretically analyze the system efficiency of OWPT system through several mediums such as human skin, water and air. Moreover, the power transmission system efficiency of OWPT is also compared with theoretical analysis of other WPT technique which shows the superiority of OWPT compared with other WPT system. Furthermore, possible application of OWPT which has been theoretically analyzed is also demonstrated in simple OWPT system.

The second contribution of this research is to propose, design and develop a new and applicable OWPT system using Galvano mirror as beam steering technology and simple web camera with image processing software to recognize the target of OWPT system. This simple technology is more feasible than other target recognition method to be applied in the application of OWPT in daily life because there is no need of attaching possible heavy equipment at the target such as retrodirective mirror or four elements photodiode which will decrease the mobility of the target devices. Moreover, the system which is designed and developed in this research is simpler than other beam steering and target recognition methods which are existing nowadays.

1.7 Flow of Research

The first step of this research is to theoretically analyze the possibility of OWPT system by analyzing its performance in terms of power transmission system efficiency. In this step, theoretical analysis of OWPT system efficiency is performed using Matlab and Python programming software. The system efficiencies of induction coupling and microwave WPT are also calculated and the results are compared with the efficiency of OWPT system to analyze the superiority of OWPT and the characteristics of each WPT methods.

The mediums of OWPT in theoretical analysis are air, water and human skin. In this case, the attenuation and absorption characteristics of each mediums are analyzed theoretically. As the receiver in OWPT system, Silicon (Si) solar cell is assumed because Si solar cell is the most common solar cell in the market which is easily produced and has considerably high power conversion efficiency. From this theoretical analysis, the superiority of OWPT for long distance power transmission can be confirmed. Possible applications of OWPT which has never been explored before are also analyzed and confirmed theoretically.

The next step of this research is to design and develop OWPT system which can be applicable for daily life especially OWPT through water and free space (air). In this case, simple OWPT through water system is developed and the performance of this system is also evaluated. OWPT system through air which can be used to transmit power to moving target is also designed and developed. Since the beam size of laser is small, beam steering and target recognition technology is needed. In this research Galvano mirror and web camera with image processing software are used as beam steering and target recognition method respectively. This system is developed for one-dimensional moving target, two-dimensional moving target and multi-moving target system. Each applications of this system bring their own problems and challenge, in this case, the problems for each application are identified based on experimental results and solved by modifying the system and target recognition software.

The next step of this research is to improve the performance of OWPT system using Galvano mirror and camera, hence, it can be used for all conditions of environment. In this case, target recognition method and marker at the target is modified in order to create a better target recognition method for indoor and outdoor applications of OWPT system. The performance of such system is experimentally analyzed.

Lastly, the possibility of OWPT system through water and transmitting power and data at the same time which will be useful to increase the value of OWPT system are proposed and the systems are designed and developed. The performance of these applications of OWPT systems are also evaluated.

1.8 Organization of Thesis

This dissertation is organized as follow: In Chapter 2, basic theory of magnetic induction coupling WPT and microwave WPT is explained in detail. Theoretical analysis of system efficiencies of magnetic induction coupling WPT and microwave WPT is explained and the calculation results are presented and analyzed. The applications and some restrictions of each method are also explained. In Chapter 3, theory of OWPT is explained. The calculation of system efficiency of OWPT and comparison with other WPT methods are performed and the results are presented and analyzed.

In Chapter 4, existing and potential target recognition and beam steering methods which can be used in OWPT system are introduced and the characteristics of each method are analyzed and compared. In Chapter 5, target recognition method and beam steering method in OWPT system to moving target, which was developed in this research, is introduced. The performance of the system is analyzed and the improvement of the system to design a robust and reliable system which is insensitive to environmental condition is explained in detail. The evaluation of system efficiency of the proposed OWPT system to moving target is also presented.

In Chapter 6, applications of OWPT systems which are OWPT system through water and hybrid OWPT and Free Space Optical (FSO) communication system which can be used to transmit power and data at the same time are proposed, designed and the results are presented. The performances of these systems are also analyzed. Lastly, in Chapter 7, the summary and list of publications are presented.

CHAPTER 2

SYSTEM EFFICIENCY OF MAGNETIC COUPLING AND MICROWAVE WIRELESS POWER TRANSMISSION

In this chapter, basic theory of Wireless Power Transmission (WPT) is explained in detail. One of the main parameters to evaluate the performance of WPT system is the system efficiency, hence, in this chapter, the theory to calculate system efficiency of magnetic coupling WPT and microwave WPT which is including the factors that affect the system efficiency are explained.

2.1 Basic Theory of System Efficiency in WPT System

The easiest way to evaluate the performance of WPT system is to evaluate the system efficiency of the system. System efficiency is the ratio of electric power which is inputted to the transmitter and the electric power which is received by the receiver and can be used to power the electronic devices up. In the other words, the system efficiency shows how much fraction of electric power that can be transmitted successfully in WPT system [10]. The basic diagram of WPT can be seen from Figure 1.2 and revisited in Figure 2.1. In this case, there are three main components of WPT system which are transmitter, medium and receiver. Hence, basic equation of WPT system efficiency can be simply expressed as:

$$\eta_{sys} = \eta_T \times \eta_{med} \times \eta_R \quad , \tag{2.1}$$

Where η_T, η_{med} and η_R are the conversion efficiency of electric power into electromagnetic wave in transmitter, the efficiency of the medium which represents the loss during the propagation in the medium and the conversion efficiency of the transmitter to convert from electromagnetic wave into electric power that can be used directly to power the electronic devices up.

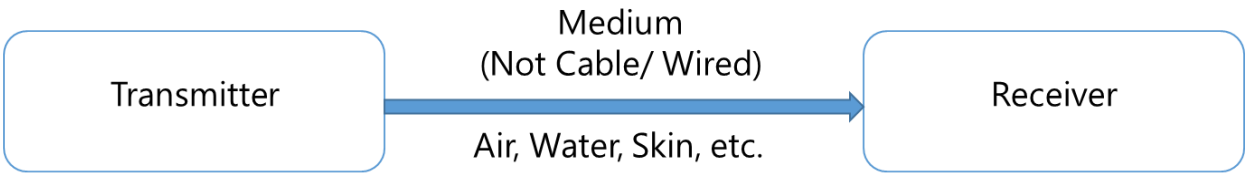

Figure 2. 1 Basic diagram of wireless power transmission (WPT) system (Revisited).

2.1.1 Efficiency of Transmitter and Receiver

The efficiency of transmitter, η_T shows the ability of the transmitter to convert electric power to electromagnetic wave and can be described as the ratio of the amount of electric power which is inputted to the transmitter and the power of electromagnetic wave which is produced by the transmitter to be transmitted in WPT system. It can simply be expressed as:

$$\eta_T = \frac{P_{in}}{P_{elec}} \quad , \tag{2.2}$$

Where P_{in} and P_{elec} are the inputted electric power and output electromagnetic power of the transmitter respectively.

On the other hand, efficiency of the receiver is the ability of the receiver to receive the electromagnetic wave and convert it back into electric power that can be used directly by electronic devices. It can be simply expressed as:

$$\eta_R = \frac{P_{elec}}{P_{out}} \quad , \tag{2.3}$$

Where P_{out} is the output electric power of the receiver. Note that the transmitter and receiver in WPT system can be similar objects such as coils in magnetic induction coupling WPT and antennas in microwave WPT or different objects such as laser and solar cell in Optical Wireless Power Transmission (OWPT).

2.1.2 Loss in Medium

The efficiency of the medium represents the loss of electromagnetic wave power during its propagation in the medium. The power of electromagnetic wave that propagates through medium exponentially decreases and can be expressed as:

$$\eta_{med} = \mathrm{e}^{-\alpha \mathrm{d}} \quad , \tag{2.4}$$

Where α and d are the attenuation coefficient of the medium and distance between transmitter and receiver where the electromagnetic wave propagates, respectively.

There are two mechanism that contributes to decrease the power of electromagnetic wave during its propagation. They are absorption and scattering. Hence the attenuation coefficient α can be described as:

$$\alpha = \alpha_{abs} + \alpha_{scat} \quad , \tag{2.5}$$

Where α_{abs} and α_{scat} are the absorption and scattering coefficient of the electromagnetic wave by the medium.

The absorption is the mechanism in which the energy of propagated electromagnetic wave is absorbed by the particle of the medium and transformed into other form of energy such as lattice

vibration (heat). The absorption of electromagnetic field by the medium can be analyzed from the equation of electromagnetic wave as:

$$E = E_0 \exp j(\omega t - kz) \quad , \tag{2.5}$$

Where E_0, ω and k are the amplitude, angular frequency and propagation constant of the electromagnetic wave respectively. For the electromagnetic wave which propagates in the medium, propagation constant k can be described as:

$$k = k' - jk'' = \frac{2\pi N}{\lambda} \quad , \tag{2.6}$$

Where N and λ are the complex refractive index of medium and wavelength of the electromagnetic wave respectively. The complex refractive index N can be analyzed as:

$$N = n - jn'' \quad , \tag{2.7}$$

Where n and n'' are the real part and imaginary part of refractive index of the propagation medium. The real part of refractive index determines the polarization of the medium and phase of the electromagnetic wave during propagation in the medium. On the other hand, the imaginary part describes the losses in the medium.

By substituting eq. (2.6) to eq. (2.5), the equation of magnetic wave can be rewritten as:

$$E = E_0 \exp(-k''z) \exp j(\omega t - k'z) \quad , \tag{2.8}$$

From eq. (2.8), it can be clearly seen that the amplitude of electromagnetic wave in the medium decays exponentially during its propagation in z-direction. The power of electromagnetic field is proportional with the square of electric field as:

$$P \propto |E|^2 \propto \exp(-2k''z) \quad , \tag{2.9}$$

Hence, it can be seen that the absorption coefficient α_{abs} of the electromagnetic wave can be described as:

$$\alpha_{abs} = -2k'' \quad . \tag{2.10}$$

The absorption in the medium can also be correlated with the relative permittivity of the medium as:

$$N = n - jn'' = \sqrt{\epsilon_r} = \sqrt{\epsilon_r' - j\epsilon_r''} \quad , \tag{2.11}$$

Where ϵ_r' and ϵ_r'' are the real part and imaginary part of permittivity of medium respectively and can be expressed as:

$$\epsilon_r' = n^2 - n''^2 \quad , \tag{2.12}$$

$$\epsilon_r'' = 2n \times n'' \quad , \tag{2.13}$$

The values of real part and imaginary part of refractive index of medium are dependent to the medium itself and frequency of electromagnetic wave. [11]

During the propagation of electromagnetic wave in inhomogeneous medium, there is possibility that some part of the electromagnetic field is radiated away from its original propagation direction, in this case, the power of electromagnetic field in the direction of propagation of electromagnetic field will decrease and the power will be scattered to some directions as illustrated in Figure 2.2. This phenomenon is called scattering of electromagnetic wave. This phenomenon is caused by the difference in local refractive index in a small area of the

medium due to existence of particles with different refractive index in inhomogeneous medium such as air. During the propagation, the power of electromagnetic field decays exponentially as:

$$P(z) = P_0 \exp(-\alpha_{scat} z) \quad , \quad (2.14)$$

Where α_{scat} is the scattering coefficient of the medium.

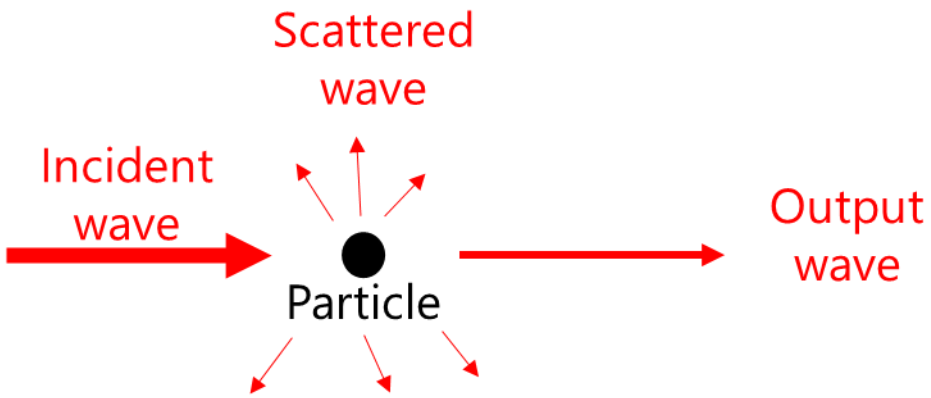

Figure 2. 2 Illustration of electromagnetic wave scattering by particle.

Based on the size of scattering agent in the medium, the scattering process can be categorized into two phenomena: Rayleigh scattering and Mie scattering. Rayleigh scattering is the scattering process in which the size of the scattering agent in the medium is much smaller than the wavelength of electromagnetic wave. The fraction of electromagnetic wave which is scattered in Rayleigh scattering will be scattered to all direction. The amount of Rayleigh scattering is inversely proportional with the wavelength of the electromagnetic wave. In the other words, the higher the frequency of the electromagnetic wave, the more power will be scattered during its propagation in the medium. Hence, the Rayleigh scattering is more sever in OWPT than in microwave WPT because the wavelength of light which is used in OWPT is shorter than microwave. Rayleigh scattering particularly happens to the light propagation through air and optical fiber. Rayleigh scattering also happens in the propagation of microwave through the air in

some weather conditions [12]. The scattering coefficient of Rayleigh scattering can be expressed as:

$$\alpha_R \propto \frac{1}{\lambda^4} \propto f^4 \quad . \tag{2.15}$$

The scattering phenomenon in which the size of scattering agent is bigger or comparable to the wavelength of electromagnetic wave is called Mie scattering. In Mie scattering phenomenon, it is assumed that the refractive index of the scattering agent is significantly different with the surrounding medium. The majority fraction of power which is scattered in Mie scattering phenomenon will scatter to front direction. Mie scattering particularly happens to light in a medium which such as air with high pollution, smoke and fog. Mie scattering is less dependent with the wavelength of electromagnetic wave than Rayleigh scattering and highly dependent to the ratio size of scattering agent and the wavelength of light.

The attenuation of electromagnetic wave during the propagation in medium is affected by absorption and scattering phenomena. In this case, the efficiency of medium in eq. (2.1) can be expressed as exponentially decay function:

$$\eta_{med} = \exp\{-(\alpha_{scat} + \alpha_{abs})\} = \exp(-\alpha) \quad . \tag{2.16}$$

2.2 Induction Magnetic Coupling WPT

2.2.1 Calculation of System Efficiency

The transmitter and receiver in induction magnetic coupling WPT are coils as can be seen from Figure 2.3. The efficiency of magnetic coupling WPT can be analyzed from the Maxwell's equations which describes the electric and magnetic field in vacuum [2,13-15]:

$$\text{Gauss' law: } \nabla \cdot D = \rho \quad , \tag{2.17}$$

$$\text{Gauss' law for magnetism: } \nabla \cdot B = 0 \quad , \tag{2.18}$$

$$\text{Faraday's law of induction: } \nabla \times E + \frac{\partial B}{\partial t} = 0 \quad , \tag{2.19}$$

$$\text{Ampere's law: } \nabla \times H - \frac{\partial D}{\partial t} = J \quad , \tag{2.20}$$

Where D, B, E and H are the electric displacement field, magnetic flux density, electric field and magnetic field strength respectively. The electric displacement field, D is related with electric field E and magnetic flux density, B is related with magnetic field strength, H, as:

$$D = \epsilon_0 \epsilon_r E \quad , \tag{2.21}$$

$$B = \mu_0 \mu_r H \quad , \tag{2.22}$$

Where ϵ_0, ϵ_r, μ_0 and μ_r are the permittivity of vacuum, relative permittivity, permeability of vacuum and relative permeability, respectively.

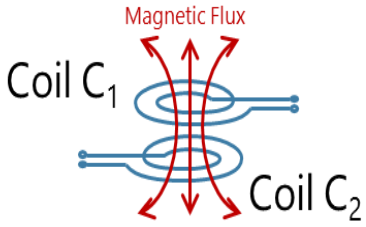

Figure 2. 3 Illustration of magnetic induction coupling WPT.

Consider a one turn coil C with an area S and magnetic flux density B passing through coil C in vacuum. Then by substituting eq. (2.21) to eq. (2.19), the Faraday's law of induction in this system can be modified as:

$$\int_S \nabla \times E.dS + \int_S \mu_0 \frac{\partial \mathrm{H}}{\partial \mathrm{t}} dS = 0 \quad , \tag{2.23}$$

By Stokes theorem, eq. (2.23) can be written as:

$$\int_C E.dr + \frac{\partial}{\partial t} \int_S \mu_0 \mathrm{H}\, dS = 0 \quad . \tag{2.24}$$

The induced electromotive force (EMF), ϵ in coil C can be expressed as:

$$\epsilon = -\frac{\partial}{\partial t}\int_S \mu_0 H.dS = -\frac{d\Phi}{dt} \quad , \tag{2.25}$$

Where Φ is the magnetic flux in circuit C.

In this analysis, by assumption that there is no flux leakage from the coil C_1 to C_2, the electromotive ϵ_2 in C_2 which is generated by current in C_1 and the electromotive force at coil C_1 can be analyzed as:

$$\epsilon_2 = -N_2 \frac{d\Phi}{dt} = -\frac{\mu N_1 N_2 S}{l}\frac{dI_1}{dt} = M_{21}\frac{dI_1}{dt} \quad , \tag{2.26}$$

$$\epsilon_1 = -\frac{\mu N_1 N_2 S}{l}\frac{dI_2}{dt} = M_{12}\frac{dI_2}{dt} \quad , \tag{2.27}$$

Where N_1, N_2, M_{21} and M_{12} are the number of turns of coil 1, number of turns of coil 2, mutual inductance at coil 2 due to current at coil 1 and mutual inductance at coil 1 due to current at coil 2, respectively. The M_{12} and M_{21} can be assumed to be similar and can be expressed as:

$$M = M_{12} = M_{21} = -\frac{\mu N_1 N_2 S}{l} \quad , \tag{2.28}$$

Where l is the length of the solenoids (coils).

In order to analyze the system efficiency of the magnetic inductive coupling WPT, the equivalent circuit of the system can be analyzed as in Figure 2.4. From the Kirchhoff's 2nd law, the following equation can be obtained:

$$\begin{bmatrix} I_1 \\ I_2 \end{bmatrix} = \frac{v}{Z_1(Z_0 + Z_2) + (\omega M)^2} \begin{bmatrix} Z_0 + Z_2 \\ -i\omega M \end{bmatrix} \quad , \tag{2.30}$$

Where ω, Z_0, Z_1 and Z_2 are the angular frequency of the system, load impedance of the circuit, equivalent impedance of coil 1 and equivalent impedance of coil 2, respectively.

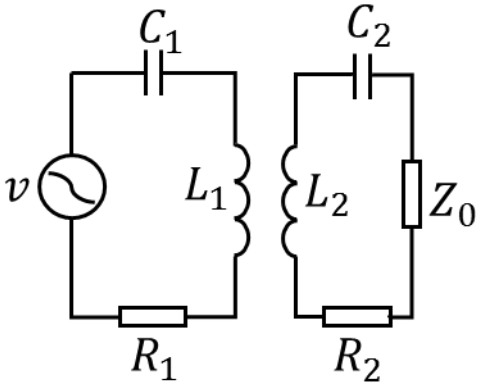

Figure 2. 4 Equivalent circuit of magnetic induction coupling WPT system.

The mutual inductance M is dependent to the distance between two coils as[13-15]:

$$M = \frac{\mu N_1 N_2 r_1^2 r_2^2}{\sqrt{(r_1 + r_2)^2 + d^2}\{(r_1 + r_2)^2 + d^2\}} \quad , \qquad (2.31)$$

Where r_1 and r_2 are the radius of coil 1 and coil 2 respectively.

The transfer efficiency then can be analyzed as:

$$\eta = \frac{P_{out}}{P_{in}} = \frac{Z_0 \omega^2 M^2}{\{Z_1(Z_0 + Z_2\} + (\omega M)^2 (Z_0 + Z_2)} = \frac{1}{\left\{\frac{R_1 R_2}{\omega^2 M^2}\frac{Z_1}{R_1}\left(\frac{Z_0}{R_2} + \frac{Z_2}{R_2}\right) + 1\right\}\left(1 + \frac{R_2}{Z_0}\right)} \quad . \qquad (2.32)$$

For simplification:

$$\frac{\omega^2 M^2}{R_1 R_2} = fom^2 \quad . \qquad (2.33)$$

Hence eq. 2.32 can be simplified as:

$$\eta = \frac{1}{\left\{\frac{1}{fom^2}\left(\frac{Z_0}{R_2} + 1\right) + 1\right\}\left(1 + \frac{R_2}{Z_0}\right)} \quad . \qquad (2.34)$$

Optimum power transmission happens when the ratio of load resistance Z_0 and internal resistance of coil 2 is:

$$\frac{Z_0}{R_2} = \sqrt{1 + fom^2} \quad , \qquad (2.35)$$

Hence the maximum power transmission efficiency can be obtained as:

$$\eta = \frac{fom^2}{\left\{1 + \sqrt{1 + fom^2}\right\}^2} \quad . \tag{2.36}$$

Figure 2.5 shows the calculated system efficiency of magnetic inductive coupling WPT for the frequency of the system are 100 kHz, 200 kHz and 500 kHz. In this calculation, the diameters of coils are 0.5 m with internal resistances of coils are assumed to be 50 Ω. It can be seen that, higher frequency of the system will result in higher system efficiency. These results can be analyzed numerically from eq. (2.36), where the efficiency is proportional with frequency of the system. Note that typical operational frequency of the inductive magnetic coupling WPT is in several hundreds of kHz region.

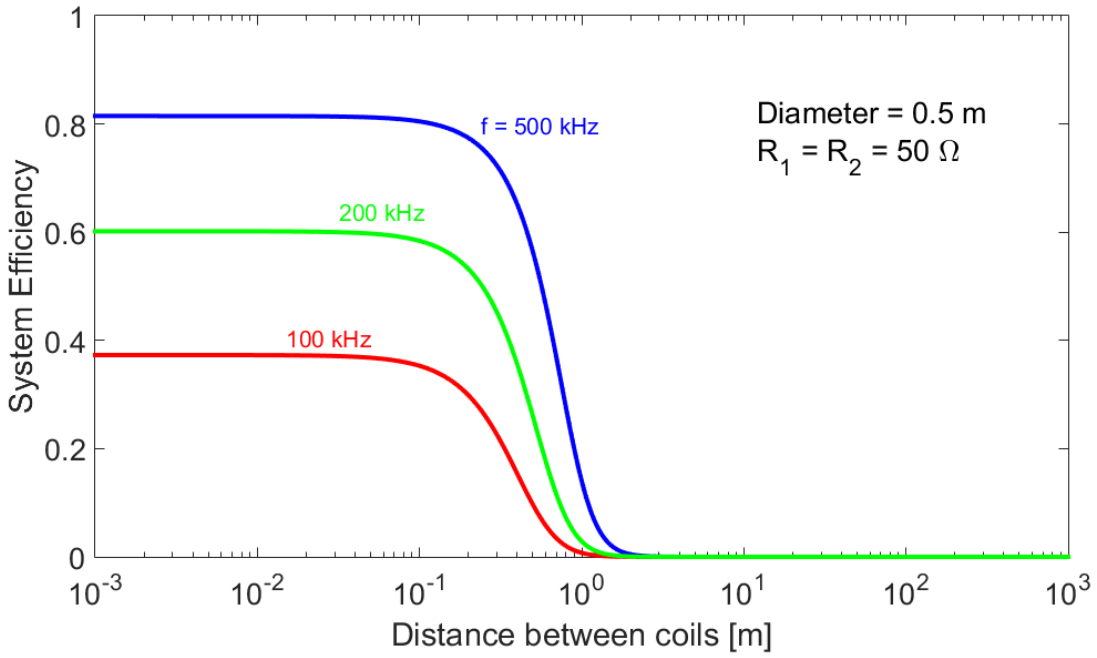

Figure 2. 5 Calculated system efficiency of magnetic induction coupling in optimal condition.

Inductive magnetic coupling WPT has some advantages in terms of high system efficiency especially for the distance between coils less than their diameters, possibility for high power transmission, ease of application and simple implementation. Therefore, this technology is very popular with mobile device wireless charging system. In 2014, MIT proposed and designed a new

magnetic inductive coupling WPT system which is called MagMIMO [16]. This system uses more than one coil as the transmitter in order to increase the range of operation of the system. It is claimed that the MagMIMO can detect a mobile device when it is in the range of MagMIMO system and automatically charge the device even though it is in the pocket.

In order to increase the efficiency and operational distance of the system, resonance circuit can be added at the transmitter and receiver. This method is called magnetic resonance coupling. The best example of this technology is the Witricity which is proposed by MIT scientist in 2007 [17-21]. The simple diagram of magnetic resonance coupling system can be seen from Figure 2.6. In this case, resonance coupling circuits which are two coils are put in front of the single turn coils at the transmitter and receiver. By this method, the transmitter and receiver will be strongly coupled, hence, the power transmission can be done for longer distance than ordinary induction coupling WPT. It is claimed that Witricity can be used to transmit power with efficiency more than 40% for the distance between transmitter and receiver is 2 meters with diameters of the coils are 0.5 m. The magnetic resonance coupling WPT operates at several MHz frequency. And it can be used to charge multiply devices at the same time.

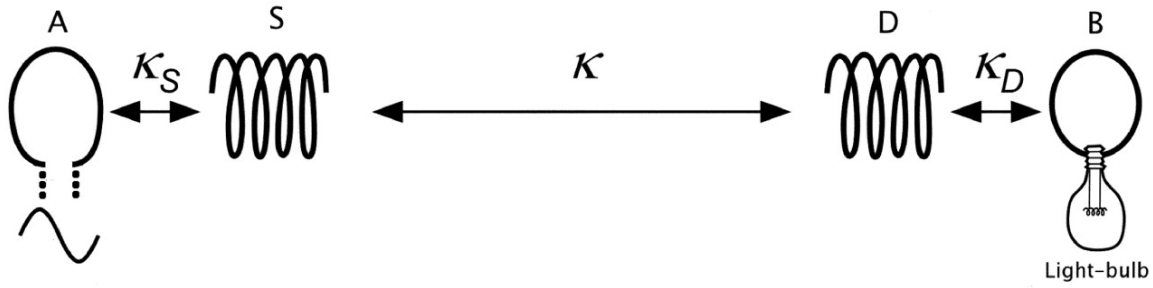

Figure 2. 6 Schematic of magnetic resonance coupled wireless power transmission system [18].

2.2.2 Applications of Inductive Magnetic Coupling WPT

There are many applications of magnetic inductive coupling WPT technologies those have been implemented in our daily life. The best example of these applications is to charge smartphone and mobile devices which is marketed and standardized as qi wireless charging. Medium power

applications of this technology include many applications for charging medical apparatuses. Applications of this technology can be found in charging implantable medical devices such as pacemaker. Since it operates in low frequency, the electromagnetic wave in WPT will not disturb the operation of pacemaker. Magnetic resonance coupling enables high power transmission for longer distance and smaller coils than induction coupling. Hence, it can be used for small implantable devices. Demonstration of WPT using coils with efficiency around 58% had been done using coils at 13.56 MHz frequency magnetic coupling WPT [22-24].

The possibility for high power transmission using magnetic coupling WPT has opened many applications of magnetic coupling WPT for high power transmission to big electronic devices and vehicles. Kilowatt applications of magnetic coupling WPT includes charging robot [25-26], underwater autonomous vehicle (UUV) by putting coils with good water insulation underwater [27-29], public transportation such as monorail system [30-32] and electric car [33-36]. Electric vehicle charging system which can transfer power more than 100 kW has been realized with 95% efficiency for the distance between transmitter and receiver is 22.5 cm [34].

2.3 Microwave WPT

2.3.1 Basic Components in Microwave WPT System

Basic microwave WPT diagram can be seen from Figure 2.7. The transmitter and receiver in microwave WPT system are a pair of antennas. The other components which are important in microwave WPT system are the DC-RF converter at the transmitter and RF-DC converter at the receiver. The DC-RF converters can be categorized into two types which are tube type such as magnetrons, klystrons, gyrotron, Travelling Wave Tube (TWT) and solid states type converter such as FET converter. The TWT microwave converter with efficiency more than 70% for space application has been reported by D.S. Komm et.al. in ref. [37]. Magnetron DC-RF converter can

be used to convert DC to RF with efficiency more than 80% [38] and theoretically, the conversion efficiency can be as high as 90% [39].

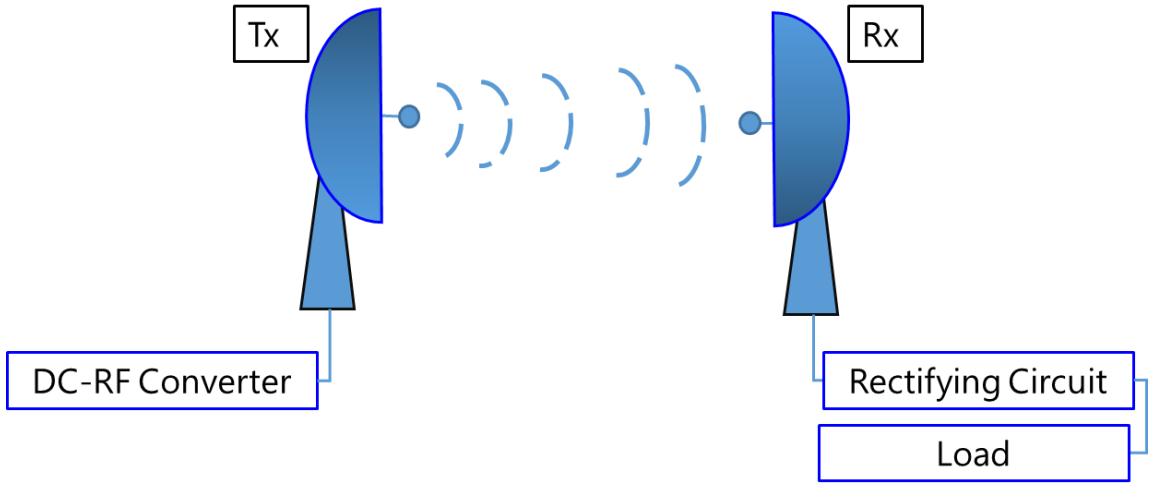

Figure 2. 7 Diagram of microwave wireless power transmission system.

At the receiver, rectenna can be used as the RF-DC converter devices. One of the records of high efficiency RF-DC conversion efficiency is 91% for 2.45 GHz frequency [40]. The other record for high efficiency RF-DC converter is 82% at 5.8 GHz frequency [41]. The other alternative of RF-DC converter that can be used for high power application is tube type RF-DC converter such as cyclotron and inverse magnetron. The highest efficiency of cyclotron is 83% with output electric power more than 10 kW [42]. 41% conversion efficiency with 23.5 kW output electric power has also been recorded using inverse magnetron [43].

There are many types of antenna which can be used for wireless communication. Some of the best examples of these types of antennas are the wire antenna, circular loop antenna, array antenna and lens antenna. Figure 2.8 shows some types of antennas which can be used for wireless communication. Among these types of antennas, due to its simple configuration, wire antenna is the most common antenna which is used for commercial purpose. For the microwave WPT transmission, one of the best options is lens antenna which is usually used to focus the

electromagnetic wave to one direction and prevent it to spread into undesired area or direction [44-45]. In lens antenna, parabolic dish is used to focus and direct the electromagnetic wave.

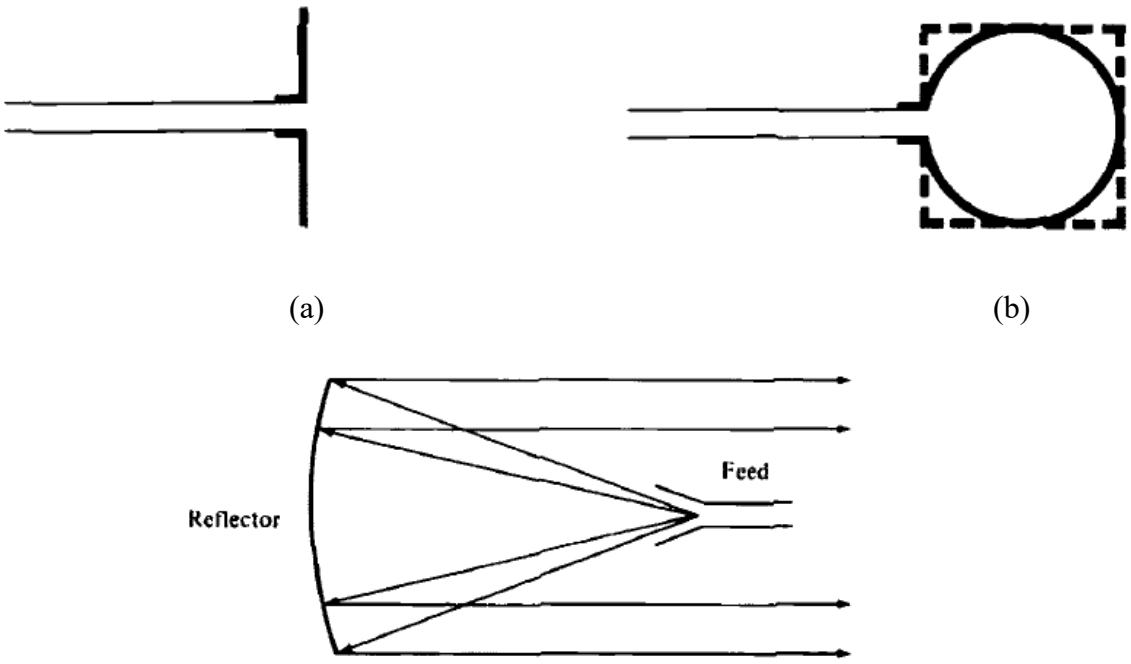

Figure 2. 8 Some types of antennas: (a) Dipole, (b) Circular (Square) Loop, (c) Parabolic lens antenna [45].

2.3.2 System Efficiency of Microwave WPT

Basic equation of system efficiency in eq. (2.1) can be modified to fit the DC to DC system efficiency in microwave WPT as follows [46]:

$$\eta_{sys} = \eta_{DC-RF} \times \eta_{TA} \times \eta_{BCE} \times \eta_{med} \times \eta_{RA} \times \eta_{RF-DC} \quad , \qquad (2.37)$$

Where η_{DC-RF}, η_{RF-DC}, η_{TA}, $\eta_{RA}$and η_{BCE} are the conversion efficiency of DC to RF converter at the transmitter, conversion efficiency of DC-RF converter at the receiver, transmitting antenna efficiency, receiving antenna efficiency and beam collection efficiency which shows the fraction

of transmitted power than can be received well by the antenna, respectively. The η_{DC-RF} and η_{RF-DC} have been described in Section 2.3.1 and have high value which are more than 80%.

When the antenna radiates electromagnetic wave, there is possibility of losses at the antenna due to many factors such as: conduction loss due to the conductivity of metal that makes the antenna, dielectric loss due to conductivity of dielectric materials near the antenna and impedance mismatch loss. Small antennas which are used in mobile phones typically have loss around 20% to 70%, on the other hand, lens parabolic dish antenna which does not have any disturbance by dielectric materials around it can have efficiency almost 100%.

The atmospheric attenuation coefficient, α, of the RF wave can be seen from Figure 2.9 for standard atmosphere (the water vapor density is 7.5 g/m3) and dry air (0 g/m3). In microwave WPT, the frequency of microwave is around 2.45 GHz to 10 GHz [47] which is the Industrial, Scientific and Medical (ISM) band. The attenuation coefficient of RF wave through atmosphere is very small, which is around 0.01 dB/km to 0.02 dB/km. Attenuation coefficient of 0.01 dB/km means that after the transmission for 150 to 300 km distance from the transmitter, only half of the transmitted power will remain due to attenuation in the atmosphere. Hence, the efficiency of medium in microwave WPT for several hundreds of meters can be assumed to be almost unity.

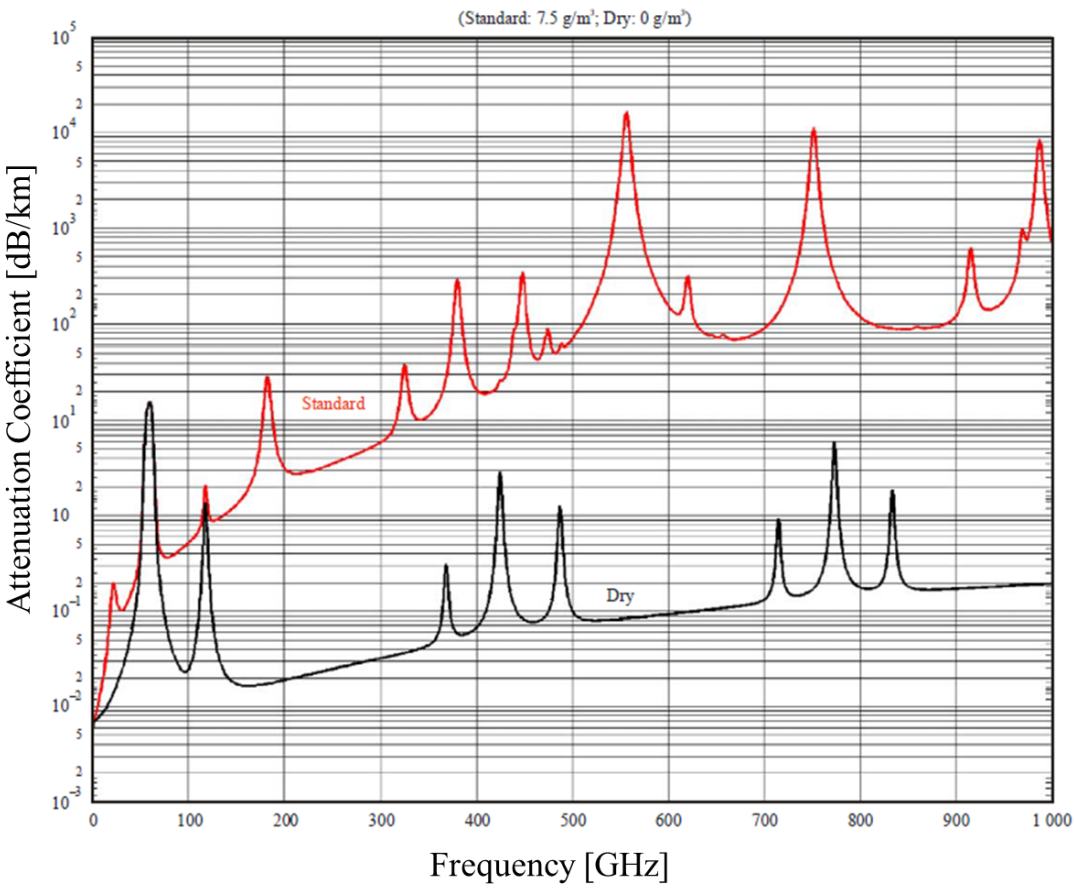

Figure 2. 9 Attenuation coefficient of microwave by atmosphere [48].

The absorption coefficient of microwave through water can be calculated from the imaginary part of permittivity of water as can be seen from Figure 2.10 which is adopted ref. [49]. From the imaginary part of permittivity, absorption coefficient can be calculated using eq. (2.10) until eq. (2.13). The absorption coefficient of 2.45 GHz and 10 GHz microwave by pure water molecule at 20° C can be calculated as 72.23 m^{-1} and 896.5 m^{-1} respectively. In the other words, the power of microwave which is transmitted through water will become half after the transmission through 9.6 mm and 0.8 mm of water for 2.45 GHz and 10 GHz of microwave, respectively. In this case, the absorption coefficients for 2.45 GHz and 10 GHz are very high, hence, it is almost impossible to transmit microwave through water.

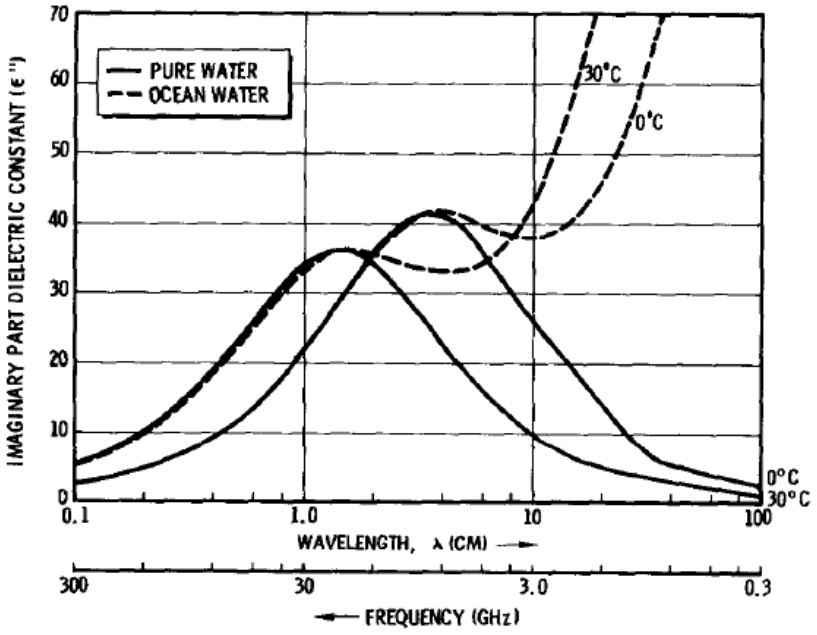

Figure 2. 10 Imaginary part of dielectric constant dependence on wavelength in water [49].

For long distance microwave WPT, the main important factor in calculation of system efficiency is the beam collection efficiency. In wireless communication system, Friis equation is used to calculate power density which can be received by antenna in long distance transmission as:

$$S_r = \frac{P_t G_t}{4\pi d^2} \quad , \tag{2.39}$$

Where P_t, G_t and d are the power which is transmitted by the transmitting antenna, gain (directivity) of transmitting antenna and distance between transmitter and receiver, respectively. Gain of antenna can be analyzed as:

$$G = \frac{4\pi A_{eff}}{\lambda^2} \quad , \tag{2.40}$$

Where A_{eff} is effective area of the antenna and can be expressed as:

$$A_{eff} = A \times \eta_{eff} \quad (2.41)$$

Where A and η_{eff} are the area and area efficiency of receiving antenna, respectively. By assumption that the receiving antenna is a dish type rectenna, typical area efficiency is 70%.

By assumption of plane wave which happens in far field region (Fraunhofer region), the power which is received by the antenna in far field region can be calculated as:

$$P_r = \frac{P_t G_t G_r \lambda^2}{(4\pi d)^2} \quad . \quad (2.42)$$

Then the beam collection efficiency based of Friis formula can be expressed as:

$$\eta_{BCE\_Friis} = \frac{G_T G_T \lambda^2}{(4\pi d)^2} \quad . \quad (2.43)$$

The region around antenna can be divided into reactive near field region, radiative near field region (Fresnel region) and far field region (Fraunhofer region) as can be seen from Figure 2.11. In reactive near field region, the power transmission efficiency can be very high because there is high magnetic coupling between transmitter and receiver. However, the distance is limited. Microwave WPT can be conducted in the far field region. However, it is found in ref. [50], the transmission efficiency becomes considerably low and in order to compensate large dispersion angle of microwave, the receiver size has to be very big. Based on these facts, most of microwave WPT is conducted in Fresnel region. Unfortunately, Friis formula cannot be used in Fresnel region because it assumed plane wave which is the characteristics of electromagnetic wave in far field region.

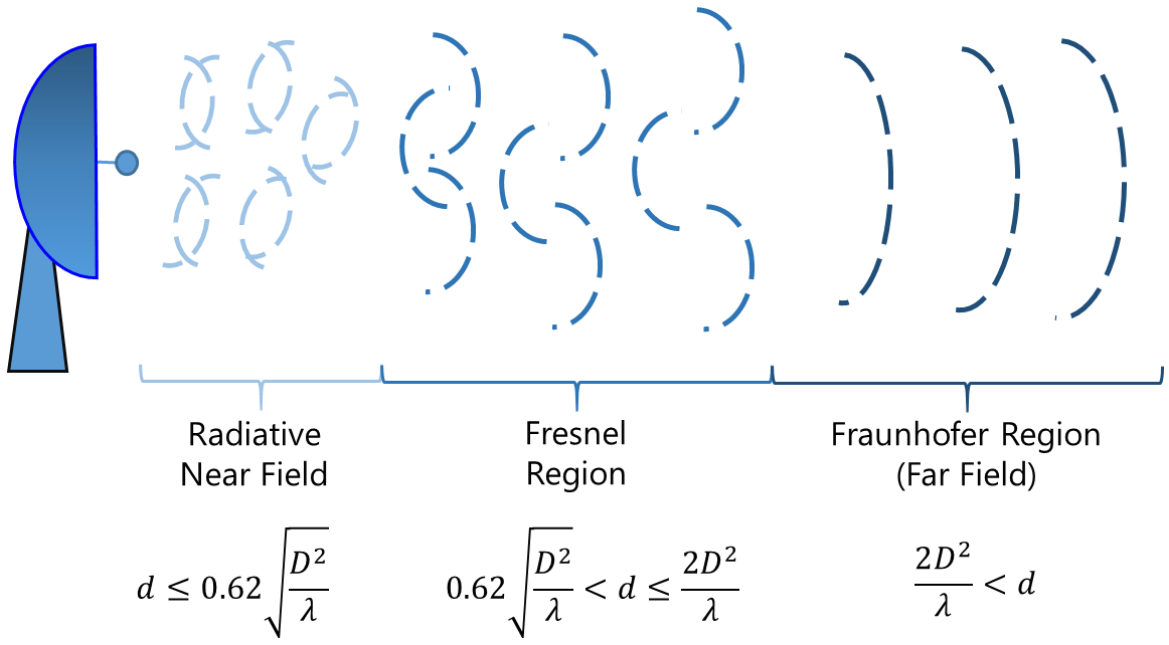

Figure 2. 11 Near field and far field region of antenna transmission.

In 1968, Goubau et. al. proposed a new formula which can be used to calculate the beam collection efficiency of optimized system [51]. The formula which was proposed by Goubau et.al. is:

$$\eta_{BCE-G} = 1 - \exp(-\tau^2) \quad , \tag{2.44}$$

Where τ is the transmission parameter which can be expressed as:

$$\tau = \frac{\sqrt{G_T G_R}\lambda}{4\pi d} \quad . \tag{2.45}$$

Note that the Goubau's formula is used to analyze the beam collection efficiency in optimized condition. Hence, it tends to be higher than in real experiment.

Figure 2.12 shows the results of calculation of system efficiency of microwave WPT through atmosphere for 2.45 GHz and 10 GHz frequency and diameter of transmitting and

receiving antennas are 1 m. The DC-RF conversion efficiency at transmitter and RF-DC conversion efficiency at the transmitter are assumed to be 0.8. In this analysis, parabolic dish lens antennas are used as the transmitter and receiver, hence, there is no loss at the antennas during the transmission. For the same size of antennas, 10 GHz microwave can be used to transmit power to longer distance than 2.45 GHz microwave. This condition can be analyzed from the dispersion angle of the electromagnetic wave. Dispersion angle of electromagnetic wave is larger for lower frequency (longer wavelength). Since, the size of the antennas for 2.45 GHz and 10 GHz transmission are assumed to be similar, more fraction of power can be collected in 10 GHz microwave WPT system than in 2.45 GHz WPT system.

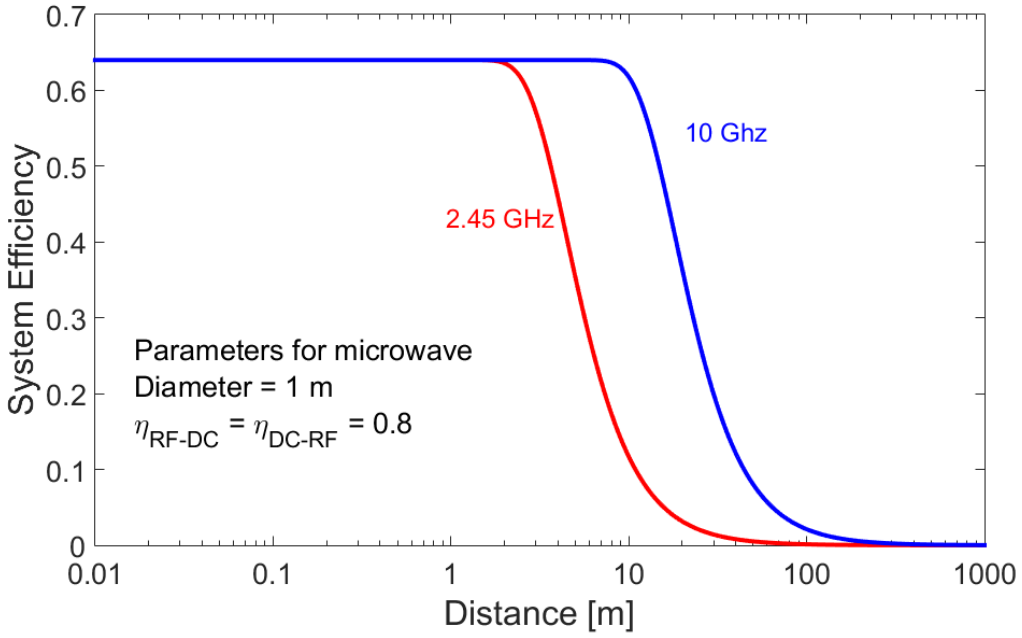

Figure 2. 12 Calculated system efficiency of microwave wireless power transmission.

2.3.4 Applications and Issue of Microwave WPT

The first development of microwave WPT technology can be traced back to W.C. Brown in 1960s [52-53]. He demonstrated microwave WPT to a wired helicopter in 1964 and a free flied helicopter in 1968. Then in 1975, he tried to increase the efficiency of microwave WPT system

can successfully demonstrated microwave WPT with 54% system efficiency and 495 W output DC power using magnetron. Then in the same year, he and his team successfully demonstrated one of the biggest microwaves WPT system with 26 m diameter of parabolic dish antenna as the transmitter and 24.48 m^2 of array rectenna as the receiver. This successful demonstration opened a new possibility of Space Power Satellite (SPS) as one of the applications of microwave WPT [54].

Due to its low attenuation by the atmosphere, power beaming from satellite to earth in microwave frequency region has been proposed in ref. [55-58]. In the concept of this system, the electric power is harvested at the satellite using solar cell, then the power is transferred to earth using microwave. In order to realize this application, high directivity antennas are needed. Based on eq. (2.40), the gain (directivity) of antenna is proportional with its radius, hence, in order to design high gain antenna, the radius of this antenna will be very large. Microwave power transmission link between satellite has also been proposed [59]. The other ground-to-air application of microwave WPT such as to transmit power to helicopter has been demonstrated and developed extensively [60]. The other application is to charge electric vehicle (EV). This application has been demonstrated by Shinohara et.al. [61].

Since 1980s, there has been an assumption that microwave is harmful for human and animal. Based on this false acclaim, there were many oppositions to microwave WPT and SPS. However, this false acclaim has been answered by Osepchuk in ref. [47]. In 1996, Osepchuk reviewed the risk of microwave exposure to human's life. It was found that most of the claims those circulated during those days such as the claims that microwave could cause cancer, it would be harmful for human's and animal's body and disturbed human's hearing were based on questionable sources and experiments which were unsupported by further researches. It was found that, exposure to microwave indeed caused thermal effects on human's skin and birds, however, the effects were mild and human tent to tolerate this kind of thermal effects for microwave more than 2.45 GHz [47]. The effects of exposure to microwave in WPT and SPS which is under maximum exposure for human's body were found to be very mild and tolerable.

The main issue which is faced by the microwave WPT is the Radio Frequency Interference (RFI). The Industrial, Scientific and Medical (ISM) band which are usually used for microwave WPT is also used for many applications of microwave such as for microwave ovens, Bluetooth and Wi-Fi.

In this case, there is possibility that microwave power transmission will interfere with the communication system which operates in this band and causes disturbance. In 1996, Osepchuk advocated the possibility to reserve the 2.4 GHz to 2.5 GHz band of frequency for microwave power transmission. However, unfortunately, nowadays this band of frequency is used for many wireless communication systems. The RFI problem is also one of the issues in the application of microwave for charging medical apparatuses such as implantable pacemaker.

CHAPTER 3

BASIC OF OPTICAL WIRELESS POWER TRANSMISSION AND COMPARISON WITH OTHER METHODS

In this chapter, basic theory of Optical Wireless Power Transmission (OWPT) is explained in detail. Basic theory about components such as light sources, attenuation of mediums, solar cell and other parameters those affect the performance of OWPT system in terms of system efficiency is explained briefly. Then the performance of OWPT system efficiency is compared with the other method to find the merit and advantage of OWPT in long distance Wireless Power Transmission (WPT). Lastly, some existing OWPT applications are given.

3.1 Basic of OWPT System Efficiency

Basic schematic of OWPT system can be seen from Figure 3.1. [62] In this case, the main components of OWPT system are the light source, medium of propagation of light and solar cell. Note that the OWPT system is a line of sight system which means that in order to successfully transmit power from transmitter to receiver, there has to be a direct line of sight space between transmitter and receiver without any object in between them. Light source is used to convert electric power into light which is electromagnetic wave and solar cell is used to convert back light into electric power which can be used to power electrical devices up. Unlike microwave WPT in

which DC-RF converter circuit and RF-DC converter circuit are needed, OWPT system operates in DC because light source such as laser and LED are operated using DC current and the output of solar cell is also DC current, hence, DC-RF and RF-DC converter are not needed and the system is generally simpler than microwave WPT.

Figure 3. 1 Basic diagram of OWPT system.

By taking advantage of the characteristics of laser which are small size, small divergence angle and high power density, OWPT is known to be able to be used for long distance WPT. The system efficiency of OWPT can simply be analyzed as:

$$\eta_{sys} = \eta_T \times \eta_{med} \times \eta_R = \eta_T \times \exp(-\alpha d) \times \eta_R \quad . \quad (3.1)$$

During the transmission in long distance WPT system, the beam size which is transmitted by transmitter through the medium will becomes larger, at some point, the beam size will become larger than the solar cell, hence, in the analysis of system efficiency of long distance WPT system, one more component can be added in the analysis of system efficiency which is called beam collection efficiency of laser, η_{col}. This efficiency shows the fraction of optical power which is captured successfully by the solar cell. Then the equation of system efficiency can be modified as:

$$\eta_{sys} = \eta_T \times \eta_{med} \times \eta_R = \eta_T \times \exp(-\alpha d) \times \eta_{col} \times \eta_R \quad . \quad (3.2)$$

Basic theory of laser and LED will be briefly explained in section 3.2 and in section 3.3, the attenuation of light by medium such as atmosphere, water, optical fiber and human skin and other phenomenon in medium that can decrease the performance of the system is explained in detail. In section 3.4, basic theory of solar cell and the calculation of conversion efficiency of Silicon (Si) solar cell is explained in detail. Then in section 3.5, the light beam divergence during the transmission in medium especially atmosphere and its effect to the system efficiency of OWPT is explained.

3.2 OWPT Component: Light Source

In OWPT system, the most popular light source is laser. Laser is an abbreviation of Light Amplification by Stimulated Emission Radiation. Basic structure of laser can be seen from Figure 3.2. Laser basically consists of laser materials which is an active gain material, pumping mechanism (energy support) and mirrors [63-64]. The active gain material and mirrors construct the laser cavity. The active gain material is the component which produces optical wave. The energy support can be DC electric current in semiconductor laser or optical power in solid state laser. The main purpose of pumping mechanism is to excite electrons in the lower energy band of gain material to higher energy band.

The optical wave which is produced by the gain materials due to the transition of electron from higher energy level to lower energy level will be reflected by the mirrors. Hence, the light wave will be reflected back and forth by the front and back mirrors in the laser cavity. In each passing of optical wave through gain materials, the light wave will be amplified. The reflectivity of the front mirror of laser is not 100%. Hence, at some point, the light will pass through mirror and escape the cavity. This light is called output light. In order to maintain the lasing condition, it is important to manage the amplitude and vibrational phase of optical wave after each cycle in the laser cavity. These three components are the main components which need to be available for all types of laser.

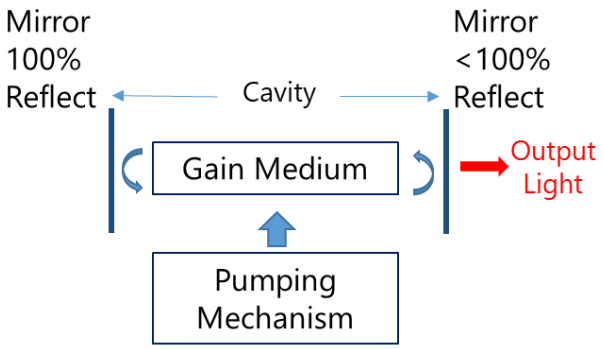

Figure 3. 2 Basic components of laser [63].

Based on the laser materials, laser can be categorized into some groups: semiconductor laser, solid state laser and gas laser. The energy support components (pumping mechanism) for each type of laser are also different. In semiconductor laser (laser diode), DC current injection is used as the pumping mechanism, on the other hand, in solid state and gas laser, optical pumping and gas discharged pumping method is used. The differences between these three types of laser can be seen from Table 3.1.

Table 3. 1 Several types of lasers.

Type of Laser	Materials	Operating Wavelength	Pumping Mechanism
Gas Laser	He-Ne	632.8 nm	Gas Discharge
	Ar	488 nm – 514.5 nm	
	CO2	10500 nm	
Solid Laser	YAG (Nd3+ . Y3Al3O2(	1060 nm	Optical illumination
	EDF (Er3+ . SiO2)	155 nm	
Semiconductor Laser	AlxGa1-xP	350 nm – 430 nm	Direct Current Injection
	AlxGa1-xAs	750 nm – 850 nm	
	GaxIn1-xAsyP1-y	850 – 1600 nm	

To understand how laser works, it is important to understand the concept of absorption and emission in laser material. For simplification, the concept of optical pumping in solid state laser. Two level energy is assumed as can be seen from Figure 3.3. In this case, electron is located in energy band E_1. When a photon which has energy same or higher than the band gap energy between E_1 and E_2 ($h\nu_g \geq E_2 - E_1$) comes to the material, the photon energy will be absorbed by the electron. The electron which has absorbed the photon energy will be excited into higher energy level E_2. This phenomenon is called absorption. The condition where the number of electrons in E_2 is higher than the number of electrons in E_1 is called population inversion.

The electron which is located in energy level E_2 can transit back into lower energy level E_1 by emitting photon. There are two mechanism that can happen in this situation. The first is spontaneous emission in which the electron transit to lower energy level by emitting photon without any stimulation from other photon. This phenomenon is illustrated in Figure 3.3 (b). There is also possibility that other photon which has photon energy $h\nu_g = E_2 - E_1$ comes to the system and stimulated the electron to transits from high energy level to lower energy level by emitting photon. This emitted photon will have the same phase and energy as the incoming photon. This phenomenon is called stimulated emission and illustrated in Figure 3.3 (c). [11,63-65]

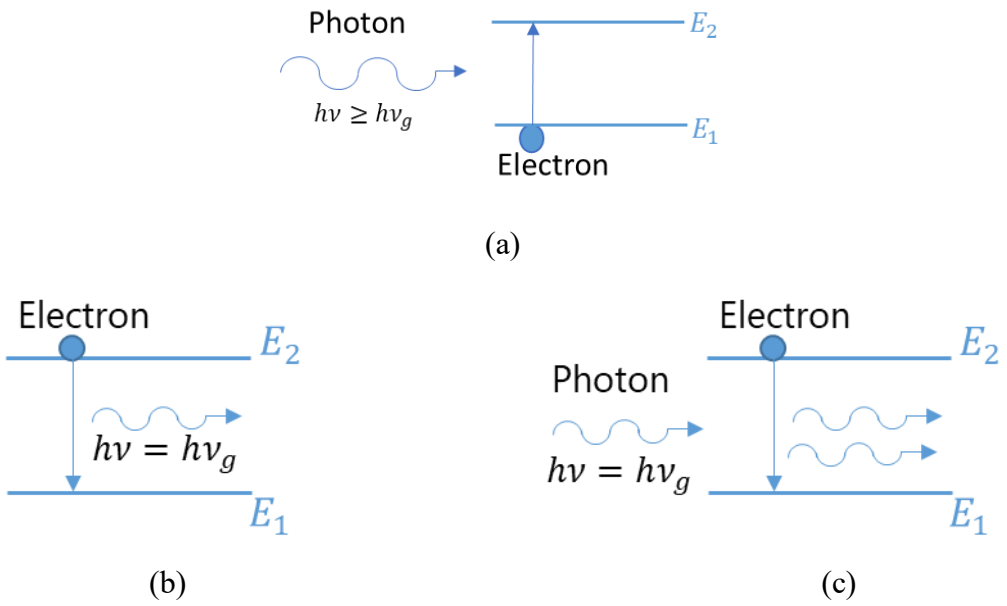

Figure 3. 3 Illustrations of: (a) Absorption, (b) Spontaneous emission and (c) Stimulated emission of light.

In the laser material, after the electron is excited to high energy level by the energy support component (pumping mechanism), the electron will transit back to low energy level by emitting photon as spontaneous emission. Then this spontaneous emission photon will stimulate the stimulated emission of other electron, hence, the power of the first spontaneous emitted light will be amplified during the propagating in laser cavity by stimulated emission until the total gain of the light can overcome the total absorption in the cavity. Then the light will escape the cavity and becomes output light of laser.

The main parameter of laser which contributes to the performance of WPT system is the conversion efficiency of laser. The conversion efficiency of laser can be expressed as:

$$\eta_{LS} = \frac{P_{opt}}{P_{el}} \quad , \tag{3.3}$$

Where P_{opt} and P_{el} are the output optical power and input electric power of laser. In the other words, conversion efficiency of laser measures how efficient the laser can convert from electric power to optical power. This power conversion efficiency is also called wall-plug efficiency.

Among three groups of lasers in Table 3.1, gas laser is the first laser which was developed to produce high power continuous wave light. This is also the first laser which can directly convert electric power into optical power. The basic schematic of He-Ne laser which is one of the gas lasers can be seen from Figure 3.4 (a). The strong electric field which is applied to the upper chamber of discharge chamber will cause electrical discharge that ionize the He+ ion in the chamber. Hence, the electron in He^+ atom will be excited to upper energy level. There is finite possibility that this excited atom will collide with the Ne atom. During the collision, the excited He atom will transfer its energy to Ne atom and excites the electron of Ne atom to upper energy level. This excited electron will decay to lower energy level. When the electron decays to lower energy level, photon will be emitted. He-Ne laser emits 632.8 nm red laser. The advantages of gas laser are its cheap and high availability of the laser gain materials and its possibility to emit high output optical power. However, in order to ionize the He+ atom in the upper chamber, high voltage power electric power source is needed, hence, the electric to optical power conversion efficiency

is relatively low. Typical power conversion efficiency of gas laser is around 0.01% to 15%. CO2 laser is the gas laser with highest power conversion efficiency and emits 10.5 μm light [66-68].

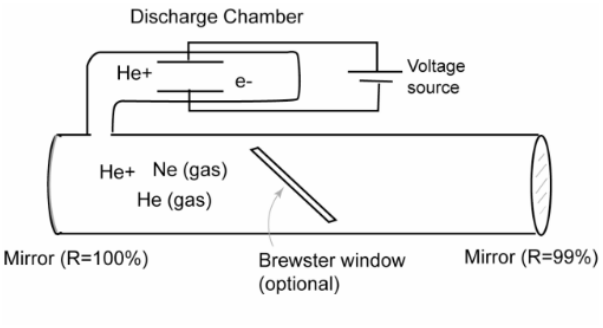

(a)

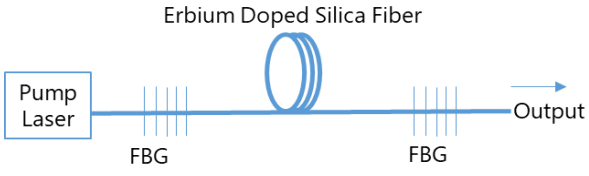

(b)

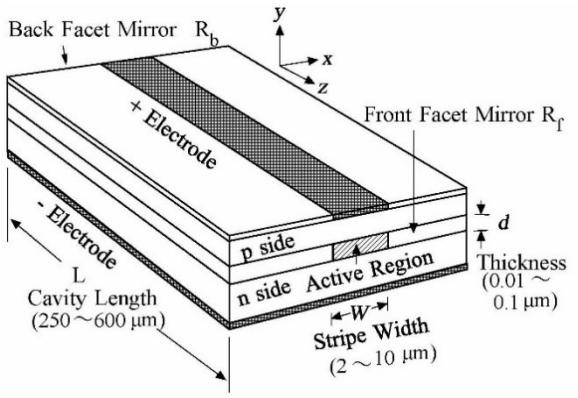

(c)

Figure 3. 4 Typical basic structure of: (a) Gas laser, (b) Solid state fiber laser and (c) Semiconductor laser [63].

Solid state laser is usually pumped with optical illumination. The gain materials in solid state laser can be either ordinary Silica fiber which is doped by rare earth element such as Erbium or rod such as in Nd:YAG laser [68]. The simple schematic of solid-state laser can be seen from figure 3.4 (b). In this case, Erbium Doped Fiber Laser (EDFL) is assumed as the example. In EDFL, the pump laser usually has wavelength of 980 nm and 1480 nm. The photon of pump laser will be absorbed by the electron of the gain material. The electron will be excited into higher energy level and decays back to lower energy level by emitting photon. The EDFL usually emits 1530 nm to 1570 nm output light, hence, it can be used for optical communication at 1550 nm. The overall electric to optical power conversion is lower than semiconductor laser because due to the optical

illumination pumping mechanism, there are two steps of power conversion in solid state laser. The first is from electric to optical power in pump laser which is usually a semiconductor laser (diode laser) and the second step of conversion is optical to optical conversion in the gain material.

In 1990, the typical efficiency of neodymium solid state laser was only 1%. [68] However, the recent development of high efficiency solid state laser has pushed the typical efficiency into more than 10%. The other materials such as Ytterbium offers higher efficiency which is typically 30% and the best in the market can exceed 50% [69-70]. The solar pumped solid-state laser has also been developed since 1966 [68,71-73]. In ref. [71-73], solar pumped Nd:YAG laser was reported. The solar pumped laser can be used for WPT system; however, the design and setting of this laser which is complicated and the heat sink system which needs large space and complicated design, restricts the application of this type of laser for OWPT application.

Semiconductor (diode) laser is the type of laser which has the highest electric to optical power conversion efficiency. The structure of diode laser can be seen from Figure 3.4 (c). The pumping mechanism is DC electric current. Typical power conversion efficiency of diode laser is around 30%. This efficiency can be increased further into more than 50% to 70% [74]. In early 2000s, Defense Advanced Research Projects Agency (DARPA) of USA launce a program which is called Super High Efficiency Diode Source (SHEDS) which aimed to obtain more than 80% efficiency high power laser diode. Under this program in ref. [74], more than 65% power conversion efficiency high power GaAs based laser has been reported. In ref. [75], nlight reported 73% power conversion efficiency 980 nm laser using micro channel diode laser bar. Moreover, in ref. [76-77], it is reported that the efficiency of 73% at 970 nm using diode laser bar can be achieved.

Vertical Cavity Surface Emitter Laser (VCSEL) can also be used as the light source in OWPT [78-82]. The other possible light source is high brightness LED. However, since the dispersion angle of LED is generally larger than laser, for long distance application of OWPT, LED has to be focused. The possibility of LED as power source in OWPT has been analyzed and demonstrated in ref. [83-87].

3.3 OWPT Component: Mediums

Light which is used to transmit power in OWPT passes through medium from transmitter to receiver. During this propagation, the power of light decays exponentially due to absorption and scattering phenomena. These absorption and scattering phenomena have been explained in Section 2.2.3. In this section, the attenuation characteristics of several mediums are discussed.

2.3.1 Atmospheric and Water Attenuation

Light which propagates in the atmosphere suffers considerably higher loss than microwave. This condition can be explained using Rayleigh scattering equation in eq. (2.15). The Rayleigh scattering is inversely proportional with the wavelength of electromagnetic wave. Since the wavelength of light is shorter than microwave, the Rayleigh scattering is more severe in optical propagation than microwave propagation. For simplification, in meteorology, visibility is used as the parameter for calculating the attenuation of light by atmosphere. Literally, visibility is the distance where the object can be recognized and discerned well by human's eyes. Higher visibility means that the attenuation by atmosphere is lower than low visibility condition. In ref. [88-89], this simple method can also be used to analyze the attenuation empirically as:

$$\alpha = \frac{16.97}{vis}\left(\frac{\lambda}{550}\right)^{-Q} \quad [dB/km] \qquad , \tag{3.4}$$

Where vis, λ and Q are the atmospheric visibility in km, wavelength of light in nm and power factor which depends on the scattering particle size distribution, respectively. The value of Q can be obtained based on the visibility. In this analysis, 30 km visibility ($Q = 1/3$) and 1 km visibility ($Q = 0.585 \times vis^{\frac{1}{3}}$) are chosen as the parameters for high visibility and low visibility respectively. The wavelength dependency of atmospheric attenuation can be seen from Figure 3.5.

The absorption and scattering coefficient spectra of light by water can be seen from Figure 3.6. The absorption coefficient is adopted from ref. [90-93] and the scattering coefficient is

calculated theoretically as in ref. [94]. In this case, pure water at room temperature condition is assumed. The absorption coefficient of light by water tends to decrease for longer wavelength, however the scattering coefficient tends to decrease for longer wavelength. The absorption coefficient is much higher than the scattering coefficient of water which implies that absorption is the dominant factor in attenuation of light by water. Since the absorption coefficient of blue laser by water molecule is low, it can be used for OWPT through water.

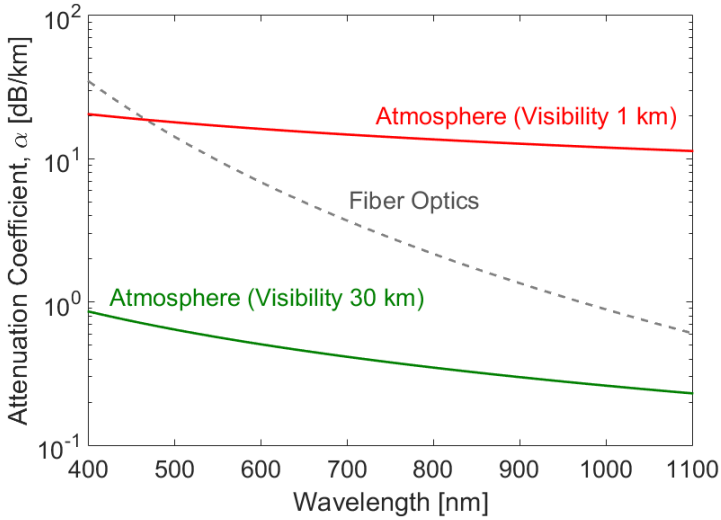

Figure 3. 5 Atmospheric attenuation coefficient.

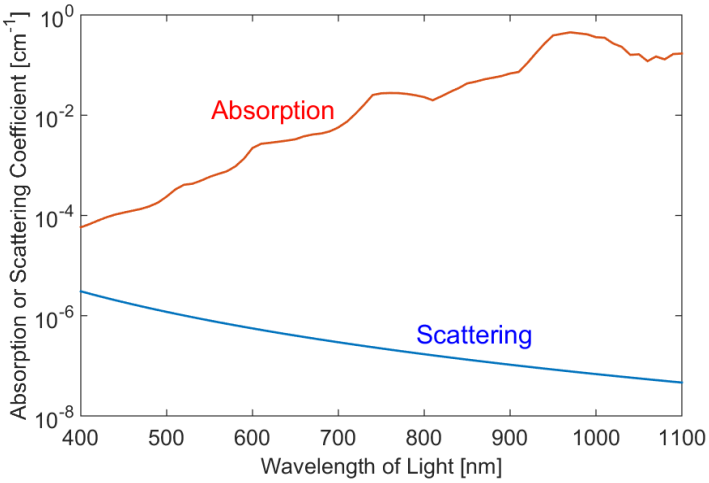

Figure 3. 6 Absorption and scattering coefficient of light by water molecule.

2.3.2 Skin

The absorption coefficient of skin is calculated as in [95]. The skin can be divided into 7 layers which are (from the top layer of skin): stratum corneum, living epidermis, papillary dermis, upper blood dermis, reticular dermis, deep blood dermis and subcutaneous fat. Each layer of skin has its own characteristics, water content and blood content. In this case, each layer has its own absorption coefficient. The stratum corneum layer and epidermis layer does not contain blood. The epidermis layer contains melanin. The absorption coefficient of stratum corneum and epidermis layer can be calculated as [95]:

$$\mu_a^{stratum}(\lambda) = \left((0.1 - 0.3 \times 10^{-4}\lambda) + 0.125\mu_a^{(0)}(\lambda)\right)\left(1 - C_{H_2O}\right) + C_{H_2O}\mu_a^{H_2O}(\lambda) \quad , \quad (3.5)$$

$$\mu_a^{epi}(\lambda) = \left(C_{mel}\mu_a^{mel}(\lambda) + (1 - C_{mel})\mu_a^{(0)}(\lambda)\right)\left(1 - C_{H_2O}\right) + C_{H_2O}\mu_a^{H_2O}(\lambda) \quad . \quad (3.6)$$

Here, $\mu_a^{(0)}$, μ_a^{mel} and $\mu_a^{H_2O}$ are the absorption coefficient of medium free of any other absorber (basic absorption of skin), the absorption coefficient of melanin (pigment of skin) and absorption coefficient of water respectively. The absorption coefficient of water is adopted from [90-93]. The $\mu_a^{(0)}$ and μ_a^{mel} can be expressed as [95-97]:

$$\mu_a^{(0)}(\lambda) = 7.84 \times 10^7 \times \lambda^{-3.225} \quad , \quad (3.7)$$

$$\mu_a^{mel}(\lambda) = 5 \times 10^9 \times \lambda^{-3.33} \quad . \quad (3.8)$$

The C_{H_2O} and C_{mel} are volume fraction of water in the skin layer and melanin (ranging from 0.02 for light skin until 0.43 for very dark skin) respectively.

The absorption coefficient of skin layers that contains blood can be calculated as [95]:

$$\mu_a^{layer}(\lambda) = (1-S)\gamma C_{blood}\mu_a^{Hb}(\lambda) + S\gamma C_{blood}\mu_a^{HbO_2}(\lambda) + (1-\gamma C_{blood})C_{H_2O}\mu_a^{H_2O}(\lambda) + (1-\gamma C_{blood})\left(1-C_{H_2O}\right)\mu_a^{(0)}(\lambda) \quad . \qquad (3.9)$$

Here, μ_a^{Hb} and $\mu_a^{HbO_2}$ are the absorption coefficient of deoxyhemoglobin and oxyhemoglobin respectively. The value of μ_a^{Hb} and $\mu_a^{HbO_2}$ are adopted from [98]. C_{blood}, S, and γ are volume fraction of blood, oxygen saturation and volume fraction of hemoglobin in blood. In this calculation, the oxygen saturation value is assumed to be 0.6 [95]. Noted that volume fraction of water and blood of each skin layer are different and can be seen in Table 3.2. The volume fraction of hemoglobin in blood is assumed to be similar for each blood contain layer and can be calculated as:

$$\gamma = F_{Hb}F_{RBC}H_t \quad , \qquad (3.10)$$

Where F_{Hb}, F_{RBC} and H_t are volume fraction of hemoglobin in erythrocyte ($F_{Hb} = 0.25$), volume fraction of erythrocyte in the whole blood volume ($F_{RBC} = 0.99$) and hematocrit ($H_t = 0.45$ for male and $H_t = 0.4$ for female) respectively.

Table 1 shows the value of C_{blood}, C_{H_2O} and thickness of each layer of skin. Note that the thickness of subcutaneous fat depends on the body weight, shape and area of skin. This thickness of subcutaneous fat can vary between 2 mm until 10 mm [99-100].

Table 3. 2 Parameters of skin layers.

Layer	C_{blood}	C_{H_2O}	**Thickness (μm)**
Stratum Corneum	0	0.05	20
Epidermis	0	0.2	80
Papillary dermis	0.04	0.5	150
Upper blood dermis	0.3	0.6	80
Reticular dermis	0.04	0.7	1500
Deep blood dermis	0.1	0.7	80
Subcutaneous fat	0.05	0.7	Until 8000 or more

The scattering coefficient of skin is calculated as in [97]. The scattering coefficient are calculated by taking into account the Rayleigh scattering and Mie scattering of light by skin. The scattering coefficient of each layer is assumed to be similar. The reduced scattering coefficient of skin can be calculated as [97]:

$$\mu_s'(\lambda) = a'^{\left(f_{Ray}\left(\frac{\lambda}{500\ (nm)}\right)^{-4}+(1-f_{Ray})\left(\frac{\lambda}{500\ (nm)}\right)^{-b_{Mie}}\right)} \quad , \qquad (3.11)$$

Where a', f_{Ray}, b_{Mie} are the scaling factor, fraction of Rayleigh scattering and Mie scattering scaling factor. Note that the eq. (7) comes from phenomenological analysis and fitting parameters

based on experimental results are assumed in this equation [97]. The wavelength, λ, is in nanometer. The value of a', f_{Ray}, b_{Mie} are 42.9 cm^{-1}, 0.76 and 0.351 respectively. These values come from approximation by Jacques for human skin in [96].

Reduced scattering coefficient is the coefficient which represent the scattering when photon diffuse in anisotropy medium such as skin. In this case, it is assumed than photon takes random path and in each steps of the path, it suffers isotropic scattering. The scattering coefficient can be calculated from reduced scattering coefficient as:

$$\mu_s = \frac{\mu_s'}{(1-g)} \quad . \tag{3.12}$$

Here g is the anisotropy of skin which has typical value 0.9. This value indicates that photon is assumed to take 10 mean free steps when penetrating the skin.

After we calculate absorption coefficient, μ_a and reduced scattering coefficient of skin, μ_s', we can calculate the effective attenuation coefficient of skin as [101]:

$$\alpha_{skin} = \sqrt{3\mu_a(\mu_a + (1-g)\mu_s)} \quad . \tag{3.13}$$

Then we assume the refractive index of skin to be 1.45 [102-103]. In this case, by assumption that light enter the skin at 90^o, the reflection at the surface of skin can be analyzed by using simple Fresnel equation.

Figure 3.7 and 3.8 show the attenuation of human skin and transparency of human skin respectively. The attenuation of human skin decreases for longer wavelength. Higher penetration of skin by light can be achieved by using around 900 nm wavelength of light. Note that in this calculation, the subject is assumed to be human male with low melanin level (Fair skin).

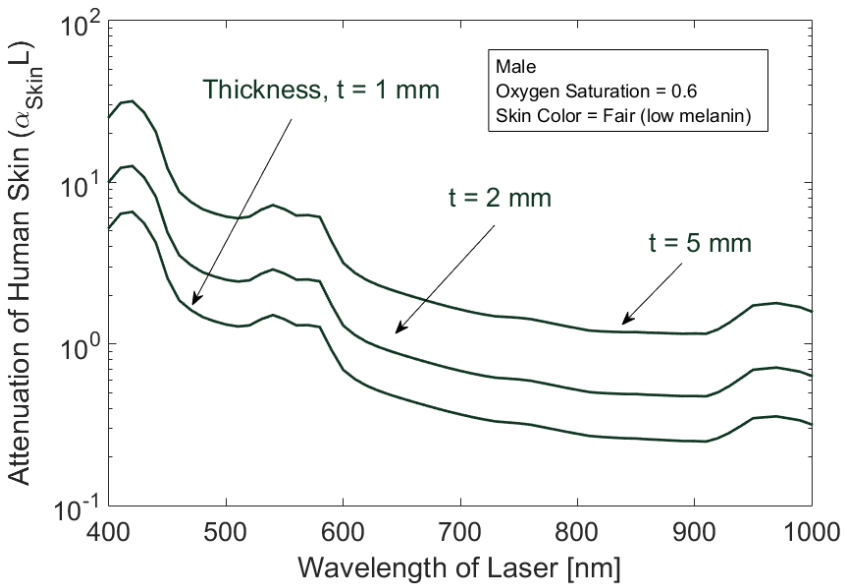

Figure 3. 7 Attenuation of human skin.

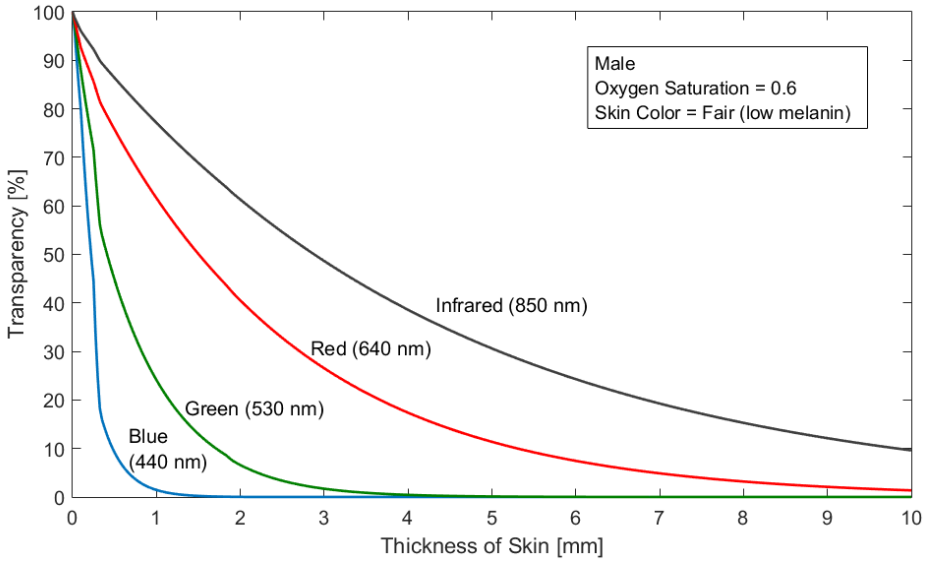

Figure 3. 8 Transparency of human skin for several wavelengths of light.

The calculation of attenuation of human skin is based on fitting parameters from experimental results. The result of experiment and calculation may be different because there are many factors which affect the attenuation of skin such as, gender, pigment and melanin contents, skin condition, area of the body where skin is taken, body mass index and many other factors. For the same test subject, the attenuation of the same area of skin may also vary from time to time due to many external and internal factors but we believe and hope that the tendency and characteristics might be almost similar where the longer wavelength (around 900 nm) might penetrate more than shorter wavelength (400 nm).

3.3.3 Other Phenomenon: Reflection

In OWPT, through other mediums than atmosphere such as water and human skin, it can be assumed that the light comes from outside the medium. In this case, there is reflection of light at the interface between two mediums with different refractive indices as can be seen from Figure 3.9. The fraction of light which is reflected at the interface between two mediums when the incoming light is normal to the surface ($\theta = 0$) can be analyzed as:

$$Ref = \left|\frac{n_1 - n_2}{n_1 + n_2}\right|^2 \quad , \tag{3.14}$$

Where n_1 and n_2 are the refractive index of medium 1 and medium 2 in Figure 3.9. The refractive index of air and water are 1 and 1.33, respectively, hence in OWPT through water where the light comes from the air above the water and normal incident of light is assumed, the reflection is 2% which means that 98% of light is transmitted into the water.

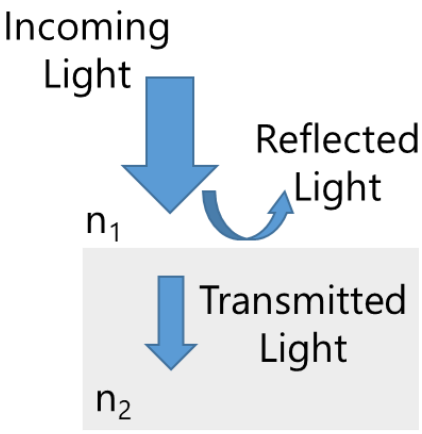

Figure 3. 9 Transmission and reflection of light at interface between mediums with different refractive indices.

3.4 OWPT Component: Solar Cell

Solar cell is the component which is used to convert light into electric power. The principle of solar cell can be seen from Figure 3.10. Simple solar cell is constructed from the pn junction. Thin p-type semiconductor is grown on top of thick n-type semiconductor to create a solar cell. Then electrodes are attached to the pn-junction. The area between p-type and n-type of semiconductor is called depletion region. In depletion region, mobile charge carrier has been diffused away due to the electric field, hence, this region acts like an insulator. The photons that falls into this region in solar cell are the only photon that will contributes to the photocurrent generation [11].

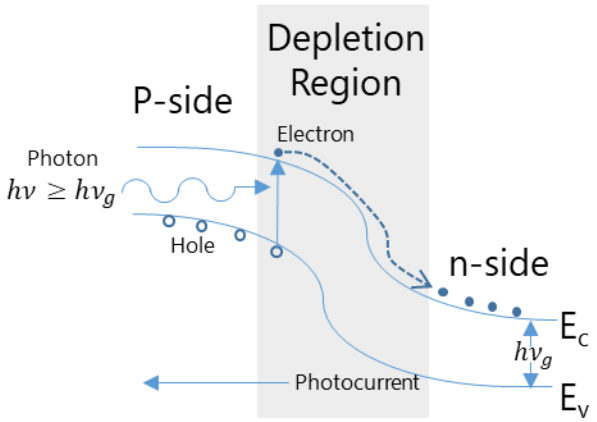

Figure 3. 10 Illustration of photocurrent generation in solar cell.

The principle of solar cell is as follow: when a photon which has same or higher energy as the band gap energy of the semiconductor ($E_g < h\nu$) comes to the solar cell, it will pass through very thin layer of p-type semiconductor into the depletion layer. In the depletion region of solar cell, the electron in the valence band will absorb the energy of photon and excites into the conduction band and creates the hole-electron pair. The electron then will drift from p-side of pn-junction into the n-side of junction, at the same time, the hole will move to the p-side of the junction. The movement of electron and hole will cause the current to flow from the n-side to p-side of the junction. This current is called photocurrent. Since this current flow from the n-type which has lower potential than p-type in pn-junction, this current is called reverse biased current.

To analyze the conversion efficiency of solar cell, firstly, it is better to understand the characteristics of incoming light to the solar cell. The spectrum of incoming light has Gaussian distribution as can be seen from Figure 3.11. In Figure 3.11, only the red colored area of spectrum of light will be absorbed by the solar cell and contribute to photocurrent generation, since the wavelength is shorter (higher photon energy, higher frequency) than wavelength which correspond with band gap, λ_g. Only the photon of light which has higher or similar energy as the band gap energy of the semiconductor will contribute to the photocurrent. The total power of incident light can be analyzed as:

$$P_{tot} = \int_0^{\infty} \frac{P_0}{\sqrt{2\pi\sigma^2}} \exp\left\{\frac{\nu - \nu_c}{2\sigma^2}\right\} d\nu = \int_0^{\infty} S(\nu) \times h\nu \, d\nu \quad , \qquad (3.15)$$

Where P_0, ν_c and σ are the maximum power of the Gaussian distribution, central frequency of light and standard deviation of the Gaussian distribution, respectively. $S(\nu)$ is the number of photon and h is Planck constant. The standard deviation σ is related with the Full Width Half Maximum (FWHM) of the Gaussian distribution as:

$$\sigma = \frac{FWHM}{\sqrt{2 \ln 2}} \quad . \qquad (3.16)$$

FWHM is the width of the Gaussian distribution when the amplitude is half of the maximum amplitude.

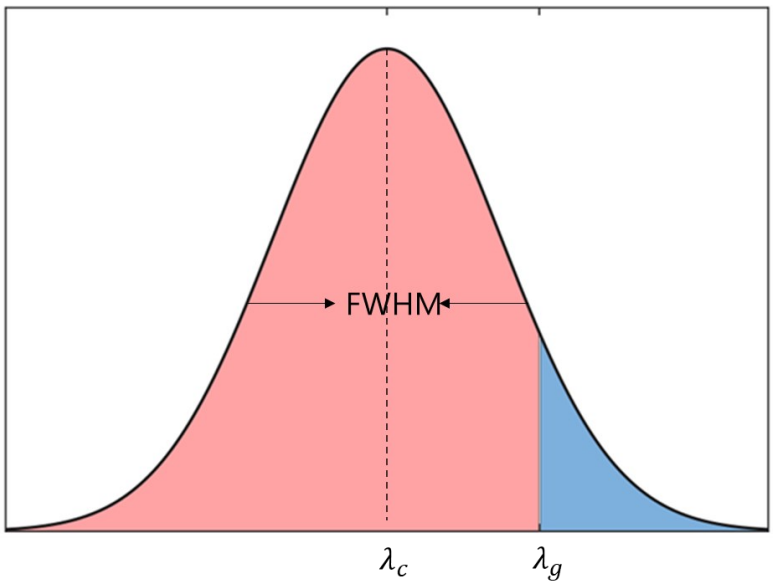

Figure 3. 11 Illustration of spectrum of incoming light of solar cell.

Only the photon which has higher or similar energy than the band gap energy of semiconductor will contribute to the generation of photocurrent, hence the power of incident light that will contribute to the generation of photocurrent can be analyzed as:

$$P_{inc} = \int_{\nu g}^{\infty} \frac{P_0}{\sqrt{2\pi\sigma^2}} \exp\left\{\frac{\nu - \nu_c}{2\sigma^2}\right\} d\nu \quad , \tag{3.17}$$

Where νg is the frequency which is related with the band gap energy of semiconductor. The degree of absorption of photon energy by the electron in solar cell depends on the frequency (wavelength) of light and the material of solar cell. In this case, Silicon (Si) is assumed as the material of solar cell. The absorption spectra of Si can be seen from Figure 3.12 [104]. The fraction of incident optical power that is absorbed by the solar cell can be expressed as:

$$P_{abs}(\nu) = \int_{\nu g}^{\infty} \frac{P_0}{\sqrt{2\pi\sigma^2}} \{1 - \exp(-\alpha_m(\nu) d_m)\} \exp\left\{\frac{\nu - \nu_c}{2\sigma^2}\right\} d\nu \quad , \tag{3.18}$$

Where $\alpha_m(\nu)$ and d_m are the absorption of light by material and the thickness of material of solar cell, respectively. Note that the absorption of light by material has frequency dependency. In this calculation, for simplification, Internal Quantum Efficiency (IQE) is assumed to be 1. It means that one photon that is absorbed by the solar cell is assumed to excite exactly one electron which contributes to the generation of photocurrent. Then External Quantum Efficiency (EQE) which expresses the fraction of total incident photons that contributes to the generation of electron in photocurrent is:

$$\eta_{EQE} = \frac{P_{abs}}{P_{tot}} \quad . \tag{3.19}$$

The number of electron-hole pairs which is created due to absorption of photon and contributes to the generation of photocurrent can be analyzed from eq. (3.15) and eq. (3.18) as:

$$S_{abs} = \int_{\nu g}^{\infty} S(\nu) d\nu \quad . \tag{3.20}$$

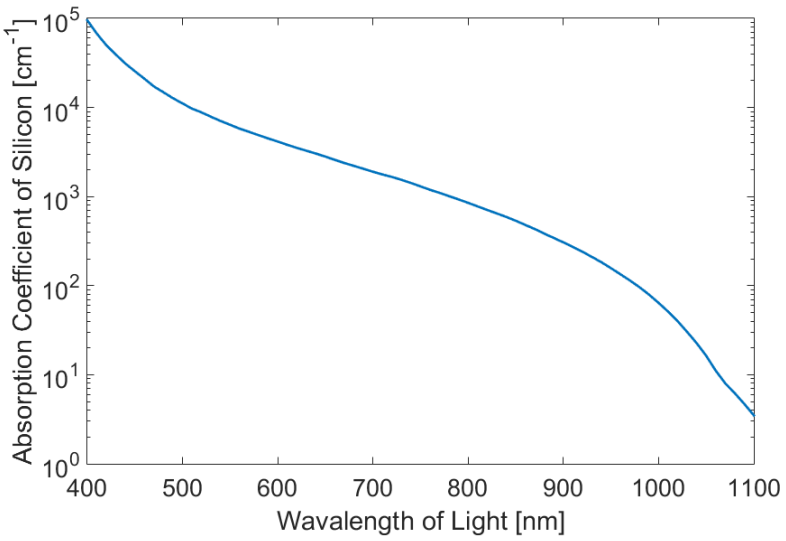

Figure 3. 12 Absorption coefficient spectrum of silicon [104].

This number of electron-hole pairs is related to photocurrent as:

$$I_L = qS_{abs} \quad , \tag{3.21}$$

Where q is the charge of electron ($q = 1.69 \times 10^{-19}$ Coulomb).

Based on Shockley-Queisser Theorem, in the solar cell, an absorption of photon creates electron-hole which will contributes to the generation of photocurrent, however, based on the principle of detailed balance, the other way around phenomenon can also happens where the electron meets hole and recombine by emitting photon. The solar cell has its own temperature; hence, it can act as blackbody. The recombination of electron and hole in the cell is affected by the thermal voltage across the junction that can be calculated as:

$$V_C = \frac{kT_C}{q} \quad , \tag{3.22}$$

Where T_c is the temperature of solar cell in K (in case of room temperature, 300 K). When the temperature of the solar cell is not 0, there is voltage across the junction, then, the concentration

of electron-hole in the solar cell will also change. The rate of this recombination which is correlated with the blackbody photon above the bandgap energy of the cell can be expressed as:

$$F_0 = \int_{vg}^{\infty} \frac{1}{\left(\exp\left(\frac{h\nu}{kT_C}\right) - 1\right)} \frac{2\pi\nu^2}{c^2} d\nu \quad . \tag{3.23}$$

Then the dark current which is the current flows when the solar cell is not illuminated by light is:

$$I_0 = qF_0 \quad . \tag{3.24}$$

Based on Shockley-Quiesser theorem and by assumption that the solar cell is an ideal diode, the current in the solar cell can be calculated as:

$$I = I_0 \left\{\exp\left(\frac{qV}{kT_C}\right) - 1\right\} - I_L \quad . \tag{3.25}$$

Note that the negative value of photocurrent I_L indicates that the photocurrent flows to different direction with the dark current and it flows from negative to positive potential of junction. The calculated IV characteristics for several wavelength of incident light for 1 W/cm^2 optical power can be seen from Figure 3.13.

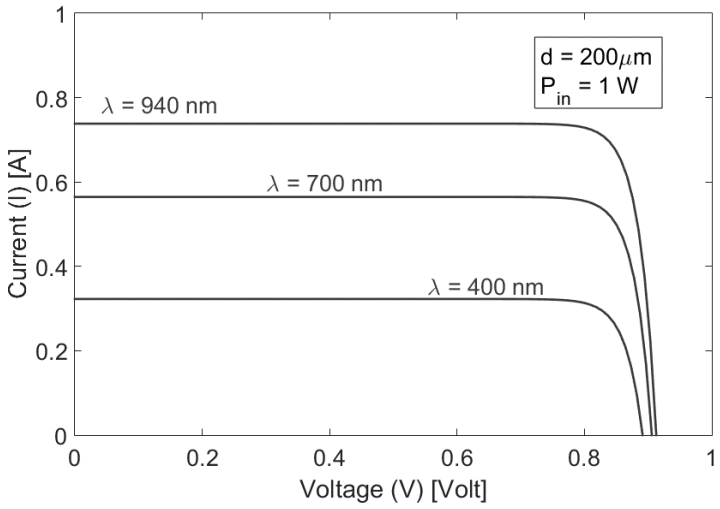

Figure 3. 13 Calculated IV characteristics of solar cell.

The short circuit current which is the current when the voltage across junction is 0, can be expressed as:

$$I_{sh} = I_L \quad . \tag{3.26}$$

The open circuit voltage which is the voltage across junction of solar cell when the current is 0 can be calculated as:

$$V_{OC} = \frac{kT_C}{q} \ln\left(\frac{I_L}{I_0} + 1\right) \quad . \tag{3.27}$$

The current in eq. (3.25) can be correlated with eq. (3.27) as:

$$I = I_0 \left\{ \exp\left(\frac{qV}{kT_C}\right) - \exp\left(\frac{qV_{OC}}{kT_C}\right) \right\} \quad . \tag{3.28}$$

Then by multiplying eq. (3.28) with the voltage across junction, V, the equation of electric power produced by the cell can be expressed as:

$$P_{elec} = IV \quad . \tag{3.29}$$

Then, to find the maximum power which can be produced by the solar cell, the derivative of eq. (3.29) is evaluated as $\frac{dP}{dt} = 0$, then the voltage when the maximum electric power of the solar cell can be correlated with the open circuit voltage as:

$$V_{MAX} = V_{OC} - \frac{kT_C}{q} \ln\left(\frac{qV_{MAX}}{kT_C} + 1\right) \quad . \tag{3.30}$$

Finally, maximum electric power that can be produced by the solar cell can be calculated as:

$$P_{MAX} = I_{MAX} \times V_{MAX} = V_{OC} \times I_{SC} \times FF \quad , \tag{3.31}$$

Where FF is the fill factor which is the factor that determines the quality of the solar cell. Then power conversion efficiency (PCE) of solar cell can simply be analyzed the ratio of maximum output electric power and total incident optical power as:

$$\eta_R = \frac{P_{MAX}}{P_{tot}} \quad . \tag{3.32}$$

Figure 3.14 shows the calculated central wavelength of incident light dependency of PCE of Si solar cell. The thickness of Si layer of solar cell is assumed to be 200 μm which is the typical thickness of Si in solar cell [105]. The band gap energy of Si is 1.1 eV which is correlated with 1100 nm of wavelength of light. The power density of incident light is assumed to be 1 W/cm^2. The maximum PCE can be obtained at 940 nm central wavelength of light. Shorter wavelength of light means that the photon energy of the light is higher than longer wavelength of light. Hence, visible light has much high photon energy than the band gap of electron. In this case, the electron which absorbs photon of short wavelength of light will excite from valence band to higher energy level, releases some part of energy as heat and transits to the conduction band level. Hence, photon of short wavelength light has lower efficiency than near infrared light which is near the band gap

of Si because shorter wavelength means that more energy is released as heat. The maximum PCE is calculated to be 59% [10].

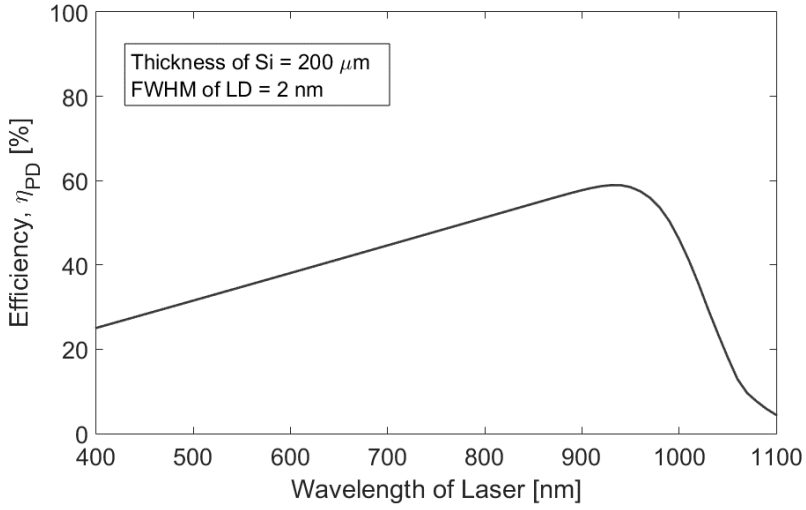

Figure 3. 14 Calculated PCE of Si solar cell.

Many researches focus on the developments of high PCE solar cell which can be used for OWPT application. There are many analyses of efficiency and performances of Si solar cell in OWPT applications [106-112]. Beside Si, other semiconductor materials of Solar cell such as InGaAs, GaN and GaP which have different band gap with Si, hence, can be applied for different wavelength of light source, have been proposed. Some of these materials of solar cell are summarized in Table 3.3 [113-126]. The other attempts to increase the PCE of solar cell have also been developed such as by putting back side mirror on the solar cell, hence the photon which passes through solar cell and has not been absorbed will be reflected back to solar cell and can be absorbed [127] and by special design of solar cell to increase its PCE [110-111]. GaN solar cell has very high band gap compared which is around 3 eV, hence it can be used for high efficiency power converter for blue laser. At this point, we learnt that matching the wavelength of operation of solar cell or the band gap of materials with the wavelength of light in OWPT is very important when choosing laser and solar cell.

Table 3. 3 Some semiconductor materials for solar cells.

Materials	Band Gap	Wavelength of Operation
InGaAs	0.75 eV	0.5 – 1.65 μm
InGaAsP	0.75 – 1.1 eV	1 – 1.6 μm
GaN	3 – 3.4 eV	0.2 – 0.4 μm
Ge	0.74 eV	0.5 – 1.8 μm

3.5 Laser Beam Divergence and Beam Collection Efficiency Problem

The Gaussian beam power distribution profile can be seen from Figure 3.15. The power distribution is Gaussian shape across its cross section and point *O* is the center of Gaussian beam. The beam diameter is defined as the diameter of the beam when the optical power is $1/e^2$ of the peak intensity. The region between the beam diameter contains around 86.5% of the total optical power of the beam.

When a laser beam is focused using a lens, its beam size will become smaller and at some point, the wavefront will becomes parallel. However, its beam size will not become a spot with near to 0 area because if the beam spot size were near zero, it would mean that the power density was infinity. The focused beam size will become smaller and after its size is at the smallest (when the wavefront is parallel), it will start to diverge and the beam size will become larger again during its propagation as can be seen from Figure 3.16. This phenomenon is called beam divergence.

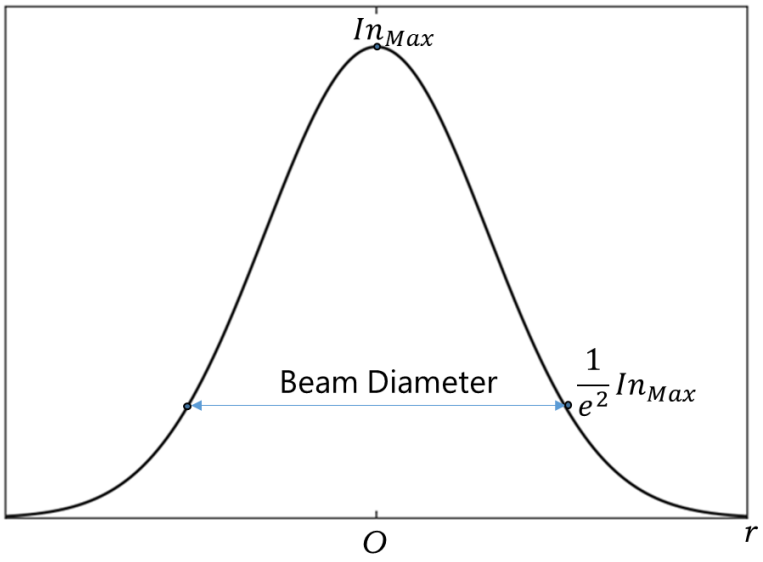

Figure 3. 15 Gaussian beam power distribution profile.

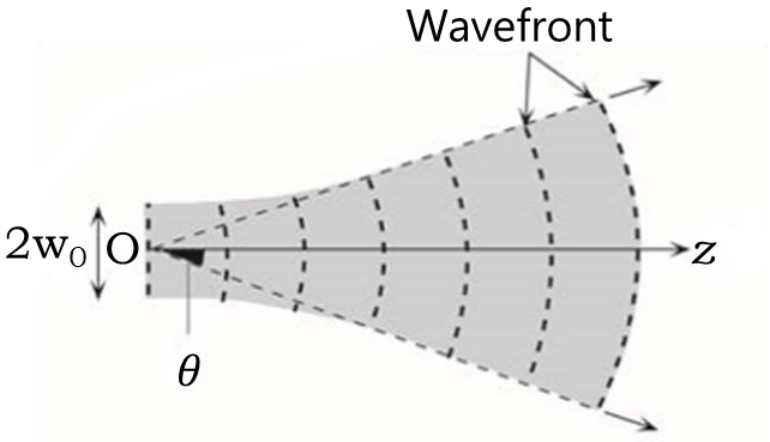

Figure 3. 16 Illustration of beam divergence during its propagation to z-direction [11].

The smallest beam size when the wavefront is parallel is called beam spot size, $2w_0$. The divergence of the beam during propagation in z-direction will make a certain angle at center of beam *O*. The angle of divergence of the beam can be expressed as:

$$\theta_d = \frac{\lambda}{\pi n(w_0)} \quad , \tag{3.33}$$

Where *n* is the refractive index of medium. In case of the free space, the refractive index is 1.

At certain distance, z_0, the beam diameter will become $\sqrt{2}(2w_0)$. This distance is called Rayleigh range and can be expressed as:

$$z_0 = \frac{\pi n w_0^2}{\lambda} \quad . \tag{3.34}$$

Then the radius of the ideal Gaussian beam for the distance z along the propagation in free space can be analyzed as:

$$w = w_0 \left\{1 + \left(\frac{z}{z_0}\right)^2\right\}^{\frac{1}{2}} = w_0 \left\{1 + \left(\frac{z\lambda}{\pi w_0^2}\right)^2\right\}^{\frac{1}{2}} \quad . \tag{3.35}$$

Calculated beam size during the propagation to z-direction for several spot size $2w_0$ can be seen from Figure 3.17. In this case, the beam is assumed to be ideal Gaussian beam. Smaller value of beam waist radius w_0 will results in larger divergence angle, hence the beam diameter of beam with spot size 1 cm becomes more than 12 cm after 1 km distance, on the other hand, laser beam with spot size 10 cm hardly changes in diameter after 1 km propagation through air.

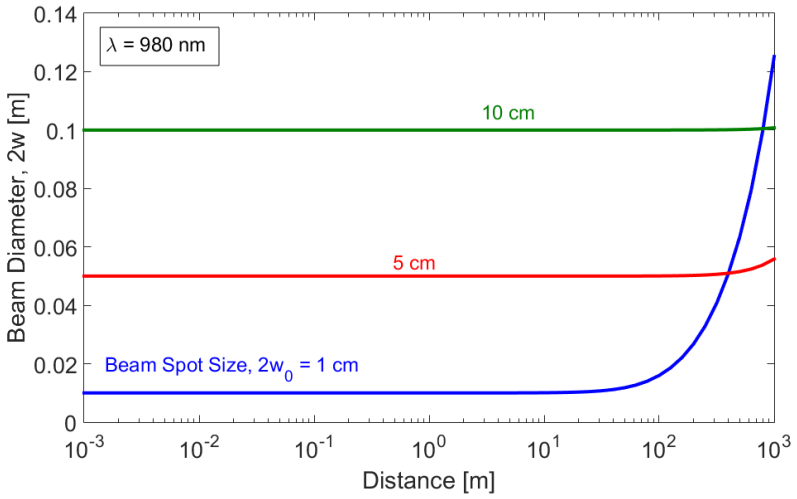

Figure 3. 17 Beam diameter of ideal gaussian beam during its propagation in atmosphere.

If the beam size is larger than the solar cell, only a fraction of the power of the laser that will be received by the receiver. Hence, some of the power which is not received by the receiver can be considered to be loss. The intensity of Gaussian beam for the position r from the center of the beam can be expressed as:

$$In(r) = In_0 \exp\left(\frac{-2r^2}{w^2}\right) \quad . \tag{3.36}$$

The shape of solar cell is assumed to be rectangle with the length and width are x_1 and y_1. Then the function of intensity in eq. (3.36) can be modified in Cartessian coordinate as:

$$In(x,y) = In_0 \exp\left(\frac{-2(x+y)^2}{w^2}\right) \quad . \tag{3.37}$$

The power which is contained in the rectangle with length x_1 and width y_1 which defines the power which is received by the solar cell by assumption that the center of the solar cell in (0,0) coordinates in Cartessian, then the power received by solar cell for all four quadrants of the solar cell can be analyzed as:

$$P_{SC} = 4 \times \int_{0}^{\frac{y_1}{2}} \int_{0}^{\frac{x_1}{2}} In(x,y)dxdy \quad . \tag{3.38}$$

Then the beam collection efficiency can be calculated as the ratio of the power which is received by the solar cell and total power of the Gaussian beam:

$$\eta_{mis} = \frac{P_{SC}}{P_{tot}} = \frac{\int_0^{y_1} \int_0^{x_1} In(x,y)dxdy}{\int_0^{\infty} \int_0^{\infty} In(x,y)dxdy} \quad . \tag{3.39}$$

The beam collection efficiency for several beam spot size parameters can be seen from Figure 3.18. In this calculation, the wavelength of light is 980 nm, the solar cell is assumed to be a square with size 10 cm x 10 cm. Laser beam with spot size 1 cm has lower beam collection efficiency after 1 km propagation through atmosphere due to the divergence of beam and the beam diameter becomes larger than the solar cell, on the other hand, the beam collection efficiency of laser with beam spot size 5 cm is almost 100% for propagation 1 km. The laser with beam spot size 10 cm has lower beam collection efficiency due to the size of the solar cell is similar with the beam diameter, hence, some parts of the laser beam is not received well by the solar cell, even though at close distance.

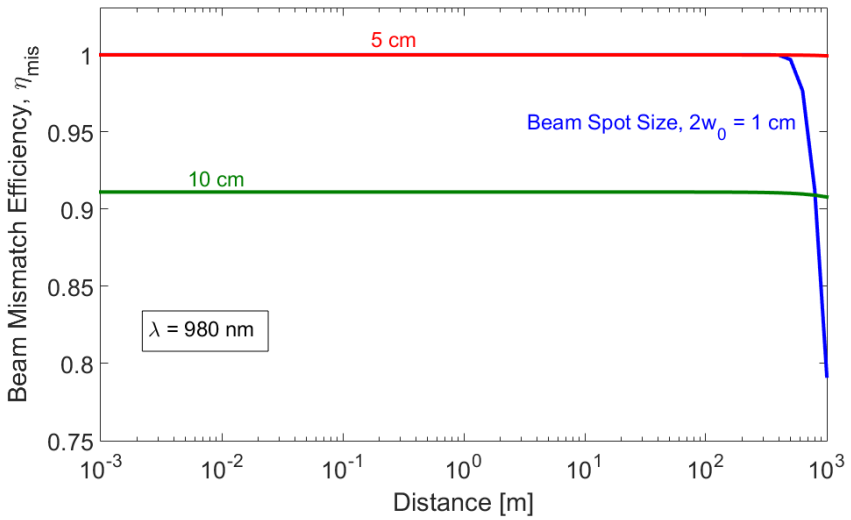

Figure 3. 18 Calculated laser beam collection efficiency.

At this point, it is understandable that the matching of size between solar cell and laser beam is one of the important conditions in OWPT. If the size of the beam is larger than solar cell, some power will be lost, on the other hand, if the beam size is much smaller than solar cell, if the solar cell is single junction solar cell, it might not be a big problem, however, if the solar cell is multijunction solar cell or solar cell array, if not all of the junction of solar cell or not all of the cells in the array are illuminated by light, the current will not flow and there would be no output of solar cell. One of the attempts to solve the beam size mismatch problem is by using fly-eye lens. Using fly eye lens, the laser power density and size can be adjusted, hence, the power density of the laser at solar cell will be evenly distributed. However, in this method, as reported in ref. [128-131], there is loss by the fly eye lens due to scattering by the material. Lenses can also be used to control the size of laser beam during its propagation [132].

3.6 Calculated System Efficiency of OWPT

The wavelength dependency of OWPT system efficiency for distance between transmitter and receiver is 1 km through atmosphere under low visibility condition (vis = 1 km) and high visibility condition (vis = 30 km) can be seen from Figure 3.19. The solar cell is assumed to be Si solar cell. For comparison, the system efficiency for power transmission through optical fiber is also calculated. For simplification, the power conversion efficiency of the laser which is the light source in this OWPT is assumed to be 70%. The optical power density of incident light is assumed to be 1 W. The maximum system efficiency around 38.7% at 940 nm, 31.85% at 950 nm and 2.38% at 960 nm wavelength of incident light for power transmission through air with 30 km visibility, optical fiber and air with 1 km visibility respectively can be achieved. In this analysis, it is assumed that there is no any laser beam collection loss. The size of solar cell and laser is assumed to be match.

The system efficiency for power transfer through optical fiber is less than 10% for visible light spectrum. In this case, air may be more suitable choice for optical power transfer medium than optical fiber if the concentration of scattering agent such as water vapor is low. In the condition of very high concentration of scattering and absorption gas in the air such as in fog or smog weather, the system efficiency can become less than 2%. [10]

Figures 3.20 and 3.21 show the system efficiency of OWPT through water and skin, respectively. In this numerical calculation, the reflection of water and human skin is taken into account by assuming normal incident light from the air (refractive index = 1) and using Fresnel equation. The refractive index (n) of water and human skin are assumed to be 1.33 and 1.45, respectively. It is found that the optical power transmission through water has maximum system efficiency at visible light. This condition is due to high absorption of water in near infrared and infrared region. The maximum system efficiency around 29.2% at 810 nm wavelength for 10 cm depth of water, 22.9% at 570 nm wavelength for 1 m depth of water, 17.85% at 480 nm for 10 m depth of water and 9.6% at 400 nm wavelength for 100 m depth of water. In this case, system efficiency of the optical power transmission through water has unique characteristics where the

maximum system efficiency shifts to longer wavelength for shorter distance or shallower depth of water.

The parameters of skin are adopted from [95-87]. In this analysis, the characteristics of alive male with light color skin for thorax area is assumed because the objective of this analysis is for optical power transfer for charging implantable device such as pacemaker. The system efficiency of optical power transmission through human skin basically increases for longer wavelength until it reaches the peak at 910 nm for all thicknesses of skin. The maximum system efficiency of 24.5%, 12.4% and 4% are achieved at 2 mm, 5 mm and 10 mm thickness of skin respectively. The system efficiency for 10 mm thickness of skin may seem small but based on [133], the consumption of energy for pacemaker is small which is only 20 μA in 24 hours. In this case, the system efficiency 4% might be sufficient to charge pacemaker.

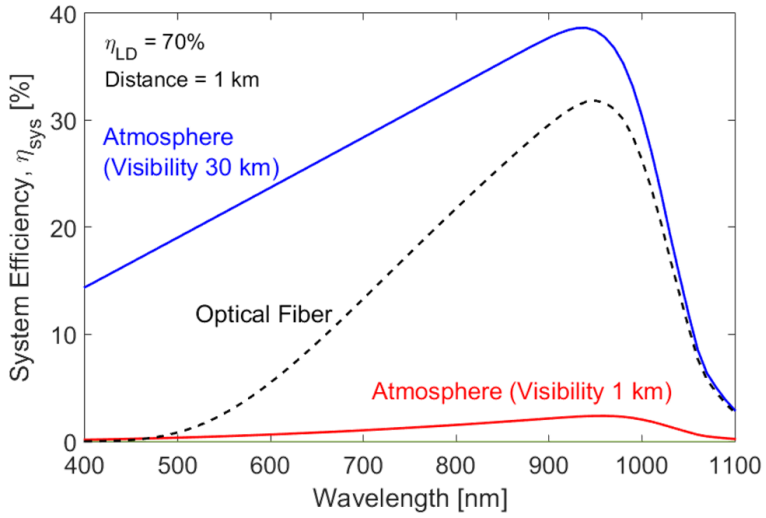

Figure 3. 19 Calculated system efficiency of OWPT through atmosphere.

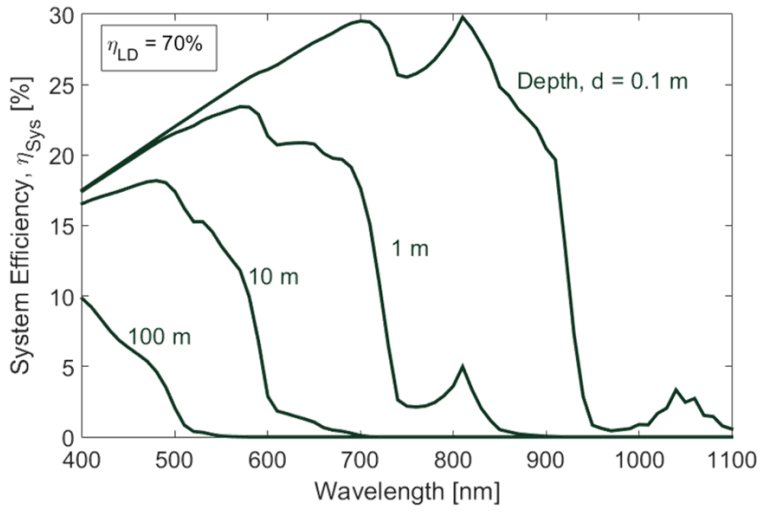

Figure 3. 20 Calculated system efficiency of OWPT through water.

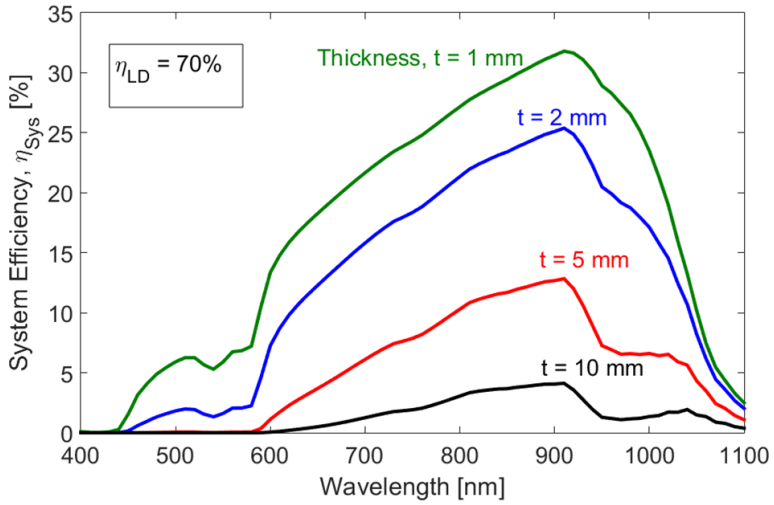

Figure 3. 21 Calculated system efficiency of OWPT through human skin.

3.7 Distance Dependency of System Efficiencies of OWPT and Other Methods

The distance dependency of system efficiency of OWPT, magnetic coupling WPT and microwave WPT through atmosphere for the central wavelength of light is 980 nm, the frequency of magnetic coupling WPT is 500 kHz and the frequencies of microwave WPT are assumed to be 2.45 GHz and 10 GHz can be seen from Figure 3.22. Among three WPT methods, OWPT is the method which has lowest back to back efficiency, however, it can be used to transmit power for longer distance than other WPT methods. Magnetic coupling WPT is the method which has highest back to back efficiency. Magnetic coupling WPT with 50 cm of diameter of coils can be used to transmit power for several tens of cm, on the other hand, microwave WPT can be used to transmit power to distance several tens of meter with 1 m diameter of antennas. Theoretically, OWPT can be used to transmit power to distance more than 100 m through high visibility atmospheric condition.

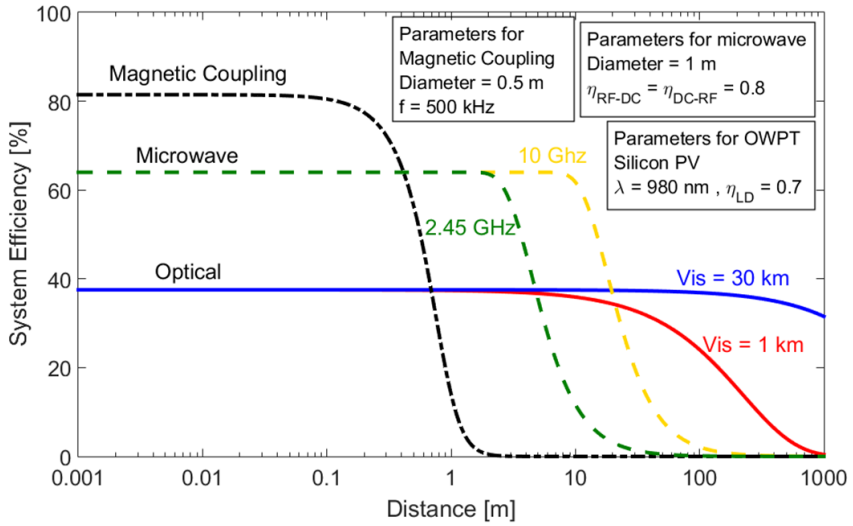

Figure 3. 22 Comparison of system efficiency of WPT methods through atmosphere.

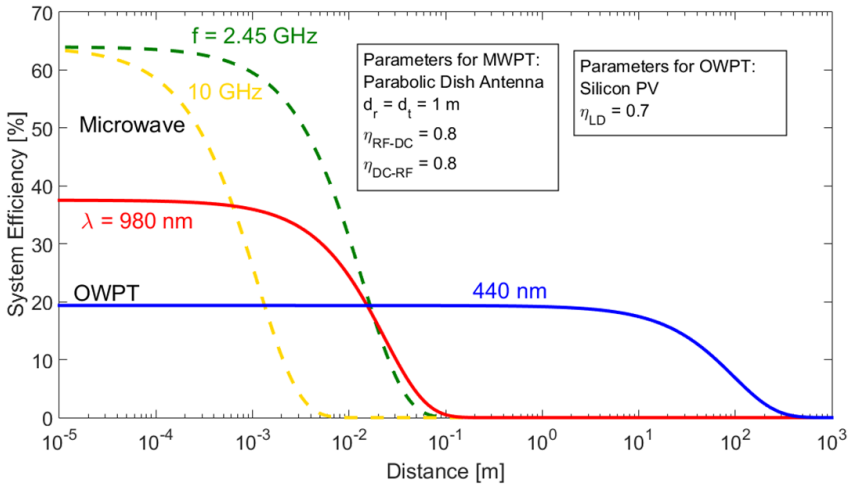

Figure 3. 23 System efficiency of MWPT and OWPT through water.

Distance dependency of OWPT and microwave WPT through water can be seen from Figure 3.23. In this calculation, it is assumed that the phenomenon in near field of antennas where the coupling between two antennas is very high for microwave WPT can be neglected, hence the only factor which is considered in this calculation is the attenuation by medium. As explained in Section 2.2.3, the absorption coefficient of microwave by water molecule is very high, hence, the microwave is highly absorbed by the water. The microwave WPT can only be used to transmit power with efficiency more than 10% for very short distance which is several mm of distance between antennas. On the other hand, OWPT using blue laser (440 nm) can be used for distance more than 1 m between laser and solar cell with considerably high system efficiency. However, the absorption of 980 nm laser which is in infrared wavelength region is very high, hence, it is not advisable to use infrared light in OWPT transmission through water. In short distance (several cm), OWPT using 980 nm laser has higher system efficiency than OWPT using 440 nm laser due to higher PCE of Si solar cell for 980 nm of light than 440 nm of light.

3.8 Existing Applications

The history of the development of concepts of OWPT can be traced back to the end of 1960s. The first documentation about the feasibility of OWPT system is in 1968 by W.J. Robinson, Jr. from National Aeronautics and Space Agency (NASA) [134-135]. In this documentation, NASA explored the feasibility wireless power transmission using either laser or microwave from an earth-orbiting space station into substation in space. During that time, gas laser was the only available light source which could deliver kW continuous wave (CW) of optical power. In this documentation, it was concluded that WPT using laser would have smaller aperture than microwave WPT, hence, WPT using laser had advantage over microwave WPT.

In the early stage of its development until the beginning of 2000s, the applications of OWPT which were developed and analyzed were mainly for space applications. NASA developed and analyzed components of OWPT for outer space applications such as laser [136-137] and solar cell [106,138]. NASA also developed and proposed concepts of OWPT systems such as OWPT between satellites, ground to space laser power transmission [139-142], power transmission from in space and from space to earth [143-158] and space elevator which is a cable where one end is attached to the surface of earth and the other end is attached to a platform outside of earth's atmosphere to send payload to satellite and to send satellite into its orbit [141].

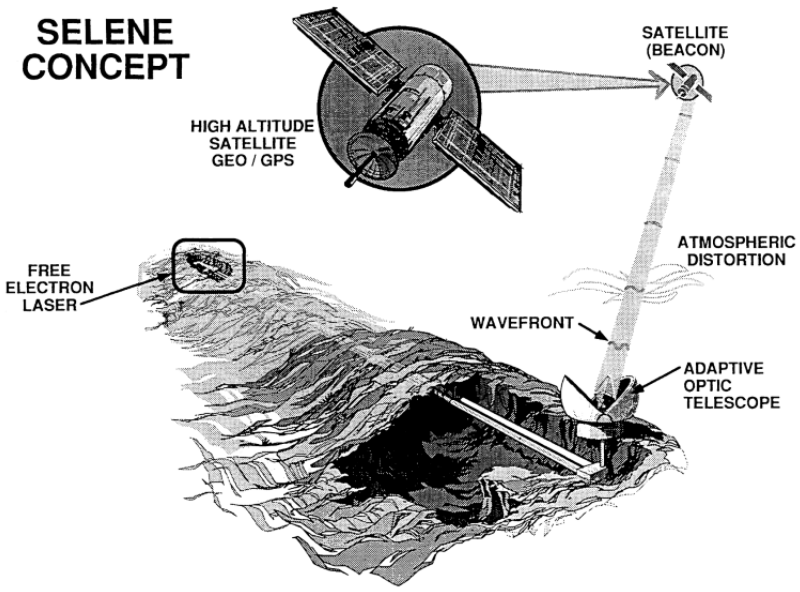

Figure 3. 24 Selene Project concept [142].

US Navy also proposed project Selene, as can be seen from Figure 3.24, which was a project to send power from ground to satellite via laser which can be used to power the satellite up to extend its lifetime [142]. N. Kawashima et.al. proposed a space application of OWPT where OWPT is used to transmit power to a rover to explore the moon [149]. This proposal is followed with successful demonstration of OWPT for 1.2 km power transmission using 30 W/cm2 output power density of laser and GaAs solar cell. The diameter of the beam at the solar cell was 80 cm and the diameter of solar cell was 67 cm [150]. The effect of power transmission in GaAs based solar cell OWPT system was also analyzed by H.W. Brandhorst and D. R. Forester in ref. [113]. Japan Space Agency (JAXA) also took part in the development of space applications of OWPT by proposing laser power beaming from space to ground station. In this proposed concept, the electric power is harvested in space by using solar cell at the satellite, then, the electric power is sent to earth using high power laser (more than MW class laser) [154]. At this point, it is clear that one of the large-scale and the most sophisticated applications of OWPT which is popular and developed for long time is space applications for exploration.

At smaller scale, OWPT can be used to power up small aircraft [152, 159-160], Unmanned Automated Vehicles (UAVs) [161-167], robots [168-170] and other electronics appliances. Application of optical wireless link which can be used for communication and power transmission for indoor small cells have also been pioneered by J. Fakidis et.al. [171-173]. The other applications of OWPT in small scale is to charge subcutaneous implantable medical devices such as pacemaker [10,133,174-177]. The possibility and feasibility of OWPT through water which can be used to power Unmanned Underwater Vehicle (UUV) up and underwater sensors have also been analyzed and demonstrated [10,178-182]. Since blue laser is absorbed less than other wavelength of light and microwave, OWPT is the only possible long distance WPT method for underwater application.

Two of the leading companies in the development of technology for OWPT applications are Powerlight Technologies and Wi-charge. In 2009, Powerlight Technologies (formerly known as Lasermotive) received $900,000 fund from NASA by becoming the champion in NASA space elevator challenge [183-185]. Since then, Powerlight Technologies has achieved 400 W power transmission using laser for 1 km distance which is the world record for the longest highest-power transmission up to date [185]. Besides the laser power transmission through free space, Powerlight Technologies also have concern in replacing copper wire with power over fiber power transmission.

If the focus of Powerlight Technologies is large scale OPWT system, Wi-charge's focus is to develop OWPT system which is safe for human and can be applied to charge mobile devices and home appliances such as smartphones, smart speaker and other home appliances. Wi-charge claimed that its system uses eye safe laser and can charge several electronics devices at the same time in an indoor environment [186-187].

3.9 Safety Issue of OWPT

The main issue in the development of OWPT system is the safety problem. It is well known that high power laser might be hazardous for human's eyes and skin. In order to better understand the hazard of laser radiation, it is better to look at the Maximum Permissible Exposure (MPE) for eyes and skin of laser based on its wavelength as can be seen from Figure 3.25 and Figure 3.26, respectively [188-190]. MPE describes maximum amount of optical energy which is still tolerable for human's skin or eyes and can be considered to be safe. Wavelength with higher MPE means that it is less harmful than wavelength with lower MPE value. The values of MPE in these figures are calculated for single burst of CW light. The MPE for eyes is calculated for 0.25 s (blink reflex time) and 1 s. For the MPE of skin, the MPE for 1 minute exposure of light is also calculated [188].

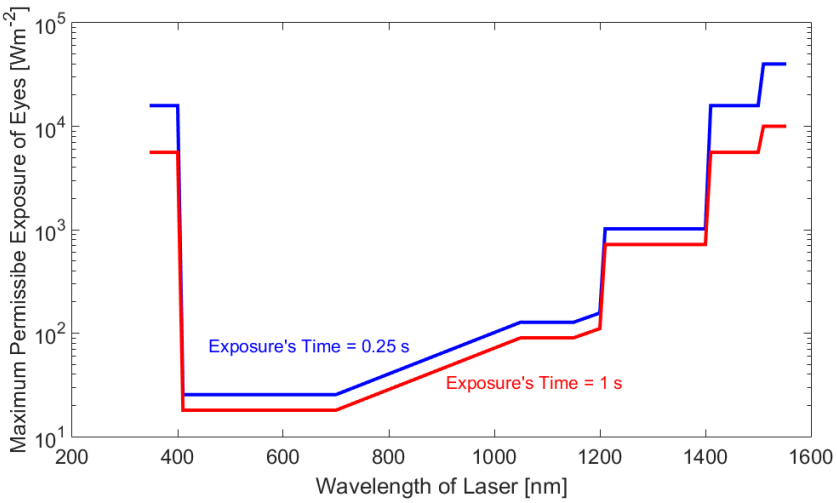

Figure 3. 25 Maximum permissible exposure of human's eyes.

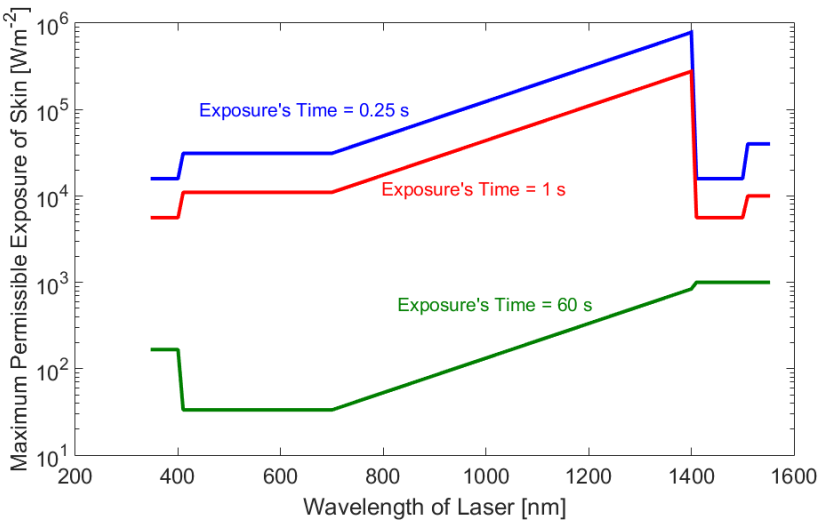

Figure 3. 26 Maximum permissible exposure of skin.

To understand the value of MPE in Figure 3.25 and 3.26, let us analyze this value by calculating the example. The value of MPE of eyes for 0.25 s of visible light is 25.46 W/m^2. By assumption that the light source is laser with the area of beam is 1 cm^2, it means that the maximum power of light which is harmless is around 2.5 mW. On the other hand, MPE of longer wavelength, for example, 1550 nm is 40000W/m^2, hence, theoretically, it is still safe to use 4 W laser with area 1 cm^2. From this result of calculation, it can be concluded that infrared light such as 1550 nm of light is less hazardous for human's skin and eyes than visible light. For comparison, the average solar irradiance on earth's surface is 1000 W/m^2. This value of solar irradiance is somehow higher than some values of MPE for several wavelengths, however, since the spectrum of sunlight is very wide, it is less harmful than light from laser which has very narrow spectrum.

Then, based on its power and wavelength, laser can be classified into several classes:

- Class 1: The laser in this class is safe to be used for normal use, it means that the maximum output power of this class of laser is much lower than MPE for human's eyes and skin. When operating this laser, there is no need to wear protective glass. One of the examples of this laser is the laser diode for optical disc drives.

- Class 1M: Lasers in this class are still safety for normal use without wearing any protective glass, however, there is potential hazard if the laser is focused using magnifying instruments such as lenses, microscope or magnifying glass.
- Class 2: This class is limited to visible wavelength of laser (400-700 nm). This class of laser is still assumed to be due to the blinking reflex of human's eyes (0.25 second). In other words, this type of laser is still safe for direct exposure less than 0.25 second. Laser diode for laser pointer is categorized in this class. The maximum output power of this lasers is 1 mW in continuous wave (CW) operation.
- Class 2M: Similar with class 1M, this class of laser is similar with class 2 laser, however, there is potential hazard if the laser is focused using magnifying instruments.
- Class 3R: This type of laser is still considered to be safe if being handled carefully. Direct exposure and intrabeam viewing are still possible, however, the output power and beam size have to be carefully considered. The maximum output power for continuous wave visible light lasers in this type is 5 mW.
- Class 3B: Lasers in this class are assumed to be hazardous for direct exposure. However, the light from this type of lasers cannot diffuse completely through paper or matte, hence, exposure to the light which has passed through paper is still considered to be safe. Exposure to the reflected light from this laser might be safe. This type of lasers is usually equipped with lock and key. Protective eyewear has to be worn when operating this type of lasers.
- Class 4: Lasers in this class is hazardous for direct or reflected exposure. Protective eyewear is a must when operating this type of lasers. Class 4 laser can cause harm to skin and the damage of direct exposure to human's eyes is permanent and devastating. This type of lasers can also burn some materials; hence, it has to be handled carefully.

Class 4 laser is the most dangerous type of lasers. The long infrared wavelength of light such as emission of CO2 laser ($\lambda = 10500$ nm) from this type of lasers can be absorbed highly by the water in human's tissue, hence, it can vaporize the water and burn the cornea of the eyes. The near infrared wavelength of lasers such as Ho:YAG ($\lambda = 2000$ nm) and EDFL ($\lambda = 1550$ nm)

will cause burn damage to cornea and lens of human's eye because this wavelength of laser will be partially absorbed and partially transmitted by the water in eye's tissue. The visible light laser of Class 4 will be transmitted through the water in the tissue and cause permanent damage to retina in the eye's [188]. Note that, even though 1550 nm of laser is called "eye safe wavelength", in case of high power Class 4 laser which operates in much higher power than MPE, it is still not safe for eyes. Nevertheless, since MPE for 1550 nm is much higher than MPE of visible light laser (400 – 700 nm), 1550 nm laser has attracted interest to be used as light source to deliver considerably high power under MPE level in OWPT system [191-193].

In OWPT, unfortunately, high power laser which is Class 4 lasers are used as the light source in most of the system. Hence, it has to be handled very carefully and protective eyewear has to be worn during the demonstration. Wi-Charge claims that in their system, they are using eye safe class 1 infrared laser as the light source [187]. However, since class 1 laser has very low output power, it has to be amplified to deliver enough power for electronic appliances, in this case, free space outer gain medium and retrodirective mirrors are needed to create external cavity laser. The details of this method will be explained in Chapter 4.

The other attempt for designing safety measure in indoor OWPT system is by using light curtain. T.J. Nugent, Jr. et.al from Powerlight Technologies proposed and designed light curtain system which consists of LED and photodetector which is arranged in ring shape which enclose the laser beam which is used to transmit power. If there is any obstacle which disturbs the LED light, the system will automatically shut the high power laser beam [194].

In ref. [195], an optical ring guard for safety measure in OWPT system to transmit power to charge smartphone in across room is proposed and designed. In this design, retroreflector is put at the receiver and LED or light source which is used to create a ring guard which enclose the high power laser beam is proposed. The light source from the ring guard will be reflected back by the retroreflector which is placed around the solar cell at the receiver, then the reflected light will be detected by photodetector at the receiver. If there is any obstacle between transmitter and receiver, the reflected light of the ring guard will be disturbed and not detected by the photodetector at the transmitter, then, the high-power laser will be cut. The system can be seen from Figure 3.27.

Due to its small beam size and high power density, high power laser which is used in OWPT might be harmful for human. Hence, special mechanism, to recognize the target receiver and steer the beam to only hit exactly at the target becomes important element in OWPT. In chapter 4, some target recognition and beam steering methods are described.

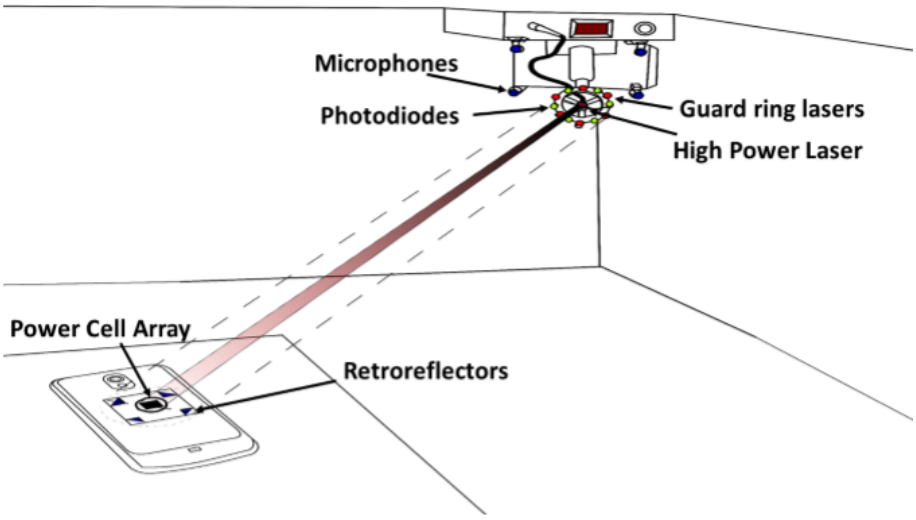

Figure 3. 27 Optical guard ring and retroreflector for safe indoor OWPT system [195].

CHAPTER 4

LASER BEAM STEERING AND TARGET RECOGNITION METHODS FOR OWPT

Laser beam has very small beam diameter. In this case, the laser beam is needed to be steered in order to point directly and only to the target. Since the lasers which are used in most of OWPT systems are high power laser, this laser steering system becomes critical in OWPT system to prevent hazardous effect which happens if the laser illuminates unintended object such as flammable materials, human skin and eyes.

The systems of free space optical (FSO) communication and OWPT are almost similar because in both cases, the laser propagates in free space (not in optical fiber). Hence, some of the beam steering methods from free space optical communication system are adopted for OWPT system. However, lasers which are used in OWPT and free space communication system might be different in terms of power. Due to different purpose of the systems, it is not necessary to use high power laser in free space communication system, on the other hand, in OWPT system, high power laser is needed to transmit power. Some methods which are unique to OWPT system have also been demonstrated.

In this chapter, some of the methods for beam steering in free space communication system those could be used for OWPT systems are discussed. Some beam steering methods which are unique to OWPT system are also discussed.

4.1 Direct Steering Using Gimbal Based Method

A gimbal is a mechanical rotary platform which is controlled by motors [196]. A high-power laser can be mounted on the gimbal and then the laser beam will be steered by the motors. A gimbal can be used to provide beam steering to two or three-axis, depends on the moving capability of gimbal. Gimbals have coarse beam pointing angle due to its large step mechanical movement from the motors. The gimbals which are available in the marker have pointing resolution in µrad region, on the other hand, the mirror-based beam pointing method can be used to steer the beam with resolution in sub-µrad region. The other limitation of gimbal-based beam steering is the reaction time of the gimbal which is limited by the performance of motors. Direct mounted gimbal-based beam steering is typically slower than mirror-based system.

To increase the capability of gimbal in terms of laser pointing resolution, Fast Steering Mirror (FSM) can be mounted on the gimbals which will provide fine steering of the laser beam, the image of this system can be seen from Figure 4.1. The FSM on gimbal will improve the pointing resolution of gimbal, however, the amount of power which can be transmitted in OWPT system will be limited by the damage threshold of the FSM. On the other hand, by directly mounting high-power laser on top of rotating gimbals, it is possible to transmit high optical power in OWPT system.

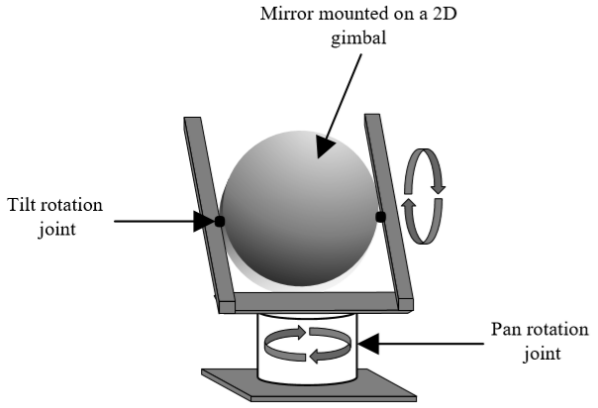

Figure 4. 1 Diagram of FSM mounted on 2D gimbal [196].

Gimbal based beam steering method for FSO communication system has been demonstrated in ref. [157]. Japan Aerospace Exploration Agency (JAXA) proposed space to ground OWPT system, the proposed system can be seen from Figure 4.2. Pilot laser beam from ground to the space unit is used to control the position and beam steering direction angle. This target method is called mutual laser link system and provide two ways communication between the ground and space unit. In this project, electric energy is harvested by the space unit using the solar panel, then the electric power is sent to ground unit on earth using high power fiber laser. The beam steering method which is used for the space unit is gimbal based with the target laser pointing resolution is 1µrad. The gimbal-based beam steering system at the Low Earth Orbit (LEO) satellite unit provides the laser steering capability for two axis steering. The laser which was used in this proposal is Yb-based fiber solid state laser (1.067 µm wavelength) with output power approximately 500 W for LEO satellite unit. As of 2014, this project was still under test and conceptual study [157].

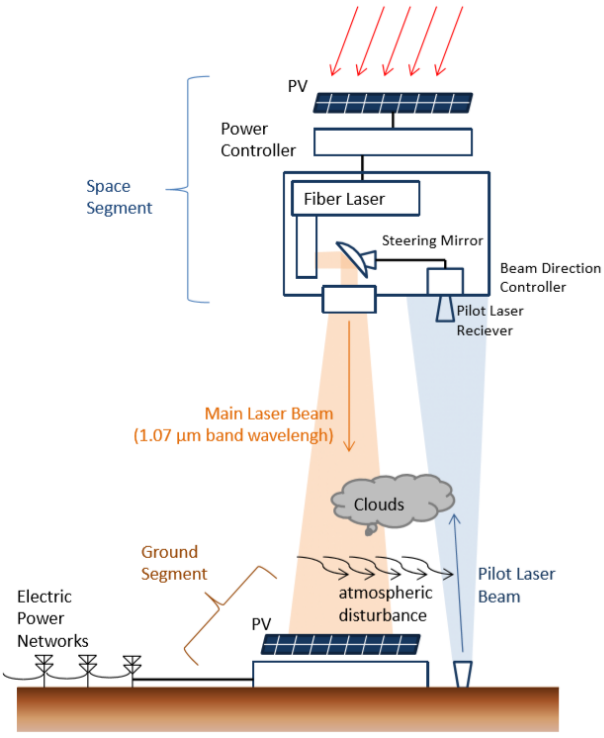

Figure 4. 2 JAXA's concept of space to ground OWPT system [157].

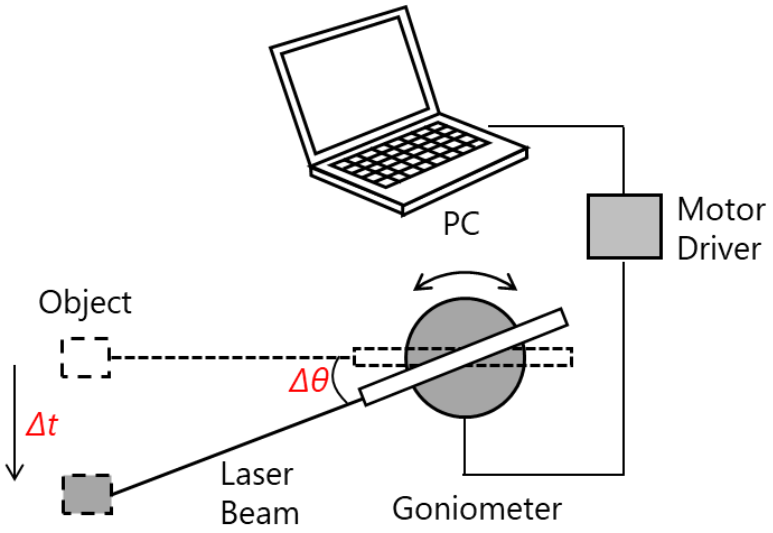

Figure 4. 3 Laser beam steering using goniometer [197].

The other direct steering method with gimbal based beam steering for OWPT can be seen from ref. [197]. The diagram of this experiment can be seen from Figure 4.3. In this experiment, goniometer which provide laser beam steering in one axis was used. This method has very coarse laser pointing resolution which was 100 µrad and the reaction time of the goniometer was slow, which was 0.78 s.

4.2 Mirror Based Method

In mirror based beam steering system, FSM is usually used to deflect the laser beam to point at the intended target or receiver. Mirror based beam steering system is usually less heavy than gimbal, hence, it can be used to provide high speed laser beam steering and high precision with pointing resolution can be less than 1 µrad. The mirror-based beam steering system in FSO is usually used for high speed applications such as for FSO communication link between high speed trains [198-200].

In OWPT system, mirror-based beam steering methods have been performed in many cases especially for moving target [161,162, 201-203]. The mirror-based beam steering system provides simple system which does not need very precision alignment between transmitter and receiver, hence, it can be used to transmit power to moving target. The other advantage of mirror-based system is its smaller dimension; hence, the system can be more compact than gimbal-based system and most of the other methods.

One of the earliest demonstrations of mirror-based laser beam steering in OWPT is in 1999 by J. T. Kare et.al. [201]. In this experiment, two gold coated mirrors were used to deflect the laser beam to the receiver. One of the gold coated mirrors was a curved mirror which was used to focus the laser beam. The other one was a flat mirror which was used to steer the beam as can be seen from Figure 4.4.

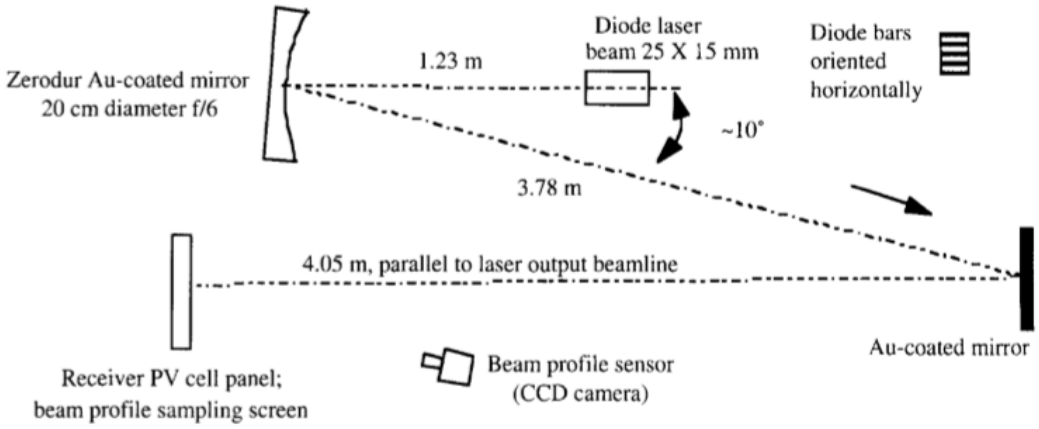

Figure 4. 4 Earlier report of OWPT system using gold coated mirrors [201].

In 2005, T. Blackwell from Alabama University demonstrated OWPT for small aircraft using mirror as the beam steering method [202]. The mirror in this demonstration was 8-inch mirror that could be steered to 2-axis. This mirror was dielectric mirror which was coated with Aluminum. This mirror was used to deflect the laser beam to a small specifically designed aircraft. The beam tracking method and target recognition in this system was still manual tracking and recognition which meant that an operator had to operate and control the mirror manually to follow a moving target.

The other mirror-based beam steering demonstration was demonstration by Powerlight Technologies (Formerly known as Lasermotive) in 2010. The concept of this system can be seen from Figure 4.5. In this case, mirror or direct steering using gimbal were used as the beam steering method for OWPT to UAV [161]. The UAV in this system was cooperative target which meant that the target's route and flying pattern was known by the beam director beforehand or the communication link between the beam director and UAV was assumed to be maintained well, hence, the laser beam steering and tracking of target in this system was simple. In accordance with this demonstration, compact UAV had been developed in 2011 [162]. This compact UAV did not need very high capacity battery because the power which is used to supply the UAV is provided by laser on the ground.

In 2015, several individually controlled mirrors are used to combine several laser beams in OWPT system using several non-coherent lasers [203]. Each of the mirrors is individually controlled, in the other words, the steering angle of each mirrors was not similar. The main purpose of this system was to focus the laser beam from several sources at the receiver as can be seen from Figure 4.6.

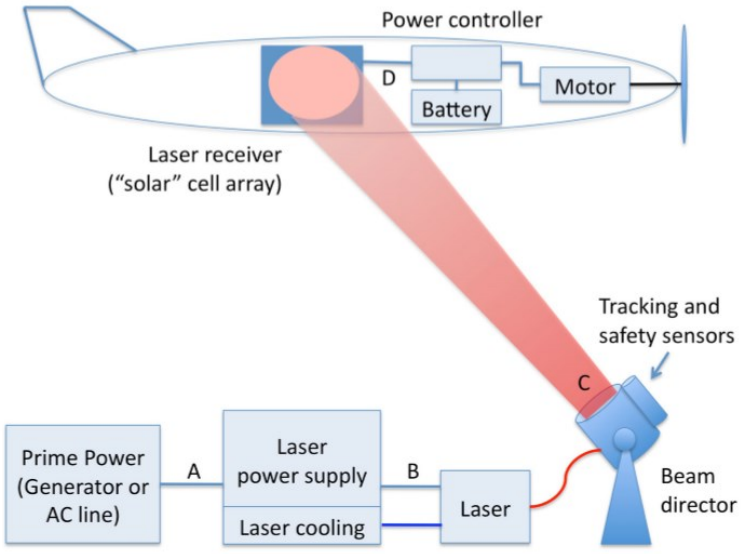

Figure 4. 5 OWPT system to UAV based on concept from Powerlight Technologies [161]

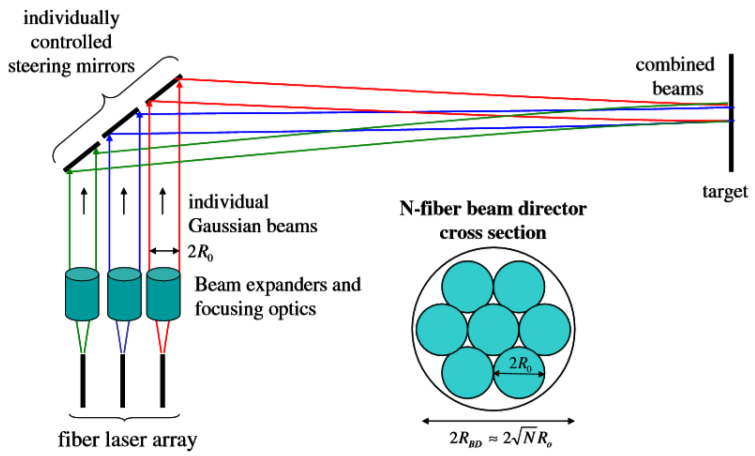

Figure 4. 6 Individually controlled mirrors for beam combiner of non-coherent light sources [203].

In the research in this dissertation, OWPT system using mirror which is electrically driven (Galvano mirror) is used as the laser beam steering system because the capability of the mirror to steer the beam to follow a high moving target and its reaction time which is much higher than goniometer. As the target recognition method, camera is used to recognize the target. Special image processing software which is called Computer Vision (OpenCV) is used to recognize the target. The details of this method will be explained in Chapter 5.

The target recognition using camera and beam steering method using mirror for FSO communication has also been demonstrated in ref. [204]. In this research, simple pattern is used as the landmark for target. This landmark (marker) is detected by camera using special pattern recognition method. This marker is put above the detector. Then infrared laser which is used for FSO is directed by micro-electro-mechanical mirror (MEMs). The mirror which was used in this system had $\pm 10^0$ of mechanical angle. In this research, it was reported that the time which is needed by the camera to capture and process the image was longer than the reaction time of the mirror. The system can be seen from Figure 4.7.

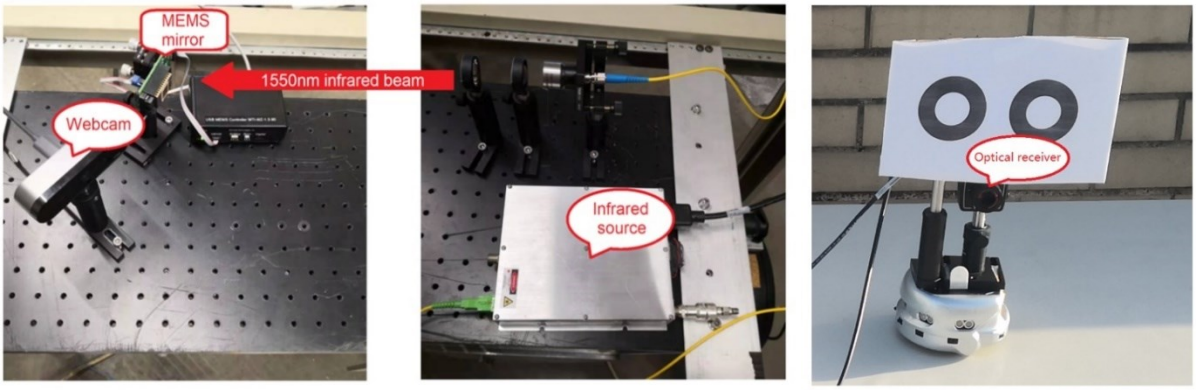

(a) (b)

Figure 4.7 FSO Communication system using mirror and camera: (a) Transmitter and (b) Receiver [204].

4.3 Liquid Lens Based Beam Steering

Liquid lens-based beam steering system uses non mechanical and can provide fine beam steering capability. Liquid lens is a device which consists of a one-dimensional array of tens of thousands of long thin electrodes which can be used to manipulate the phase of light which passes through it. The refractive index of the liquid lens can be manipulated by applying voltage to the liquid lens; hence, the focus of the lens can also be controlled by this method. Because of the change of focus of the lens, the beam can be steered to intended angle. The main disadvantage of this method is due to small size of the liquid lens, the angular motion and maximum steering angle are also limited. The process of beam deflection by liquid lens can be seen from Figure 4.8.

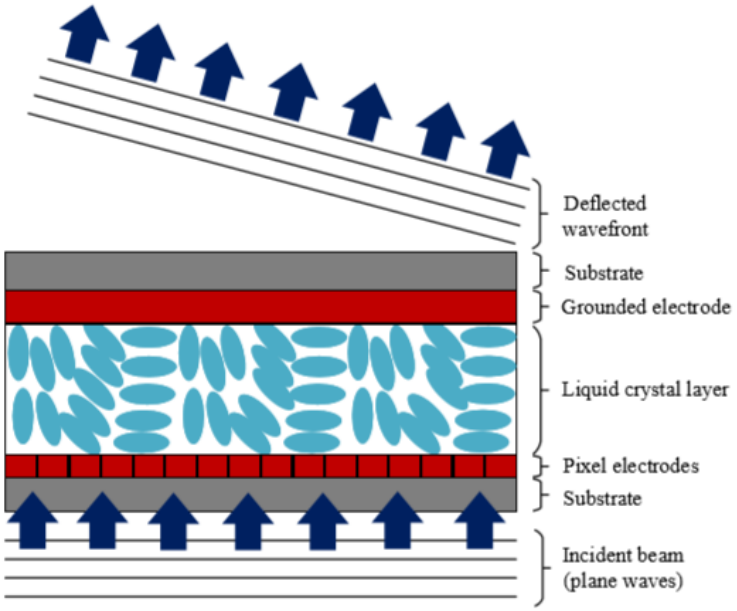

Figure 4. 8 Illustration of laser deflection by liquid lens [198].

Liquid lens for beam steering in OWPT system has been demonstrated in ref. [205]. In this demonstration, 975 nm wavelength of high power VCSEL with output power 6.3 W was used as the light source. Liquid lens from Optotune with aperture 1.6 cm was used to steer the beam. Based on the results of this demonstration, the maximum output electrical power which could be harvested by the solar cell was 450 mW. If the conversion efficiency of the solar cell was assumed to be 30%, then there was loss more than 50% between the transmitter and receiver. Hence, there was possibility that there was high loss due to the liquid lens. This loss might be cause by the localized inconsistency of the elements in liquid lens, hence, there was small and local area in the liquid lens with different refractive index than the other are, this condition caused the scattering.

4.4 Retroreflector at Receiver Method

This method of beam steering and target recognition is mainly developed by Kawashima et.al. [159] from Kinki University, Japan. In this method, it is assumed that the beam size is similar

or larger than the size of solar cell. In the center of solar cell, retroreflective mirror is attached. If high power laser with similar size or larger size with the solar cell hit the solar cell, the retroreflective mirror will reflect back some part of the optical light to the transmitter. At the transmitter, 4-elements photodiode is used to detect this reflected light. If the laser beam and the target is in line with each other, the reflected light from the retrodirective mirror at the receiver will be located at the center of 4-element photodiode. Then if the target moves, the reflected light may not be at the center of the 4-element photodiode. At this point, the laser steering system, which is direct steering in this case, will direct the beam based on the mismatch between the position of reflected beam which is detected by 4-element photodiode and center of 4-element photodiode. This method had been implemented to send power to small aircraft as can be seen from Figure 4.9. Similar method had also been used for FSO communication system with UAV [198].

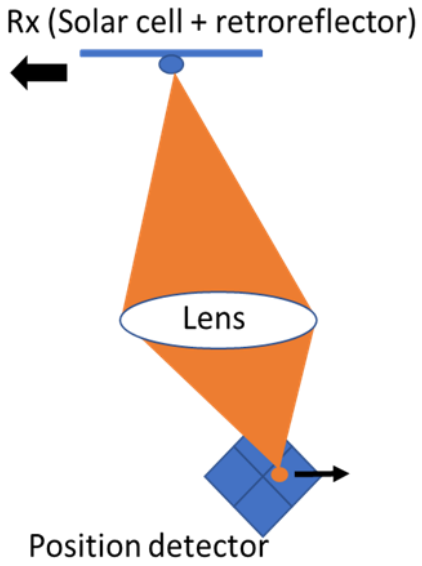

Figure 4. 9 Illustration of OWPT system to small aircraft. A retroreflector is attached on the center of the solar cell panel at the receiver [159].

4.5 Retrodirective and External Cavity Laser Methods

This method is unique to OWPT system and hybrid OWPT and FSO system. However, this method is not usually used in FSO communication system. The main idea of this method is creating an external cavity laser by using mirrors and free space gain medium in between the mirrors. There are at least two techniques which can be included in this method.

The first technique was proposed in 2007 by C.A. Schafer et.al. [206]. In this system, the receiver was equipped with laser to emit coherent pilot signal light. This signal light will be emitted to the transmitter. At the transmitter, the pilot signal light will be collected by 4 identical optical systems. This collected light will be transmitted to a series of non-linear crystals which are located in the middle of 4 different optical resonator as can be seen from Figure 4.10. The phase conjugate spherical mirrors in Figure 4.10 were photorefractive crystals which would first scatter and then transmit the light into the laser cavity. The light would be amplified in the laser cavity by the gain medium and the non-linear crystals with gain medium in the laser cavity. Then the amplified light would be transmitted back to the receiver. This method is complicated because it used non-linear crystals and required non-linear effect in the process for beam steering and amplification. Note that the laser cavity in this system was external cavity laser.

The second technique is called distributed wireless charging [186-187, 207-208]. This method was first popularized by wi-charge. In this technique, a gain medium is put in the middle of two retroreflective mirrors to create an external cavity laser as can be seen from Figure 4.11. The back retroreflective mirror is put at the transmitter and front (output) retroreflective mirror is put at the receiver. The reflectivity of the mirror at the transmitter is 100%, on the other hand, the reflectivity of mirror at the receiver is 95%. The gain medium is put the transmitter. This technique attempts to create long distance external cavity laser.

In this case, the laser beam will be reflected back and forth at the retroreflective mirrors and pass through the gain medium several times. Using this method, wi-charge claims that its system uses class 1 laser at eye-safe wavelength (1550 nm). This class 1 laser will be amplified in external laser cavity created by the retroreflective mirrors and free space gain medium in between

them until its power is enough for charging the electronic devices and if there is any obstacle, in the middle of the laser cavity, which disturbs the laser oscillation, the amplification of the optical beam will stop and power of laser will immediately drops to the class 1 laser power again. The main disadvantage of this system is it requires perfect alignment between the transmitter and receiver to create an external laser cavity. If either the transmitter or receiver is tilted, there is possibility that the laser oscillation cannot be achieved.

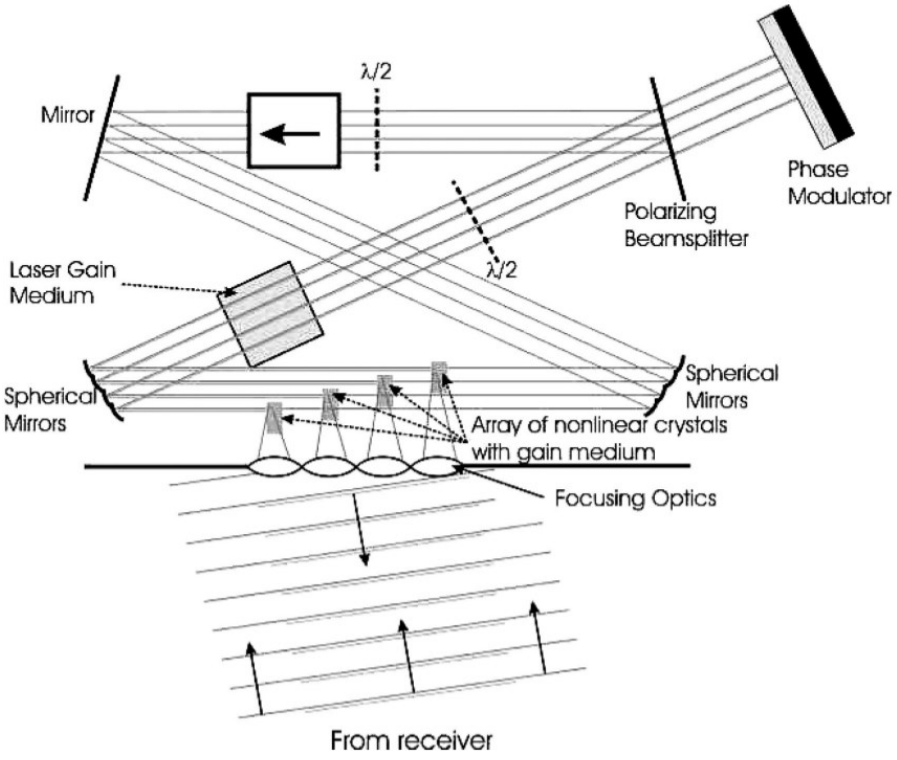

Figure 4. 10 Optical retrodirective technique using phase conjugators array [206].

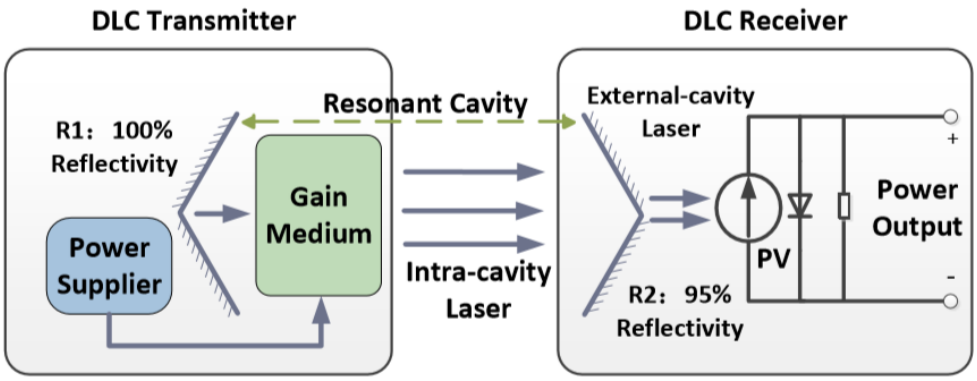

Figure 4. 11 Distributed laser charging technique [207-208].

4.6 Automatic Beamforming and RF method

In this method, the source of light was assumed to be a white LED light. A spatial Light Modulator (SLM) was attached at the LED light as can be seen from Figure 4.12. An SLM is a device that can change every pixel of space of light that passes through it. It will modulate the amplitude and phase of the light spatially and can be controlled using electric signal. The SLM that was attached at the white LED light source will beamform the white LED [209].

The location detection of the target can be performed as follows: the full possible range of beamformed light by SLM was divided into several coded area based on the angle of the beamformed light. This code was modulated to the beamformed light and the code was shared between the transmitter and receiver. If the receiver received the beamformed light which is modulated with the coded area, which gives information about the angle of light from the transmitter, it would send signal to the transmitter using RF signal. When the transmitter received the RF signal, it would focus all the light according to the angle which was responded by the receiver, then the power transmission was begun. The resolution of laser beam pointing depends on the division of the full range of the beamformed light and the beam size. Hence, the light source which was usually used in this technique was large beam source which could be LED or laser with

beam expander. One more disadvantage of this system is the complexity of the system since it needs RF communication systems between transmitter and receiver.

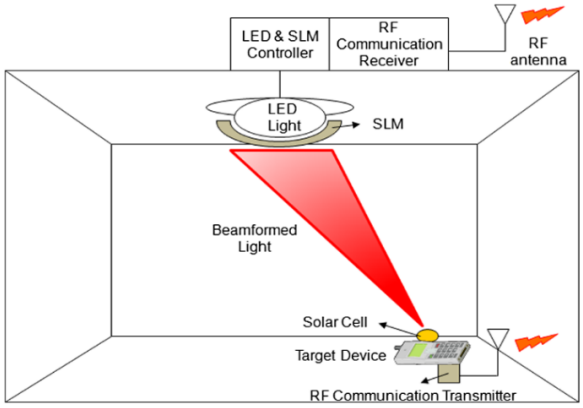

Figure 4. 12 Automatic beamforming method [209].

4.7 Summary

Table 4. 1 Summary of characteristics of beam steering methods.

Methods	Pros.	Cons
Gimbal Based	Simple system, possible for 2D and 3D laser tracking and steering, possibility of unlimited power transmission (direct mounted).	Coarse laser pointing resolution, slow reaction, large and heavier than other methods.
Mirror Based	Simple system, high speed, possible for 2D laser tracking and steering	Maximum optical power is limited by damage threshold of the mirror
Liquid lens	High speed, compact system	Steering angle is limited by its size, hence, it is not as wide as mirror based.
Retroreflector and 4-elements photodiode	Possibility to be used for long distance OWPT, can be used for moving target	Heavy and big system, target has to be captured to begin the OWPT, speed is dependent to the motors (possibly slow)
Retrodirective and External Cavity Laser	Possibility for safe OWPT,	Complicated system, cost is possibly high, perfect alignment is needed, not suitable for moving object
Automatic Beamforming and RF Method	Harmless for human, automatic targeting, possible for moving target	Complicated system, accuracy depends on the division of coded area.

CHAPTER 5

OPTICAL WIRELESS POWER TRANSMISSION SYSTEM TO MOVING TARGET

As explained in Chapter 3, Optical Wireless Power Transmission (OWPT) has many advantages compared to other WPT methods especially in terms of its capability to transmit high power density to longest distance than other WPT methods, thanks to the characteristics of laser beam which is the transmitter in OWPT system. The laser beam has small divergence angle; hence, the size of the beam will be smaller than microwave over the transmission distance. In this case, the laser beam needs to be steered to point directly at the receiver. In Chapter 4, some methods for beam steering and target recognition have been discussed.

Based on the characteristics of each method, in this research, OWPT system is developed and the performance of the system is analyzed. The mirror and camera method as the beam steering and target recognition method is chosen. The main reasons for choosing this method is the simplicity of the system where there is no need to put such complicated equipment at the target and the capability of mirror to follow a fast-moving target.

In this chapter, the design and performance of OWPT system to moving target is analyzed. Firstly, the basic system and its operation is discussed, then, the characteristics of each components are analyzed and discussed. Next, the OWPT to 1-dimensional moving target, 2-dimensional moving target and multiple targets are demonstrated. Lastly, the recognition method of the system is improved and the system efficiency of the developed OWPT system are discussed.

5.1 Components of OWPT System

5.1.1 Camera and Object Recognition Software

In the OWPT system to moving target, which was developed in this research, web camera was used as an instrument to recognize the target. The web camera was Elecom UCAM-DLI500TNBK. The picture of the camera can be seen from Figure 5.1. This we camera can capture picture with 5 million pixels which corresponds to a maximum of 2592 x 1944 pixel exceeding full high definition (HD). This camera is equipped with ¼ inch CMOS sensor. For video recording, the maximum frame rate of this web camera for YUY2 video encoding file format at 640 x 480 pixel, 1920 x 1080 pixel, and 2592 x 1944 pixel are 30 fps, 7.5 fps, and 2.5 fps, respectively. The viewing angle of this web camera is 54° diagonally. In this research, this web camera is used to capture the image of the target to determine its position. The target can move; hence, higher framerate is better in this application.

Figure 5. 1 Picture of Elecom UCAM-DLI500TNBK web camera.

Camera, as it is, is not enough to recognize which object in the captured image which is intended to be used as the target. Hence, special image processing software was used to recognize the target. This image processing software is called OpenCV. OpenCV is an open source cross platform computer vision program. As a computer vision software, the main purpose of OpenCV is to provide the capability to computer to gain high level understanding of image and video. In

other words, it is a machine learning and image processing software which allows the computer to acquire data, process and analyze digital image which is captured by the camera [210]. As a cross-platform software, it has C++, Java, Python and MATLAB interfaces. In this research, OpenCV program was written in Python programming language.

There are several methods for object recognition using OpenCV. The object recognition methods in OpenCV can be categorized into shape recognition and color recognition (color segmentation). In this system, the main target is to recognize moving target. When the target is moving, there is possibility that the size and shape of the target which is recognized by the camera will slightly changes, on the other hand, the color of the object which is recognized by the camera will not change despite its movement and speed. Based on this consideration, color segmentation method was chosen as the target recognition method in this OWPT system.

The target recognition process using color segmentation method can be explained as follow: First, the color which will be recognized as the target is chosen. The software then creates a mask based on the chosen color. The mask will be applied to the image which is captured by the camera. This mask will filter out the other color beside the chosen color, hence, in the masked picture, only the object which has the same color with the chosen color will be captured by the camera. Then, if there are several objects which have similar color as the chosen color, the software will measure the size of each object and object which has the largest size is recognized as the target. To utilize this method in our OWPT system, a color marker was put on the target which is a solar cell on top a mini car as can be seen from Figure 5.2(a). The masked image of this mini car can be seen from Figure 5.2(b). In this case, red color which was matched with the color of the marker was chosen as the target, hence, only red color was recognized by the camera. Note the circle which encircled the marker is called recognition circle. If this circle appears, it means that the target is successfully recognized by the computer.

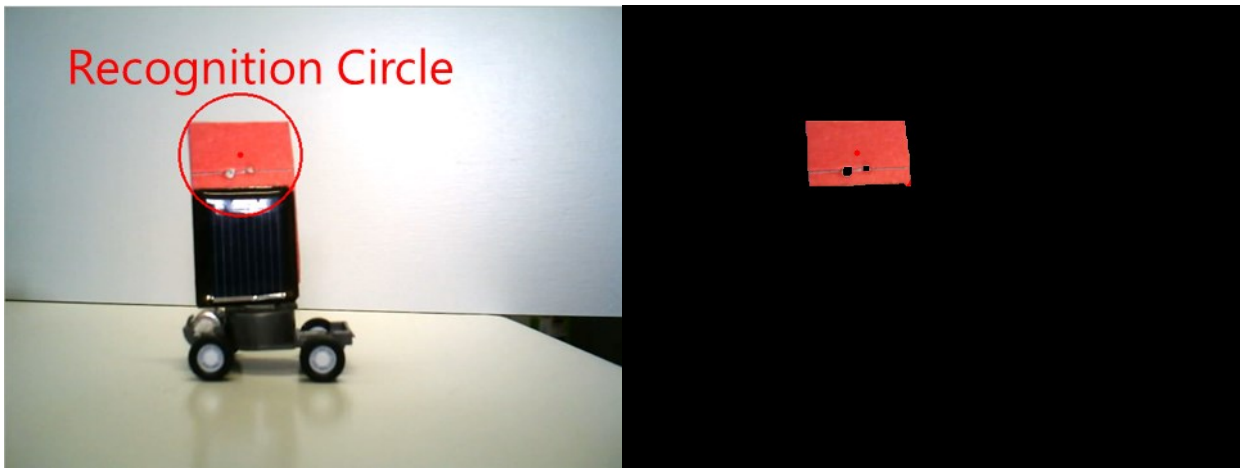

(a) (b)

Figure 5. 2 Captured image by camera: (a) Real image and (b) Color segmentation masked image.

5.1.2 Galvano Mirror

As the beam steering technology Galvano mirror was adopted. A Galvano mirror is an electromechanical instrument which can be used to deflect the light and can be controlled by inputting current or voltage. Thorlabs GVS002 2-Dimensional Galvano mirror was used in this research. This set of mirrors consist of x-axis and y-axis mirror which can be used to deflect the laser beam to a and y-axis direction respectively [211]. The mirror is coated with Silver (Ag) and the reflectively is around 100% for 500 nm to 2µm wavelength of light. The picture of this mirror set can be seen from Figure 5.3. The mirrors are driven by two servos for x and y-axis mirrors. The mirror can scan with optical angle $\pm 25^0$ which translates to ± 12.5 of mechanical angle. The response time of the mirror was measured to be 3 ms which is the time needed by mirror to scan from -12.5^0 to $+12.5^0$ of the mechanical angle. A digital to analog converter (DAC) was used to control the voltage which was supplied to the Galvano mirror.

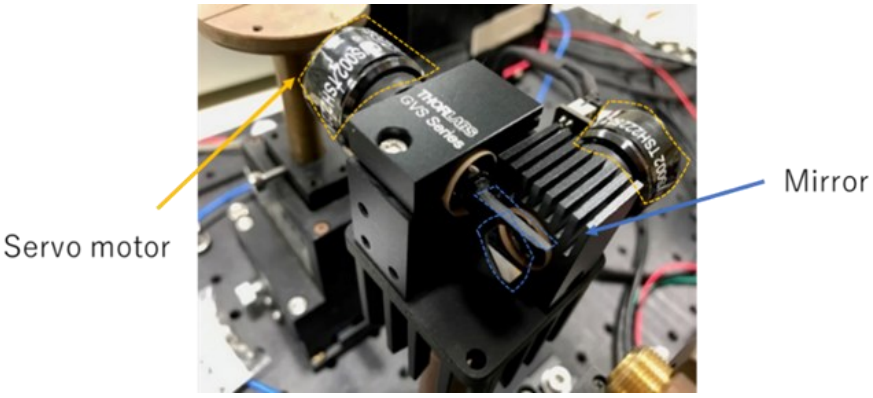

Figure 5. 3 Picture of galvano mirror set.

5.1.3 Laser

LSR980H was used as the light source in this research. The wavelength of the output light of this laser is 980 nm and maximum output optical power is 6 Watts. 980 nm wavelength of light was chosen as the light source in this research because Silicon (Si) solar cell was used as the receiver. As can be seen from Chapter 3, the conversion efficiency of Si solar cell reaches its maximum at near infrared region around 900 nm of wavelength of input light. This laser is diode laser, hence, it is electrically driven with DC current. The DC current is supplied using power supply that can be controlled. The picture of the laser and its power supply can be seen from Figure 5.4. The laser is Class 4 high power laser and equipped with key and lock. The output optical characteristics with respect to its driving current can also be seen from Figure 5.5. The threshold current of the laser was measured to be 450 mA and from the trendline, the slope efficiency of the laser was calculated as 0.59 mW/mA.

Figure 5. 4 Picture of laser module and power supply.

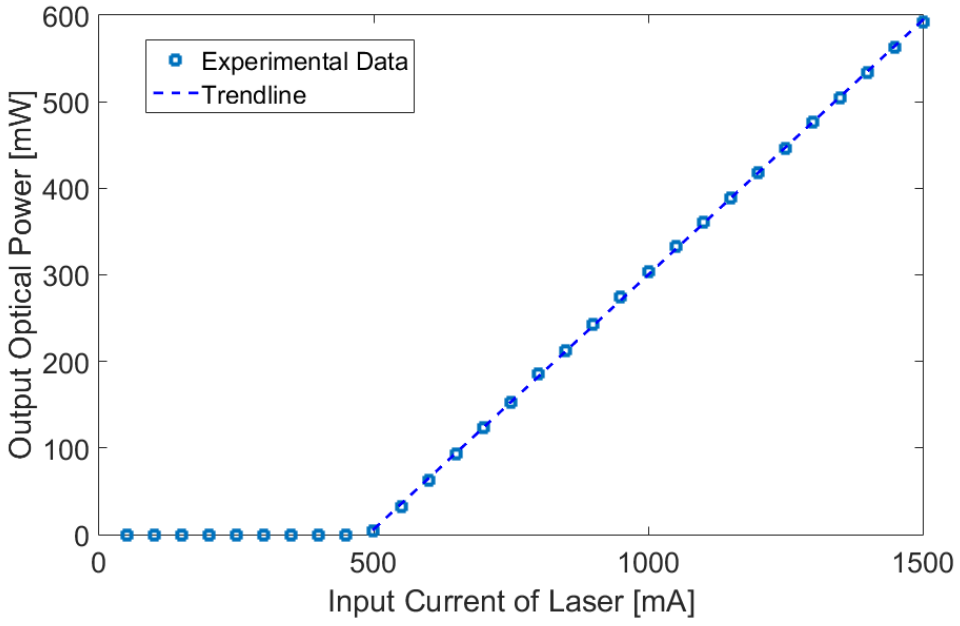

Figure 5. 5 Measured L-I characteristics of laser.

5.1.4 Solar Cell

The solar cell which was used in this research was Si solar cell which was mounted on a movable object as can be seen from Figure 5.2(a). The size of the solar cell was 2.2 cm x 2 cm. The IV characteristics of solar cell under 150 mW illumination by 980 nm laser can be seen from Figure 5.6. The distance between laser and solar cell in this measurement was 5 cm. At this distance, all of the output optical power can be assumed to be received well by the solar cell since the size of the beam can be assumed to be very small compared with the solar cell. The maximum electric power was measured to be 33 mW and the short circuit current and open circuit voltage were 100 A and 0.58 V, respectively. From these parameters, the Fill Factor (FF) of this solar cell could be calculated as 0.57. Maximum power conversion efficiency (PCE) of the solar cell was measured to be 22%.

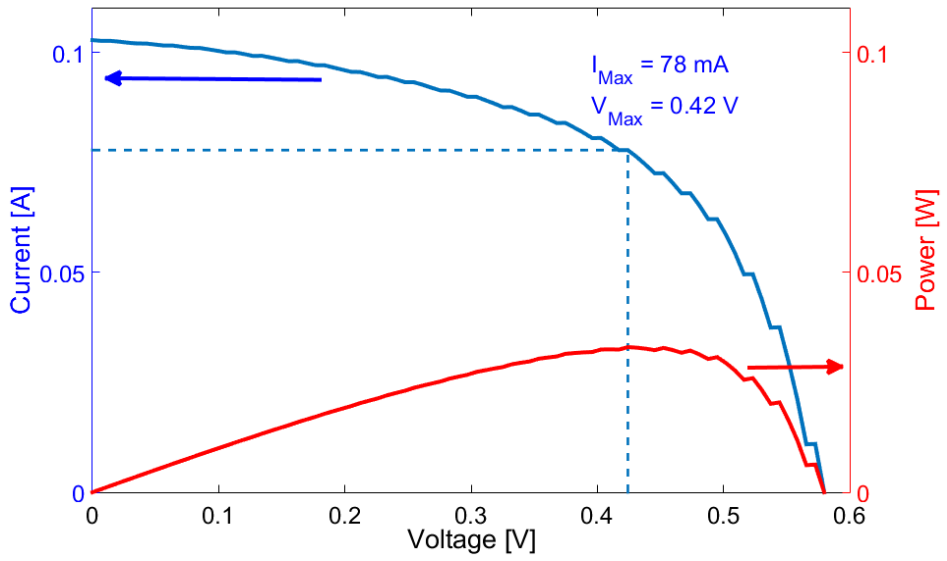

Figure 5. 6 Measured IV characteristics of solar cell.

5.2 OWPT System to 1-Dimensional Moving Target

5.2.1 Basic System of Target Recognition and Beam Steering System

Basic diagram of OWPT system to 1-dimensional moving target can be seen from figure 5.7. Target recognition and beam steering processes can be described as follow:

1. Web camera recognizes the moving target.

2. Camera sends the pixel position of target to computer.

3. Computer calculates the movement of target by calculating difference of the pixel positions of target and converts it to driving angle.

4. Computer sends the command to the drivers to drive the Galvano mirror according to the calculated angle.

5. Mirror steers the laser beam to the target.

The camera which is an ordinary web camera was set to capture image with 30 fps frame rate. Size of the captured image was 640 x 480 pixels. As the light source, 980 nm laser was used because based on theoretical analysis, infrared laser is the most suitable for OWPT through air. Small toy car was chosen as the target as can be seen from Figure 5.2(a). Si solar cell was put on top of the target to convert incoming laser beam to electric power which is used to power the mini car up. The mini car was not equipped with battery; hence, it could only move if it received enough electric power from solar cell.

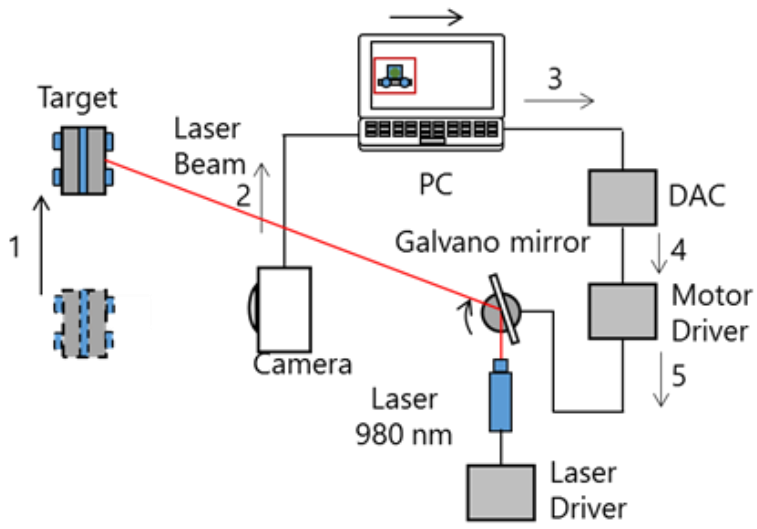

Figure 5. 7 OWPT system using camera and galvano mirror.

5.2.2 Beam Position Mismatch Problem and Solution

By using color segmentation method to recognize the target and Galvano mirror, laser beam could be steered to follow the moving target. However, when the target was moving, we found that there was position mismatch between the beam and the center of recognized moving target which was detected by the camera as illustrated from Figure 5.8. Note that, in this illustration, green laser pointer was used instead of infrared laser to emphasize the problem and to increase the visibility of laser in the image. This problem only occurred when the target was moving [212].

The position mismatch was calculated as error angle which was described as the angular difference of position between beam and center of target. This position mismatch between beam and target was proportional to the velocity of the target as can be seen from Figure 5.9. The error angle in Figure 5.9 was calculated when the distance between camera and target was fixed at 60 cm and the target velocity was from 5 to 55 ^{0}/s. Negative value of error angle indicated that the beam was directed behind the target which mean that the beam direction could not keep up with the movement of the target. This error angle was caused by the delay time needed by the camera and the program to capture the image, calculate the movement of target and direct the beam. This error angle might become big problem if the distance between

mirror and the target was far because the beam would not be able to be steered to point at the target. To overcome this problem, we adopted simple prediction method to predict the position of the target in the next frame which is detected by the camera.

The mechanism of this prediction method can be seen from Figure 5.10. From the position of the target which was captured by the camera, the velocity and acceleration of the target could be calculated. By using this velocity and acceleration data, the position of the target in the next frame which was captured by the camera, x_{n+1}, could be predicted as:

$$x_{n+1} = x_n + v_n(t_{SD} + \Delta t) + \frac{1}{2}a_n(t_{SD} + \Delta t)^2 \ , \tag{5.1}$$

Where x_n , v_n , t_{SD} , a_n and Δt are the position of the target in the n-th frame, velocity of the target in the n-th frame, system delay, acceleration of the target and the time between frame captured by camera respectively. The system delay was measured experimentally as 128 ms.

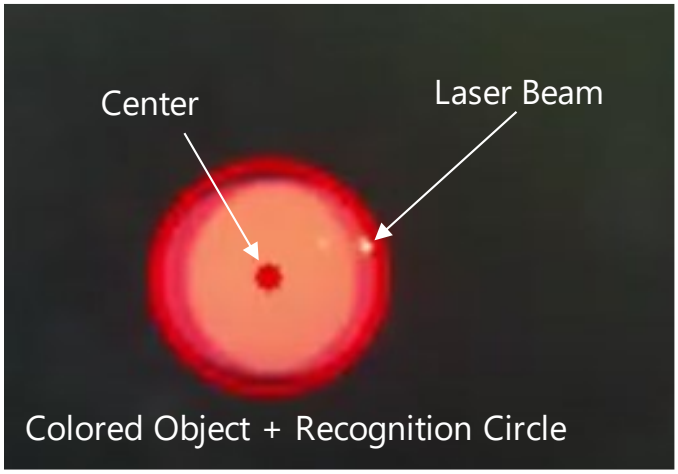

Figure 5. 8 Position mismatch (error angle) illustration.

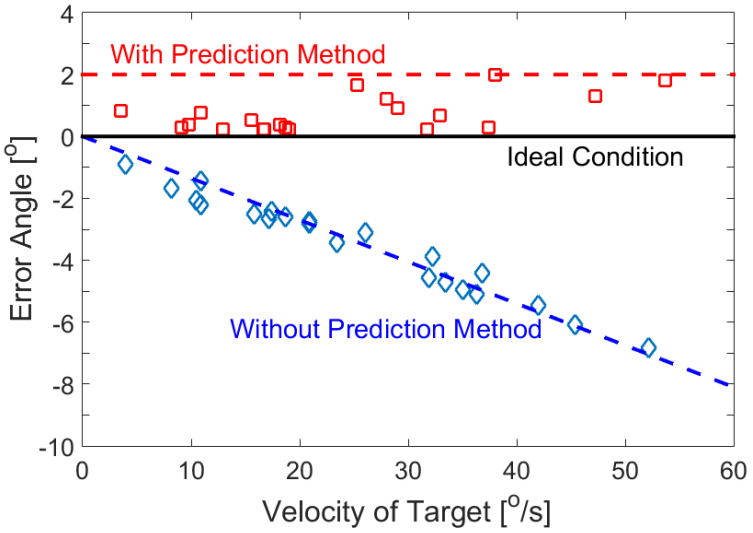

Figure 5. 9 Error angle and error angle reduction using prediction method.

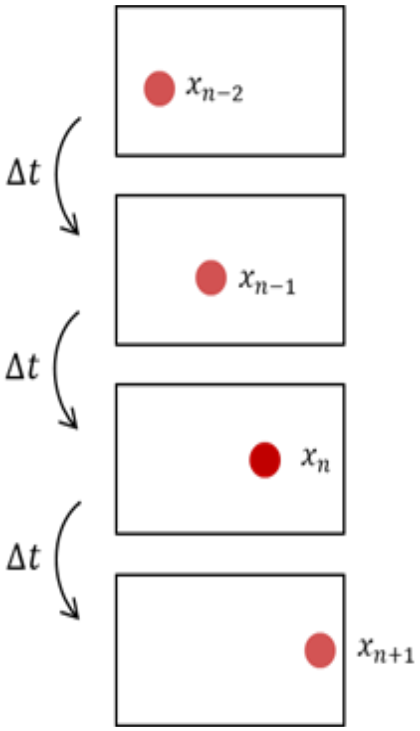

Figure 5. 10 Concept of prediction method.

The velocity and acceleration of the target could be calculated as:

$$v_n = \frac{\Delta x}{\Delta t} = \frac{x_n - x_{n-1}}{\Delta t} \quad , \tag{5.2}$$

$$a_n = \frac{\Delta v}{\Delta t} = \frac{x_n - 2x_{n-1} + x_{n-2}}{\Delta t^2} \quad , \tag{5.3}$$

Where x_{n-1} and x_{n-2} are the position of the target in the (n – 1)-th frame and (n – 2)-th frame respectively.

In the calculation of the predicted position of the target, the delay time needed by the system to steer the beam was considered. Hence, the position of the target in the next frame captured by camera could be predicted and the error angle and position mismatch between laser beam and the target could be decreased. By using prediction method, the error angle could be suppressed to less than 2° and independent to the target velocity. The positive error angle in the system using prediction method showed that the beam direction could keep up with the movement of the target. The value of 2° is still tolerable in our system because the beam can still reach the target at least until the distance between target and the beam is several meters. The moving target was driven by laser. Smooth movement of target indicated that laser was steered well to the solar cell on the target.

5.3 OWPT System to 2-Dimension Moving Target

5.3.1 Single Color Marker Problem

In this research, color segmentation method was used to recognize the target. In this case, color marker was put on the target to mark the target. Using this method, OWPT to 1-dimensional moving target has been demonstrated and the performance of the system had been evaluated in Section 5.2. However, it was found that single color marker method was not suitable for 2-dimensional moving target because there was position mismatch due to the distance between

camera and mirror system as can be seen from Figure 5.11(a). This condition would cause position mismatch between steered beam and the target when the target was moving along the course as illustrated in Figure 5.11(b). It was found that the distance between the laser beam and target was similar with the distance between the camera and mirror, d [62].

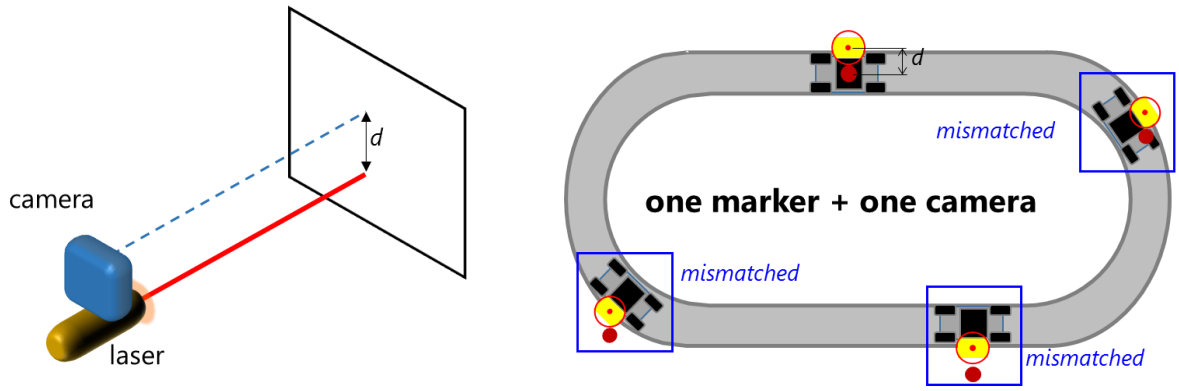

(a) (b)

Figure 5. 11 Illustrations of (a) Position mismatch problem between camera and laser and (b) Target and laser beam position mismatch problem.

5.3.2 2 Color Markers Solution and System Modification

The laser beam and target position mismatch problem could be solved using two cameras. In this case, one camera is used to record the y-position of the target and the other camera is used to record the x-position of the target. However, this solution also has its own problem. The processing time which is needed by the system to recognize the target and steer the beam should possibly be doubled. The other solution for this problem is by using two color markers. The color markers of the object were set as in Figure 5.12. In this illustration, blue color marker and yellow color marker are used and recognized as marker 1 and marker 2 respectively.

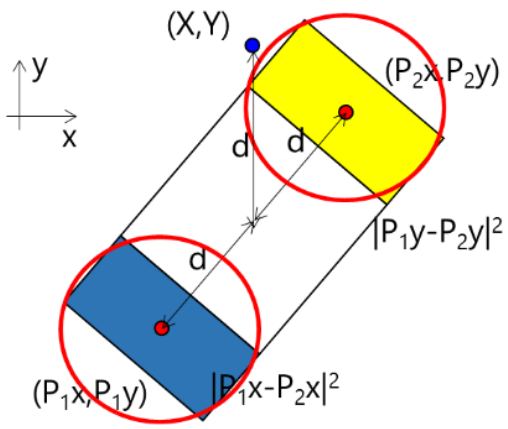

Figure 5. 12 Target and markers design for 2-dimensional moving object.

The center points of the color markers which were recognized by the camera were (P_{1x}, P_{1y}) and (P_{2x}, P_{2y}). Then the distance between center points of two-color markers could be calculated as:

$$d = \sqrt{(P_{2y} - P_{1x})^2 + (P_{2y} - P_{1x})^2} \quad . \tag{5.4}$$

Note that the distance d was the virtual distance between the center points of two-color markers. The unit of d was pixel. However, the distance between two color markers translated to the distance between camera and mirror in the real system. Hence, it could be assumed that the virtual distance d was similar with the mismatch distance d between camera and mirror in real condition.

Next, the virtual target recognition point (X, Y) which was represented as blue dot in Figure 5.13 could be calculated as:

$$X = \left| \frac{P_{2x} - P_{1x}}{2} \right| \tag{5.5}$$

and

$$Y = \left|\frac{P_{2y} - P_{1y}}{2}\right| + d \ . \tag{5.6}$$

The target recognition point was shifted to the (X, Y) point which was d distance above the center of the target. In this case, by assumption that the distance between the target recognition point and the distance between camera and mirror was same with the distance between the target recognition point and the center point of target, the laser could be steered to the center of the target while it is moving along the oval course in Figure 5.11(b). Using this method, OWPT to 2-dimensional moving object had been demonstrated as can be seen from Figure 5.13. Note that the mini toy car which was used as the target in this demonstration could move without battery because it was illuminated by laser which was steered by mirror from top.

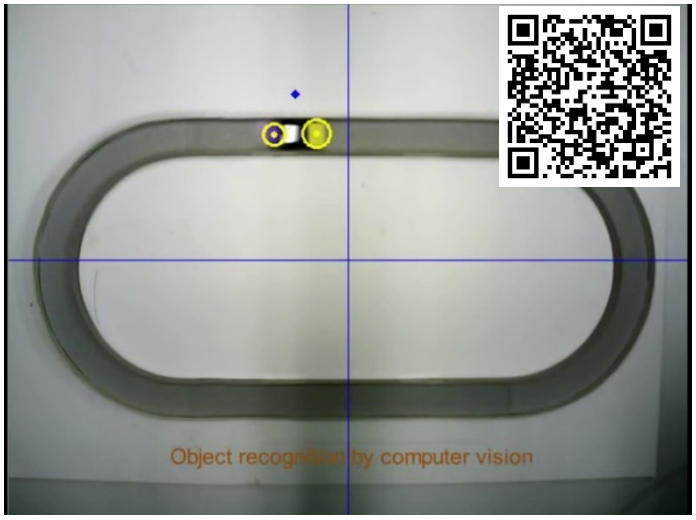

Figure 5. 13 Demonstration of optical wireless power transmission to 2-dimension moving object using single camera and color segmentation technique. (Note: Scan the QR code to watch the video.)

5.4 OWPT to Multiple Moving Targets

Galvano mirror set which was used in this experiment had fast response. By taking advantage of this characteristic, OWPT to multiple moving objects using only a single set of camera and Galvano mirror had been demonstrated. Periodic color segmentation method was used to recognize the target. Using this recognition method, the color which was recognized as the target by the recognition program would be switched every frame or several frames which were captured by the camera. In the other words, the program would periodically switch the recognized target for every frame or several frames. This method is illustrated in Figure 5.14 for the period of color recognition switching is every 1 frame. The period of color recognition switching could be adjusted from the program. Demonstration of OWPT to two moving objects using single set of camera and mirror could be seen from Figure 5.15. In this demonstration, the period of color recognition switching was adjusted to be 1 frame until 5 frames. Using this method, both targets could move smoothly using only single laser and set of Galvano mirror. This condition showed that the power could be delivered well to both moving targets.

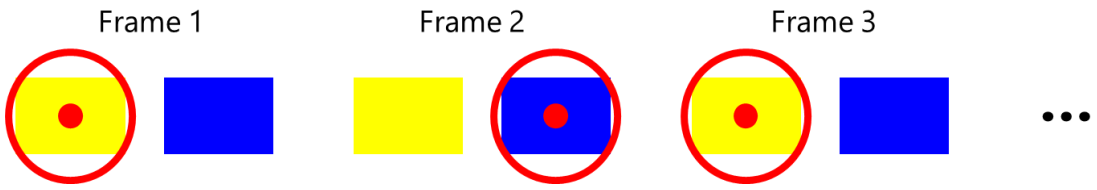

Figure 5. 14 Illustration of periodic color segmentation method for multiple objects recognition using single camera.

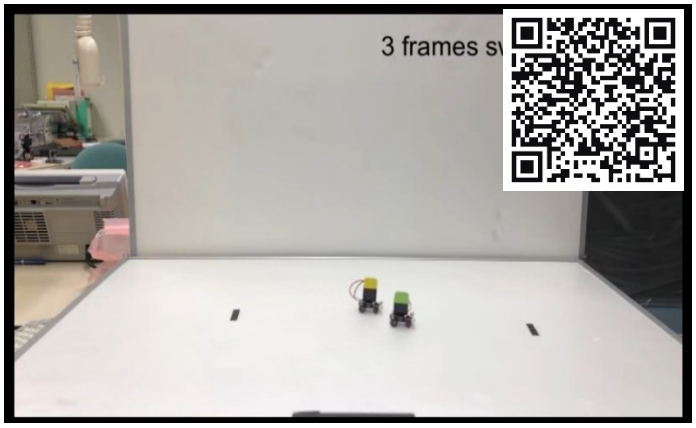

Figure 5. 15 Demonstration of optical wireless power transmission to multiple moving objects using single camera and single set of Galvano mirror. (Note: Scan the QR code to watch the video.)

5.5 Improvement of Target Recognition using Color Segmentation Method

5.5.1 Problems with Color Segmentation Method

During the demonstration of OWPT to moving target using camera with color segmentation method, some problems regarding target recognition were encountered. The main problem was the sensitivity of the target recognition to the brightness of environment and the condition of lighting of the environment. It was found that the recognized color by camera might change if the brightness of environment and the color of light source that illuminates the room changed. In this case, there was possibility that the camera would fail to recognize the target if the brightness of environment changed. In indoor condition, the color of the target which was recognized by the camera might also change depended on the color of the lamp or light source which was illuminating the environment. The best example of this problem can be seen from Figure 5.16(a) and 5.16(b). In Figure 5.16(a), the camera could recognize the red marker as the target well in the bright environment under white LED illumination. However, when the brightness of environment

changed and the color of LED which illuminates the room also changes, the color of the marker which was recgnized by the camera might changed as well as can be seen in Figure 5.16(b). In other words, the camera could not recognize the target anymore if the condition of illumination in indoor experiment changed. The main purpose of research was to develop recognition method which was insensitive to such change in the illumination and brightness of environment of the experiment [213].

(a) (b)

Figure 5. 16 Passive color marker recognition using camera at (a) Bright and (b) Dark environment.

The second problem in target recognition using color segmentation method was the disturbance by the same color objects in the environment. Color segmentation method which was used in this OWPT system recognize the target based on the color of passive color marker which was attached on the target. However, if there were other objects which have the same color as the passive color marker, the camera might recognize wrong object as the target. This condition was a big problem especially during the demonstration of OWPT at public area because in OWPT using high power laser, the laser might harm the person who was wrongly recognized as the target by camera. In Figure 5.17, it can be seen that the camera recognized wrong target because that object had same color as the intended target.

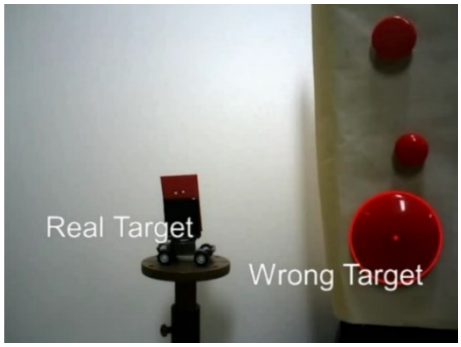

Figure 5. 17 Camera recognized other object with the same color in visible spectrum.

The sensitivity to environmental brightness problem of target recognition using color segmentation method could be solved by using active color marker such as LED instead of passive color marker which was used in previous demonstration, hence, the color of the target would not change regardless of the changes of brightness of environment. Furthermore, it was found that the web camera which was used in this demonstration could detect not only visible spectrum of light but also near infrared spectrum. In this case, to solve the disturbance which was caused by same color objects in visible spectrum, near infrared wavelength marker could be used instead of visible spectrum color marker. Then, infrared LED marker is chosen as the solution of these problems [213].

5.5.2 Infrared LED Marker Solution

Infrared LED marker is put on top of the moving target which was a mini toy car with Si solar cell as can be seen from the OWPT system diagram in Figure 5.18. The center wavelength of the light which was emitted by infrared LED marker was 850 nm. This infrared LED marker could be detected by the camera, however, to improve the detectability of the infrared LED marker and decrease disturbance by environment, optical bandpass filter lens (Thorlabs FB850-40) was put on the camera. The center wavelength of the bandpass filter was 850 nm with FWHM $\pm$ 8 nm which meant that in indoor environment, the light from the lamp in the room could be cut off perfectly. Hence, the effect of condition of the lighting of indoor environment to target recognition could be completely ignored.

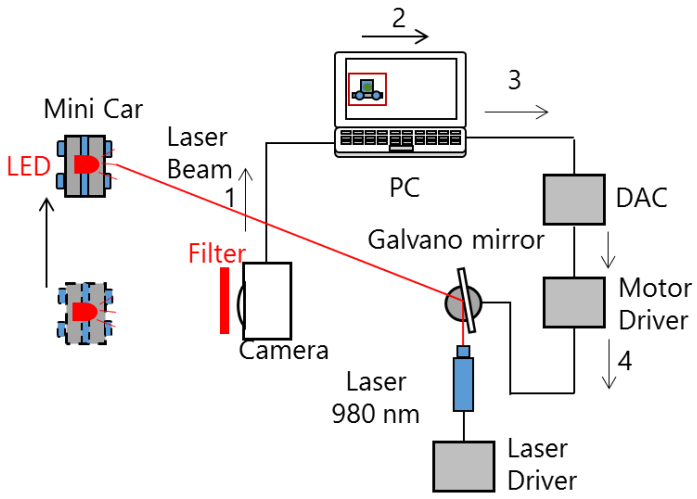

Figure 5. 18 Optical wireless power transmission system using LED marker.

OWPT to moving object using infrared LED marker had been demonstrated as can be seen from Fig. 7. The left-hand side image and right-hand side image show the images which were captured by the camera without bandpass filter and with bandpass filter respectively. In indoor environment, the light from lamp could be cut off perfectly by the bandpass filter, hence, the right-hand side image only shows the LED marker circle with black background. The red circle that encircles the LED marker image is the recognition circle. Using this method, the infrared LED marker could be detected well by the camera despite the change in brightness of the environment or the change of color of ambient light that illuminates the room.

The size of LED marker which was detected by the camera was the main limiting factor of this method. The distance dependency of the radius of infrared LED marker can be seen from Figure 5.19. In this case, single LED marker with input current 7 mA was used as the marker. The power source of this LED marker was single 1.5 V button battery. This radius was measured when the position of the LED marker was exactly at the middle point of the captured frame by camera. It is found that the operational distance for this method is only 60 cm to 70 cm distance between camera and target. For the distance more than 60 cm, the camera could still detect the marker, however, the size of LED marker would be smaller than 1 pixel. In this case, the detection might be difficult.

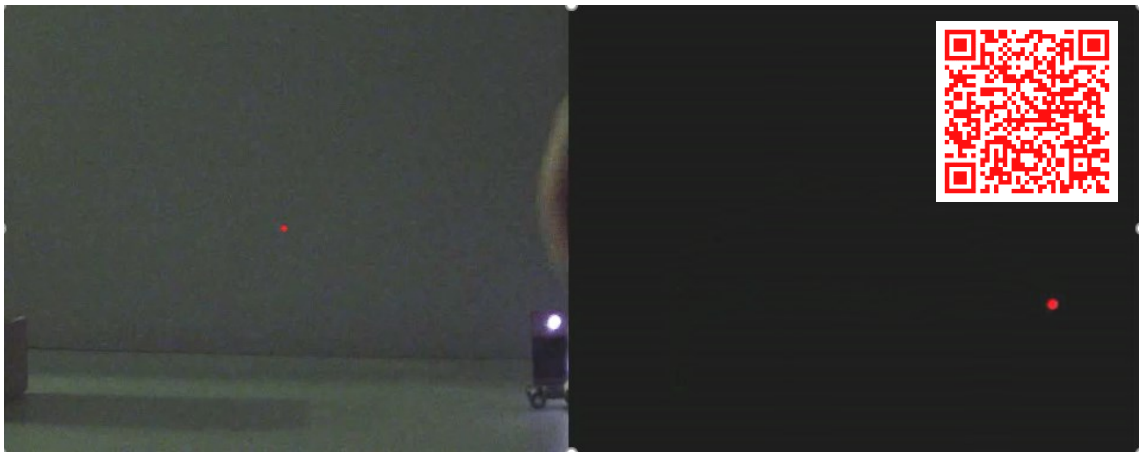

Figure 5. 19 Demonstration of optical wireless power transmission to moving object using led marker at dark environment. (Note: Scan the QR code to watch the video.)

There are several solutions to extend the operational distance of this method. The first solution is by supplying higher current to the LED marker; hence, the brightness of marker will increase and the detected size by camera will also slightly increase. The other method which is more feasible is by using LED array as the marker. The other solution that can be considered to enhance the operational distance is by using higher resolution camera [214].

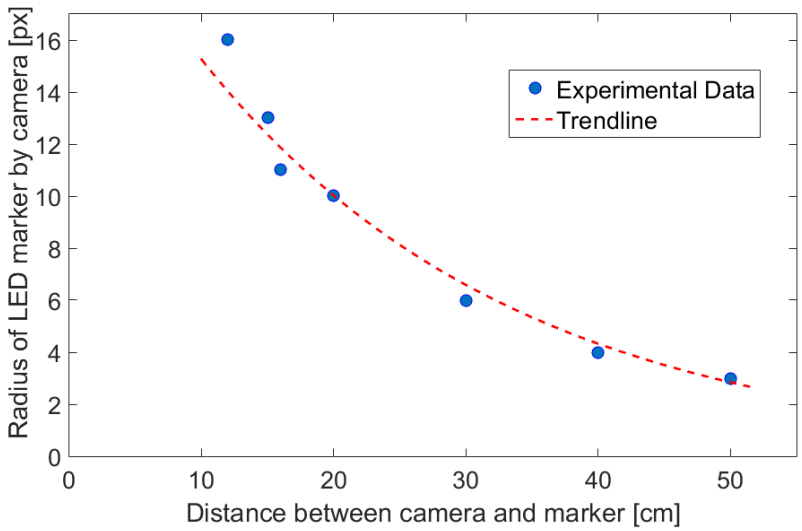

Figure 5. 20 Radius of light from LED marker which is recognized by the camera.

5.5.3 Problem with Outdoor Infrared LED Recognition and Solution

OWPT to moving object with infrared LED marker in indoor environment had been demonstrated as in Section 5.5.2. In indoor environment, the light from lamp could be cut off perfectly by the bandpass filter lens because lamp did not emit infrared light at 830 – 870 nm wavelength. However, in outdoor environment, sun emits quite high intensity infrared light. In this case, for outdoor application of infrared LED marker recognition in OWPT system, the sunlight was still detected by the camera with bandpass filter as can be seen from the captured image by the camera with bandpass filter lens in Figure 5.21. Note that, the intensity of infrared light from the sun was quite high, hence, the captured image by the camera is not completely black as in indoor condition in Figure 5.19. This condition would cause difficulty in the recognition of the target. In this case, the camera recognized other object as the target because the intensity of the LED which was recognized by the camera was very small compared with other detected objects (the sun). In the other words, camera failed to recognize the infrared LED marker [214].

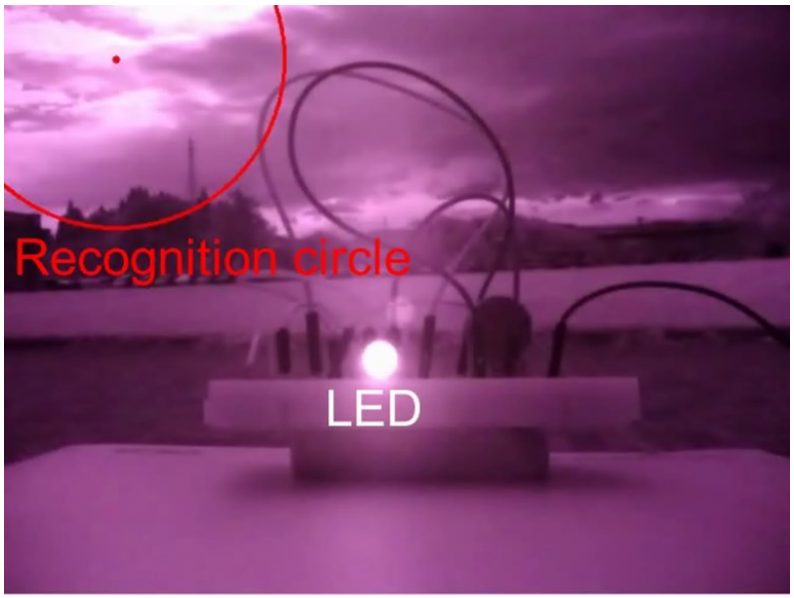

Figure 5. 21 Camera failed to recognize the LED marker at outdoor.

The solution for this problem is by using blinking infrared LED marker. The intensity of sunlight which was captured by the camera was mainly constant over time, to put it simply, the

light from the sun “did not blink”. In this case, image processing technique which was called background subtractor and blinking infrared LED marker were used for target recognition. Background subtracting technique was a technique to create image by subtracting one frame with the background model. The background model was built by considering the position and characteristics of objects for several frames. In the other words, the objects with unchanged characteristics and positions for two or several frames would be assumed as the background and would be add to the background model.

This technique is illustrated in Figure 5.22. In this case, frame 1 is subtracted with frame 2 to create frame 3. Note that, some objects such as triangle and square do not appear in frame 3 because their characteristics and position in frame 1 and 2 are same. Similar technique had been applied for target recognition in ref. [215] for indoor environment. The main difference between this method and the method in ref. [215] is the target marker and the recognition tools which is used to recognize the target. In ref. [215], the target markers are visible light LED markers on the other hand, in this research infrared LED marker is used. Note that in this research, the blinking LED method for target recognition was only applied for outdoor condition where there was disturbance from sunlight. For indoor environment, target recognition could be accomplished using non-blinking LED.

On the other hand, in ref. [215], blinking LED target recognition was used for indoor environment. The main problem by using visible light LED marker was the disturbance by the same color object in visible light spectrum. For example, if red LED marker was used as the target, the recognition of this LED marker, especially when the target was moving, would be disturbed by the existence of other red color object. In this case, the error in target recognition would occur. However, in this research, bandpass filter which cut off visible light from lamp in indoor environment completely was used, hence, there was not any disturbance from other same color object in target recognition for indoor environment.

The demonstration of blinking LED detection for outdoor application of OWPT using LED marker for target recognition can be seen from Figure 5.23. In this demonstration, the LED was driven by the signal from Arduino Uno. Frame rate of the camera was 30 fps and the frequency of

blinking LED was 15 Hz. By setting these parameters, the blinking infrared LED could be recognized well by the camera. As the conclusion, this blinking LED marker could be used as the marker for target recognition in outdoor demonstration of OWPT system.

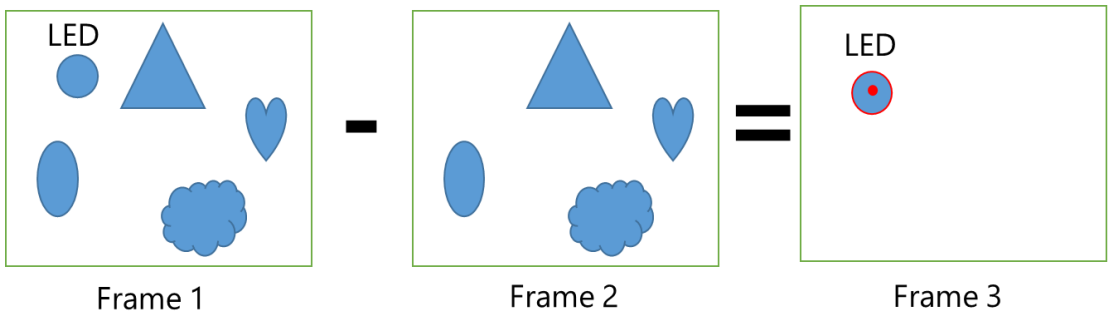

Figure 5. 22 Illustration of blinking target recognition using background subtractor technique.

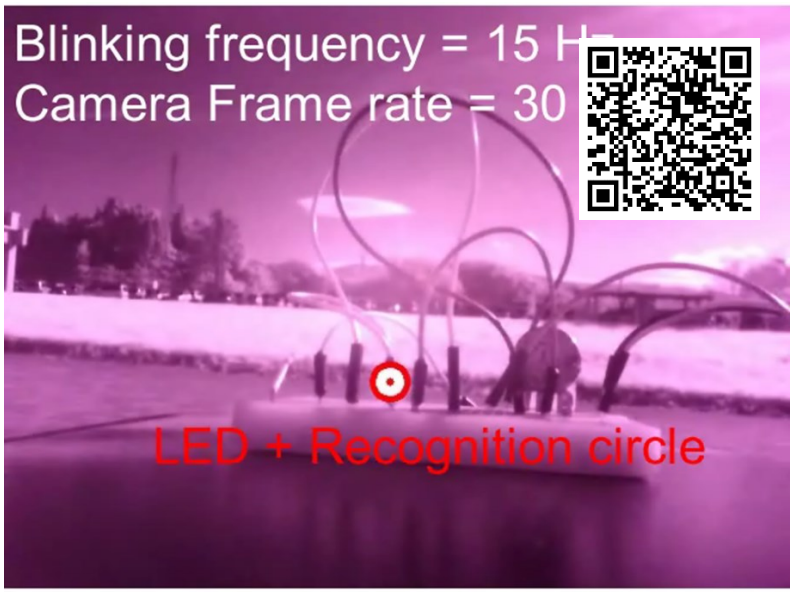

Figure 5. 23 Blinking LED marker recognition by camera. (Note: Scan the QR code to watch the Video.)

5.6 System Efficiency and Safety Evaluation

The system efficiency of OWPT system to moving target which was developed in this research can be analyzed from the characteristics of each component of the system in Figure 5.7. The first component is the 980 nm laser diode. The laser diode conversion efficiency can be analyzed from its characteristics of L-I curve in Figure 3.5. The conversion efficiency of laser diode was different according to the output optical power of the laser. In the system which was developed in this research, the laser diode driving current was set to be 600 mA to 850 mA. It was found that if the driving current of the laser was set to be less than 600 mA, at 60 cm distance between transmitter and solar cell, the target would not move because it did not receive enough power. The voltage supply for the diode laser could not be measured directly because it was enclosed in a closed case. In this analysis, it was assumed that the voltage supply to the laser was 1 V to 2 V which was typical operational voltage of 980 nm diode laser. By assumption that the output optical power of the laser was 150 mW at 750 mA driving current, the conversion efficiency of the diode laser was found to be around 20% to 10% for voltage supply around 1 V to 2 V, respectively.

The output of laser was collimated using collimator and the beam profile of the output of laser can be seen from Figure 5.24. These results were measured for the distances between laser and power meter were 20 cm, 30 cm and 40 cm. The beam profiles were Gaussian shape profiles and the beam size increased as the distance between the laser and optical power meter increased, hence, the divergence angle of the beam could be calculated. The distance dependency of beam radius of the laser can be seen from Figure 5.25. The beam radius was defined as the radius of the beam when the intensity of the laser was $1/e^2$ of the maximum intensity of the laser at the center of the beam. The divergence angle of the collimated laser beam was calculated as 0.43^0 or 7.5 mrad.

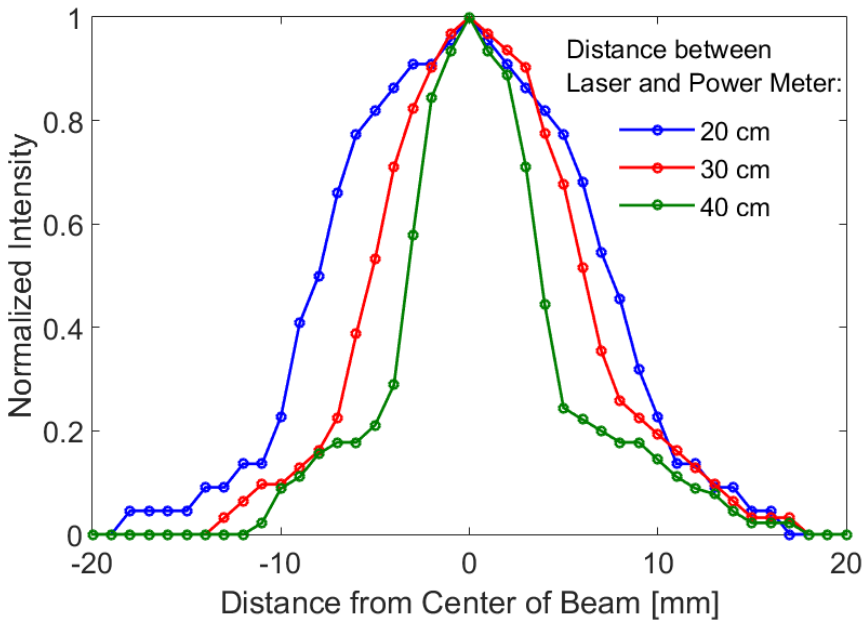

Figure 5. 24 Measured beam profiles for several distance between laser and power meter.

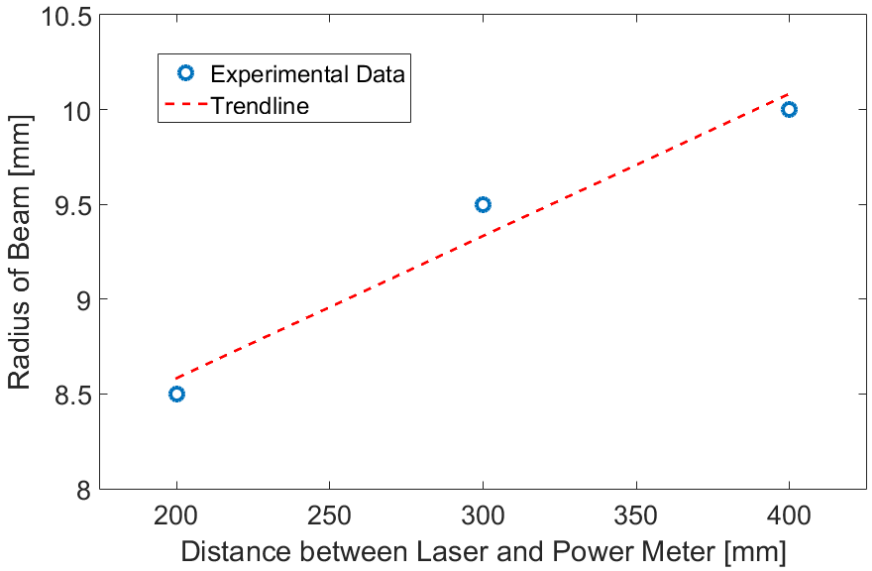

Figure 5. 25 Distance dependency of radius of laser beam.

In the OWPT system to moving target in this research, the distance between the laser and target solar cell was 60 cm and the size of solar cell was 2.2 cm x 2cm. From Figure 5.25, the beam

radius at this distance could be calculated as 1.15 cm, then the laser beam collection efficiency could be calculated as 87% which was calculated using Eq. 3.39 in Chapter 3. The output of the laser was collimated using lens; hence, it can be assumed that the size of the output of laser beam was similar with the collimator lens. Since, the Galvano mirror was larger than the collimator lens, it was assumed that all of the light from laser was deflected by the Galvano mirror, hence, there is not loss at the Galvano mirror.

The next component is the solar cell. The solar cell efficiency can be analyzed from Figure 5.6 in Section 5.1.4. For the illumination of 150 mW of light, the conversion efficiency of the solar cell was measured to be 22%. The attenuation by atmosphere was neglectable becauce the system was demonstrated at indoor environment and the distance was near. Then the system efficiency can be analyzed as:

$$\eta_{sys} = \eta_T \times \eta_{col} \times \eta_R \quad . \tag{5.7}$$

The system efficiency of the OWPT system to moving target was calculated to be between 3.83% to 1.91% for the voltage supply of laser was between 1 V to 2 V, respectively.

The power density of 980 nm laser which was used in the OWPT system to moving target was measured to be 36.1 mW/cm^2 for the distance between laser and target was 60 cm. The Maximum Permissible Exposure (MPE) values of 980 nm laser for eye at 0.25 s exposure, which can be calculated from Figure 3.26, is 9.24 mW/cm^2. The MPEs values for human skin at 1 s and 60 s exposure are 3994 mW/cm^2 and 12.1 mW/cm^2 respectively. From these values, it can be concluded that the laser which was used in this system was not safe for human's eyes and skin for long exposure. Hence, during the experiment, protective eyeglasses are a must and direct exposure to the beam should be avoided.

CHAPTER 6

APPLICATIONS OF OPTICAL WIRELESS POWER TRANSMISSION SYSTEM

In Chapter 3, the potential applications of Optical Wireless Power Transmission (OWPT) system has been analyzed theoretically. It turns out that OWPT can be used to transmit power through atmosphere for longer distance than other WPT methods, through water and even through human skin. Microwave power transmission cannot be used underwater because the absorption of microwave by water is very high, hence, it can only be used to transmit power for several centimeters as can be seen from Chapter 3. Then, the remaining WPT methods are magnetic coupling WPT and OWPT.

The magnetic coupling WPT can potentially be used for charging underwater as in ref. [216-218]. In the application of magnetic inductive coupling for underwater power transmission, the charging pad which consists of coil for transmitter in WPT has to be waterproofed well enough and has to be able to withstand the water pressure. The this charging pad has to be connected with electric cable and the Underwater Unmanned Vehicle (UUV) has to stop moving and stay on top of the charging pad all the time during the charging, in this case, the mobility of the UUV will be limited by the cable's length. In this case, the potential of transmitting power though considerably longer distance underwater which provides freedom of mobility for the target is a unique potential application of OWPT. In this chapter, simple OWPT through water is demonstrated and analyzed.

The next advanced application of OWPT is to transmit and send power and data at the same time to the target. In this chapter hybrid OWPT and FSO communication system which provides power and data transmission at the same time is demonstrated and analyzed.

6.1 Demonstration of OWPT through Water

6.1.1 Experimental Setup

Based on the theoretical analysis in Chapter 3, it is found that the infrared (around 940 nm to 980 nm) laser can be used for OWPT through water using Si solar cell for several centimeters due to high conversion efficiency of the solar cell. However, for long distance OWPT through water, blue laser (around 400 nm to 440 nm) can be used for long distance OWPT through water for distance several meters until 100 meters due to low absorption of blue light by water molecule. OWPT through water using red laser had been demonstrated in ref. [179].

In this demonstration of OWPT through water, 980 nm infrared laser and 440 nm blue laser were used as the transmitter as can be seen from Figure 6.1. The Si solar cell and tap water were used as the receiver and medium of power transmission, respectively. The water was contained in water container which was a small aquarium. The maximum distance between laser and the solar cell was 9 cm and the maximum output electric power of the solar cell was measured for the depths of water were 1 cm to 8 cm. The solar cell was single diode Si solar cell. The demonstration of OWPT through water can be seen from Figure 6.2.

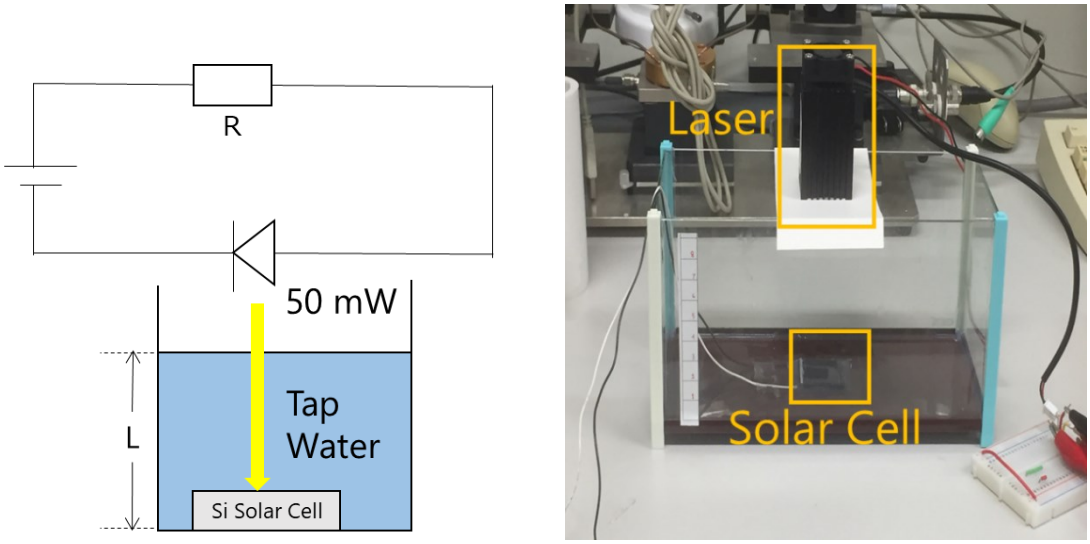

(a) (b)

Figure 6. 1 Experimental setup of OWPT through water: (a) Diagram and (b) Real image.

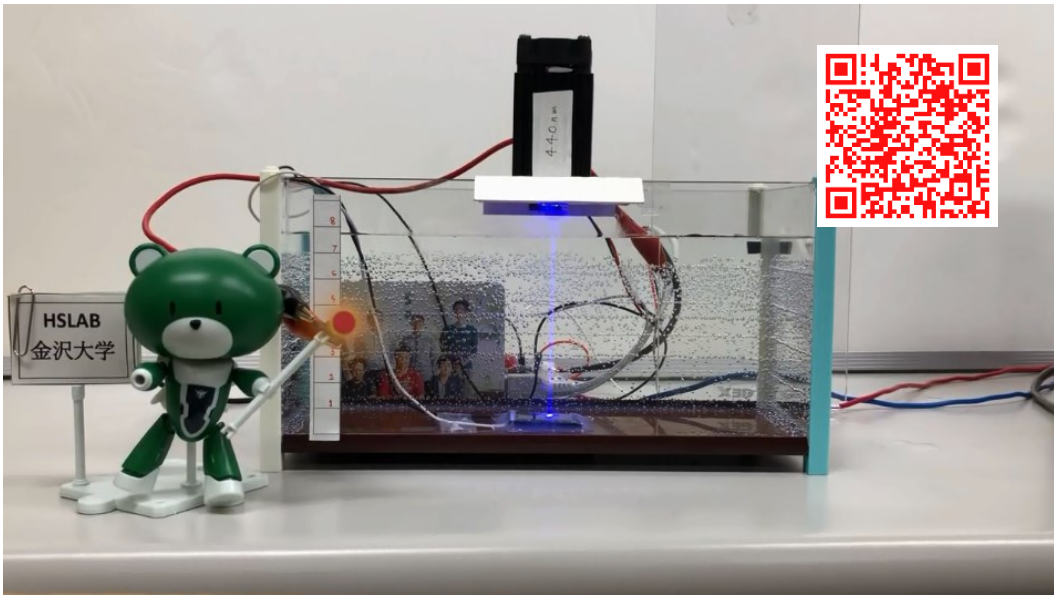

Figure 6. 2 Demonstration of OWPT through water using blue laser. (Note: Scan the QR Code to Watch the Video)

6.1.2 Results and Predicted Distance for OWPT

The output electric power of the solar cell for 440 nm (blue laser) and 980 nm (infrared laser) of input optical light for the depths of water were 1 cm to 8 cm can be seen from Figure 6.3. The short distance between laser and solar cell ensured that the size of the laser beam would be much smaller than the size of solar cell and all of the light from the laser would be received by the solar cell. The output optical powers of both lasers were set to be 50 mW.

As predicted by the theoretical analysis in Chapter 3, the output electric power of the solar cell for 980 nm illumination was higher than 440 nm of laser illumination for the depth of water was less than 3 cm depth of water, however, when the depth of water was more than 3 cm, the output electric power of the solar cell for 440 nm illumination was higher than 980 nm illumination. The absorption coefficients of the tap water for 980 nm and 440 nm of light were calculated as 0.458 cm^{-1} and 0.007 cm^{-1}, respectively. These results showed that the 980 nm infrared light was absorbed more than the 440 nm blue light.

The absorption coefficients of 440 nm blue laser and 980 nm infrared laser based on theoretical analysis were 0.0001 cm^{-1} and 0.43 cm^{-1}, respectively. These results show that the experimental result of absorption coefficients of 440 nm blue laser was 70 times larger than the theoretical value, on the other hand, the experimental result and theoretical value of absorption coefficient of 980 nm infrared laser was almost similar. These conditions could be caused by different type of water which were used for the experiment and the assumption in theoretical analysis. In theoretical analysis of pure water is assumed as the medium, on the other hand, in experiment, tap water was used as the medium, hence, there was possibility that the absorption spectra of light by the tap water in experiment and pure water in theoretical analysis would be different.

Based on the absorption coefficients which were measured in the experiment, the projected output electrical power of OWPT through water for longer distance (deeper depth of water) can be analyzed as in Figure 6.4. It was predicted that the output electric power of the solar cell will decrease into e^{-1} value of its maximum value when the distances of the laser and solar cell (depth

of water) for OWPT through water were 1.5 meter and 2 cm for 440 nm blue laser and 980 nm infrared laser, respectively. It was predicted that the performance of OWPT system and operation distance could be enhanced more by using wider bandgap solar cell such as GaN based solar cell which would increase the conversion efficiency of blue light.

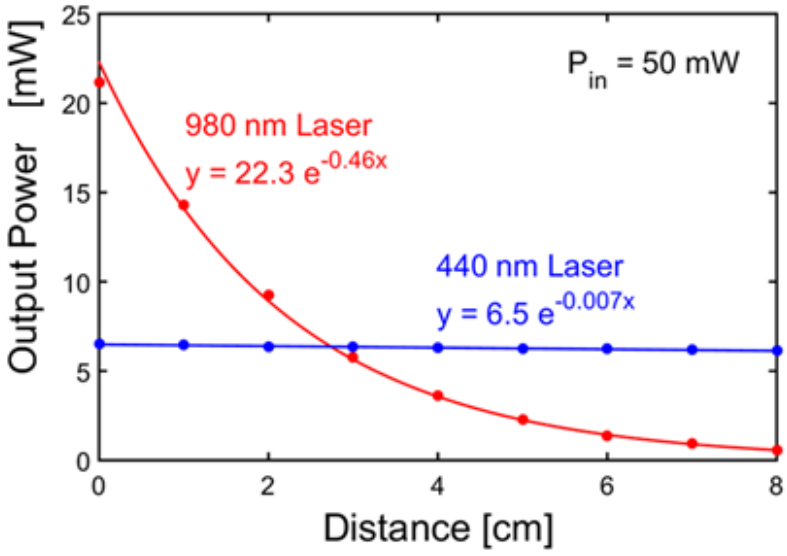

Figure 6. 3 Output electric power of Si solar cell for OWPT through water.

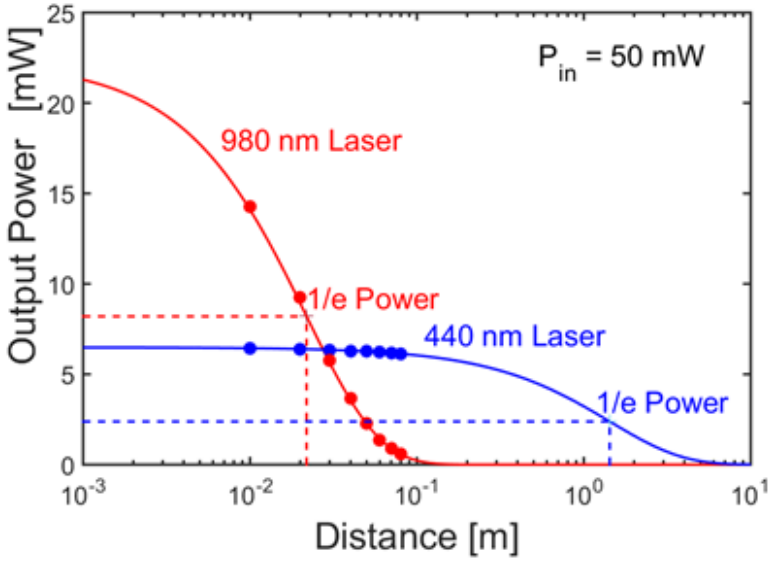

Figure 6. 4 Projection of output electric power of solar cell for OWPT through water.

6.2 Hybrid OWPT and FSO Communication System

6.2.1 System Design

FSO Communication has many advantages compared with microwave based free space communication such as Wi-Fi system. FSO provides higher bandwidth and faster data transmission than Wi-Fi system. The FSO with data transmission more than 10 Tbps had been demonstrated in refs. [219]. By combining FSO and OWPT in one system, it is possible to create a backhaul system for local wireless area network and even a satellite network [219] which can provide data and power transmission in a combined system. Such system can also be used for designing emergency base transmitter system for cellular network in disaster area.

In this section, hybrid OWPT and FSO communication system which allows data and power transmission at the same time is designed and analyzed. The system diagram can be seen from Figure 6.5. 660 nm red laser and 980 nm infrared laser were used for data transmission and power transmission, respectively. As the receivers, the Si photodetector (PD) and Si solar cell were used to detect the data transmission and convert light into electric power, respectively. The laser for data transmission was modulated using simple Intensity Modulation (IM) technique and Direct Detection (DD) method was used for detection of the modulated light.

Two identical dichroic mirrors were used to combine and separate the axes of propagation of 660 nm and 980 nm lights. The dichroic mirrors were 900 nm long pass dichroic mirror. These mirrors were transparent for wavelength more than 900 nm which meant that these mirrors would be transparent for 980 nm of light, on the other hand, 660 nm of light will be completely deflected by the mirrors. The mirrors were set to be 45^{o} angle, hence, the 660 nm red light would be deflected at 90^{o} angle. Similar method which was used to transmit data and power through single optical fiber can be seen from ref. [220]. In ref. [220], blue LED and 850 nm VCSEL were used as the light source for power and data transmission, respectively to a catheter through a single mode fiber. The axes of lights for data and power transmission were combined and separated using dichroic mirrors. However, this system was not hybrid OWPT and FSO communication system because the medium of transmission was optical fiber.

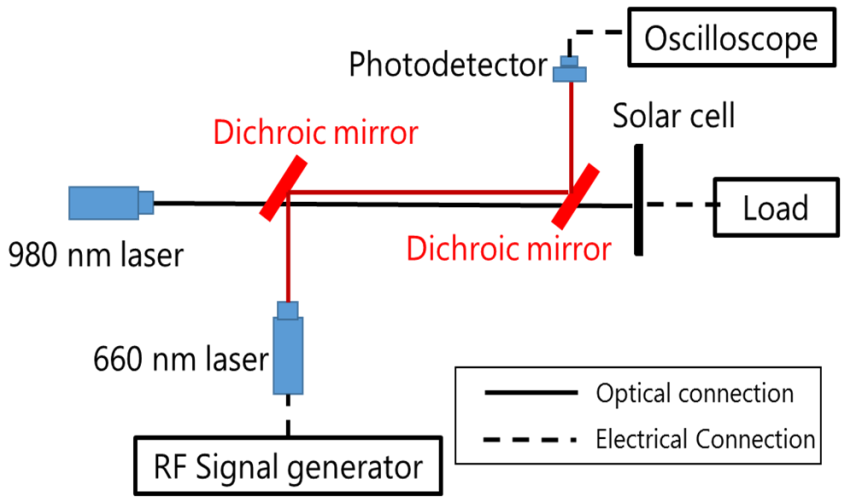

Figure 6. 5 Diagram of hybrid OWPT and FSO communication system.

6.2.2 PD Performance and Demonstration

In this system, the photodetector was Thorlabs PDA100A which was made by Silicon. The frequency response of PD can be seen from Figure 6.6. The 3-dB bandwidth of the Si PD was measured to be 10 MHz. The frequency response of the solar cell was limited by its junction capacitance which is inversely proportional with its area. The area of the Si PD was 75.4 mm^2. Hence, it was predicted that higher frequency response could be obtained by using smaller area of PD.

Hybrid OWPT and FSO communication system using dichroic mirrors and two lasers have been demonstrated and can be seen from Figure 6.7. The data which was transmitted was sound data. At the receiver, the Si PD was connected to a speaker to reproduce the sound data which was transmitted in the system.

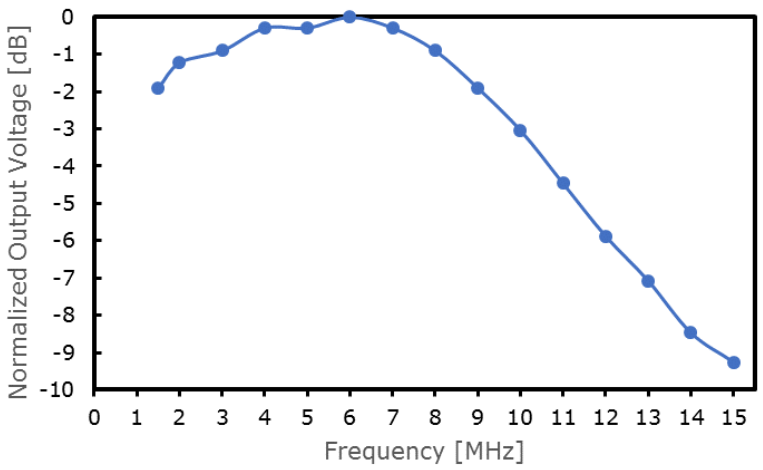

Figure 6. 6 Frequency response of PD.

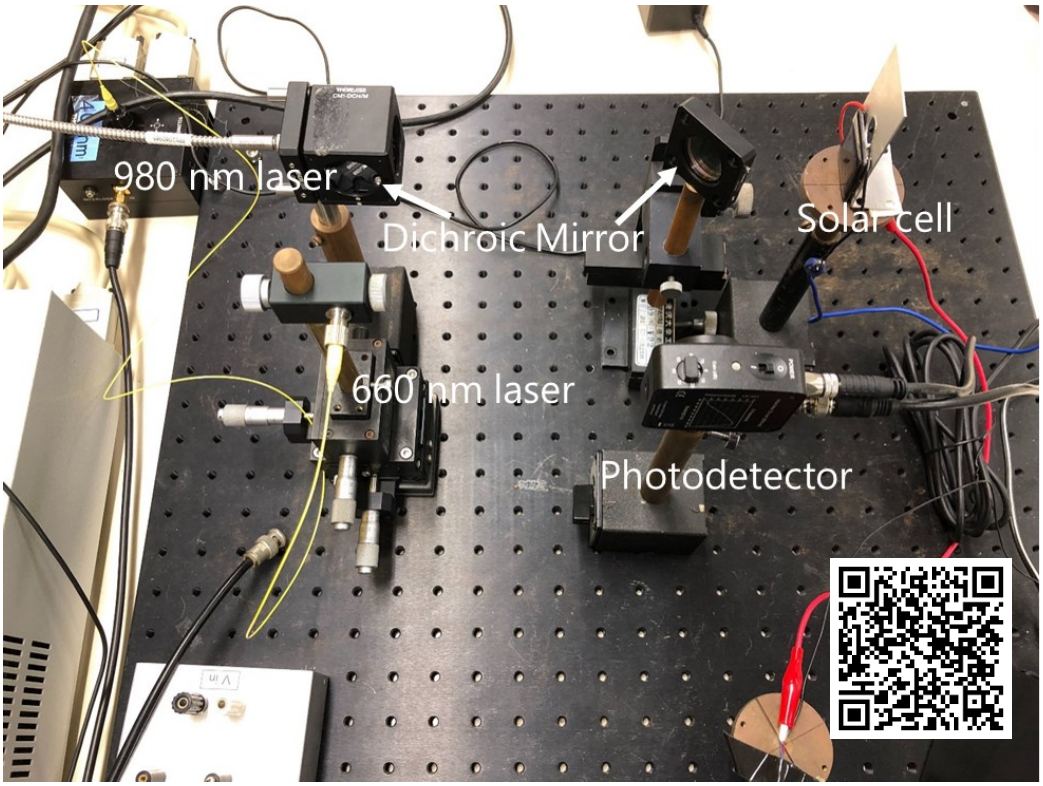

Figure 6. 7 Demonstration of hybrid OWPT and FSO communication system. (Note: Scan the QR code to watch the video).

CHAPTER 7

SUMMARY AND LIST OF PUBLICATIONS

7.1 Summary

Electronics devices need electric power as the source of energy. In electronic devices with high mobility capability such as drone, smartphone and Unmanned Underwater Vehicle (UUV), battery is used to supply power. However, the capacity of battery is limited. If the battery runs out of power, the battery of the electronics device needs to be charged using charger which is connected with electric socket using cable. In this case, the mobility of mobile electronic devices which is charged using cable is limited by the length of the cable. The other problem with mobile electronic devices is the capacity of the battery which is proportional to its size and weight. In mobile electronic devices, its performance depends on its weight and size. Hence, there is tradeoff in design of mobile electronic devices in terms of battery capacity and its mobility and weight.

Wireless Power Transmission (WPT) is a technique to transmit electric power to charge and power up electronics devices remotely without using any electric cable. In WPT, electric power is transmitted using electromagnetic wave. The development of WPT has open new possibility for unlimited operational time for mobile electronic devices such as drone and UUV because it can be charged remotely from far away and the mobility is not limited by the cable. The other advantage of WPT is a possibility to design compact and light mobile electronic devices

because there is no need for heavy high capacity battery. In WPT system, there are three main components which are transmitter, receiver and medium.

Based on the frequency of electromagnetic wave, there are three methods of WPT which are popularly developed. They are magnetic induction coupling, microwave and optical WPT (OWPT). The magnetic induction coupling WPT uses several kHz to several hundreds of MHz frequency of electromagnetic wave. Among WPT methods, magnetic induction coupling WPT is the oldest method which is developed. In this method, a pair of coils is used as the transmitter and receiver. The advantage of this method is high possibility to transmit electric power without using cable through many mediums such as air, water and human skin for short distance with high system efficiency. The system efficiency can be as high as more than 90%. However, since the operational distance of this method is very short, it cannot be used to transmit power to moving object remotely and the mobility of the object which is charged using this method is still limited by the length of the cable. Nowadays, there are many applications of magnetic induction coupling WPT such as to charge smartphone and smartwatch (Qi wireless charger), Electric Vehicle (EV) and possibility to charge implantable medical devices.

The frequency of electromagnetic wave in microwave WPT is in Industrial, Scientific and Medical (ISM) band which is usually around several GHz. The transmitter and receiver in microwave WPT are a pair of antennas. The advantage of this method is possibility to transmit power to long distance between transmitter and receiver and ease to steer the microwave beam. The back to back efficiency of microwave WPT can theoretically be more than 60%. However, the medium of transmission for microwave WPT is limited to atmosphere (air). Microwave is highly absorbed by water molecule; hence it is not possible to transmit power through water. Microwave cannot be used to transmit power to implantable medical devices because there is possibility of electromagnetic interference which will disturbs the function of implantable medical devices. The frequency band which is used by microwave WPT is also used by other electronic devices such as microwave oven, Bluetooth and Wi-Fi; hence, there is high possibility of Radio Frequency Interference (RFI). Nevertheless, some applications of microwave WPT such as to transmit power to moving small aircraft, power transmission through air for several meters of distance between transmitter and receiver. Large scale application of microwave WPT is Space

Power Satellite (SPS) where microwave is used to transmit power which is harvested by the satellite in space to a ground unit on earth.

OWPT uses light which has frequency more than 100 THz to transmit electric power. The transmitter and receiver in OWPT are light sources such as laser or LED and solar cell, respectively. The laser beam which is used in OWPT has very small diffraction angle and small size; hence, it is possible to use OWPT to transmit power over long distance between transmitter and receiver. Small size and diffraction angle of laser also give advantage which is an ease to steer the beam; hence, it can be used to transmit power to moving target. However, OWPT has lower system efficiency compared with other WPT method. The system efficiency of OWPT system can be around 40%. In this research, the characteristics of system efficiency of OWPT through several mediums such as air (atmosphere), water and human skin are analyzed. OWPT using laser and Si solar cell is theoretically analyzed. Based on the results of theoretical analysis, the ideal wavelength of OWPT through atmosphere using Si solar cell is around 940 nm with system efficiency can be as high as 38.7% for 1 km distance between transmitter and receiver. The system efficiency of OWPT through water using blue laser (400 nm) for distance between transmitter and receiver 100 m is 9.6% and 4% system efficiency of OWPT through 1 cm of human skin using 940 nm laser is theoretically possible. Based on these results, OWPT can be used to transmit power through air (atmosphere), water and human skin for long distance between transmitter and receiver.

The main purpose of this research is to develop, evaluate and improve OWPT system which can be used to transmit power to moving target and several moving targets using simple system. 980 nm high power diode laser and Si solar cell were used as the transmitter and receiver respectively. Camera and mirror are used to recognize the target and steer the laser beam to follow the moving target or targets, respectively. Color segmentation method which is one of the techniques of Open CV was used to recognize the target and a color marker was put on top of the moving target. Using this method, OWPT system to 1-dimensional and 2-dimensional moving target had been demonstrated. The mirror which was used in this research was Galvano mirror which has very high speed; hence, OWPT to multiple moving targets using only one set of mirror and camera had also been demonstrated.

Color segmentation method which was used to recognize the target in OWPT system to moving target has several limitations. The main limitations of color segmentation method were the recognition was very sensitive to the brightness of environment and there was possibility of wrong target recognition if there was any other object which has same color as the color marker of target. To solve these problems, instead of color marker which was made from color paper, infrared LED was used as the marker and band pass filter was put on the camera. The central wavelength of the LED light and the bandpass filter were matched; hence, the camera with bandpass filter would only recognize the light from the LED and the other light from environment could be completely cut off. Using this method, OWPT system to moving target which was insensitive to the brightness of indoor environment had been demonstrated. In outdoor condition, unfortunately, the intensity of sunlight was much higher than the intensity of light from LED; hence, outdoor detection of infrared LED was difficult. To solve this problem, blinking infrared LED light was used for outdoor application. The system efficiency of OWPT system to moving target which was developed in this research was around 3.8%. This system efficiency was measured when the distance between laser and the solar cell was 60 cm.

In this research, some applications of OWPT system such as the OWPT system through water and hybrid OWPT and Free Space Optical (FSO) communication system had also been demonstrated. For OWPT through water, blue laser (440 nm) and infrared laser (980 nm) were used as the transmitter and Si solar cell was used as the receiver. Tap water in an aquarium at room temperature was used as the medium. Based on the experimental results, OWPT through tap water using blue laser for distance more than 1 m with considerable high system efficiency was possible, on the other hand, OWPT through tap water using infrared laser could only be used for several cm of distance between transmitter and receiver.

Hybrid OWPT and FSO communication system had also been demonstrated. In this system, 980 nm laser and 660 nm laser were used as the transmitter for power and data transmission, respectively. Dichroic mirrors which were long pass mirrors were used to combine the axes of propagations of both lasers at the transmitter and to separate the lasers at the receiver. These long pass mirrors were transparent for light with wavelength longer than 900 nm; hence, the 980 nm

laser will be transmitted by the dichroic mirrors, on the other hand, the 660 nm light would be reflected by the mirrors.

As the conclusion, in this research OWPT system to moving target and several moving targets using camera and Galvano mirror to recognize the target and steer the beam had been successfully demonstrated and the performance of the system had been evaluated. Additionally, OWPT system through water and hybrid OWPT and FSO communication system which could be used to transmit power and data at the same time had also been demonstrated.

7.2 List of Publications

From the results of this research, the following international journal paper had been published:

- A.W.S. Putra, H. Kato, and T. Maruyama, "Infrared LED Marker for Target Recognition in Indoor and Outdoor Applications of Optical Wireless Power Transmission System," Jpn. Appl. Phys., Vol. 59, No. SOOD06, Aug. 2020.
- A.W.S. Putra, M. Tanizawa and T. Maruyama. "Optical Wireless Power Transmission Using Si Photovoltaic Through Air, Water and Skin." IEEE Phot. Technol. Lett., Vol. 31 (2), pp. 157-160, Jan. 2019.

Several results had also been presented in several international conferences as follows:

- A.W.S. Putra, H. Kato and T. Maruyama, "Demonstration of Hybrid Optical Wireless Power Transmission and Free Space Optical Communication System Using Dichroic Mirrors," 2nd Optical Wireless and Fiber Power Transmission Conference 2019, Yokohama, Japan, April 21 – 23, 2020.

- A.W.S. Putra, H. Kato, H. Adinanta and T. Maruyama, "Optical Wireless Power Transmission to Moving Object Using Galvano Mirror," Free-Space Laser Communications XXXII (LASE), Photonics West, San Francisco, California, United States of America, February 1 – 6, 2020.
- A.W.S. Putra, H. Kato and T. Maruyama, "Infrared LED Marker for Target Recognition in Optical Wireless Power Transmission to Moving Object at Dark Environment Condition," 24th Microoptics Conference, Toyama, Japan, November 17 – 20, 2019.
- H. Adinanta, H. Kato, A.W.S. Putra and T. Maruyama, "Enhancement of Beam Tracking Response Using Color Filtering Method for Optical Wireless Power Transmission," 5th International Symposium on Frontier of Applied Physics, Indonesia, October 23 – 24, 2019.
- A.W.S. Putra, T. Yoshida, H. Adinanta, H. Kato and T. Maruyama, "Optical Wireless Power Transmission through Water," 1st Optical Wireless and Fiber Power Transmission Conference 2019, Yokohama, Japan, April 22 – 26, 2019.
- H. Kato, H. Adinanta, A.W.S. Putra and T. Maruyama, "Object Recognition and Beam Steering System for Optical Wireless Power Transmission to Moving Object," 1st Optical Wireless and Fiber Power Transmission Conference 2019, Yokohama, Japan, April 22 – 26, 2019.

Several other results had also been presented in domestic conferences:

- A.W.S. Putra, H. Kato and T. Maruyama, ">1 W Power and 10 MHz Data Transmission in Hybrid Free Space Optical Communication and Optical Wireless Power Transmission," The 67th Japanese Society of Applied Physics (JSAP) Spring Meeting 2020, Sophia University, Tokyo, Japan, March 12 – 15, 2019.
- A.W.S. Putra, H. Kato and T. Maruyama, "Demonstration of Optical Wireless Power Transmission to Moving Object Using Infrared LED Marker in Dark Environment," The 80th Japanese Society of Applied Physics (JSAP) Autumn Meeting 2019, Hokkaido University, Hokkaido, Japan, September 18 – 21, 2019.

- H. Kato, A.W.S. Putra and T. Maruyama, "Development of optical axis identical laser tracking system for optical WPT to moving object," IEICE Society Conference 2019, Osaka University, Osaka, Japan, September 10 – 13, 2019.
- A.W.S. Putra, T. Yoshida, H. Adinanta, H. Kato and T. Maruyama, "Optical Wireless Power Transmission through Water," Institute of Electronics, Information and Communication Engineers (IEICE) General Conference 2019, Waseda University, Tokyo, Japan, March 19 – 22, 2019.
- H. Adinanta, A.W.S. Putra, H. Kato and T. Maruyama, "Optical Wireless Power Transmission to Multiple Moving Objects Using Computer Vision," The 66th Japanese Society of Applied Physics (JSAP) Spring Meeting 2019, Tokyo Institute of Technology, Tokyo, Japan, March 9 – 12, 2019.
- A.W.S. Putra, H. Adinanta, H. Kato and T. Maruyama, "Object Tracking Using Single Camera for Optical Wireless Power Transmission to Two-Dimensional Moving Object," Institute of Electronics, Information and Communication Engineers (IEICE) Society Conference 2018, Kanazawa University, Kanazawa, Japan, September 11 – 14, 2018.
- A.W.S. Putra, M. Tanizawa and T. Maruyama, "Numerical Calculation of System Efficiency of Optical Wireless Power Transmission Using Silicon Photovoltaic Through Various Mediums," The 65th Japanese Society of Applied Physics (JSAP) Spring Meeting 2018, Waseda University, Tokyo, Japan, March 17 – 20, 2018.

Beside the research, which was presented in this dissertation, author was also involved in other research about semiconductor optical amplifier and Erbium Doped Fiber Amplifier (EDFA) and the development of silicon slab waveguide. Based the results of these research, the following paper had been and would be published in international journals:

- A.W.S. Putra, M. Yamada, S. Ambran and T. Maruyama, "Theoretical Comparison of Noise Characteristics in Semiconductor and Fiber Optical Amplifiers," IEEE Photonics Technology Letters, Vol. 30 (8), Apr. 2018.
- W.P. Tresna, A.W.S. Putra and T. Maruyama, "Optical Properties of Si Slab Waveguide," submitted to Current Optics and Photonics (under review).

REFERENCES

[1] MIT Electric Vehicle Team, “A Guide to Understanding Battery Specifications,” Dec. 2008. http://web.mit.edu/evt/summary_battery_specifications.pdf

[2] X. Lu, P. Wang, D. Niyato, D. I. Kim and Z. Han. “Wireless Charging Technologies: Fundamentals, Standards, and Network Applications,” *IEEE Commun. Surv. Tut.*, vol. 18, No. 2, pp. 1413-1452, Second quarter 2016.

[3] E. Bertran and A. Sànchez-Cerdà, "On the Tradeoff Between Electrical Power Consumption and Flight Performance in Fixed-Wing UAV Autopilots," *IEEE Trans. on Veh. Technol.*, vol. 65, no. 11, pp. 8832-8840, Nov. 2016.

[4] R. Citroni, F. Di Paolo and P. Livreri, “A Novel Energy Harvester for Powering Small UAVs: Performance Analysis, Model Validation and Flight Results,” *Sensors*, vol. 19, pp. 1771, 2019.

[5] L. P. Wheeler, "II — Tesla's contribution to high frequency," in *Electrical Engineering*, vol. 62, no. 8, pp. 355-357, Aug. 1943.

[6] N. Shinohara, “*Wireless Power Transfer via Radiowaves*,” Iste, Wiley, 2014.

[7] B. Johns, “An introduction to the Wireless Power Consortium standard and TI’s compliant solutions,” *Analog Applications Journal*, Texas Instrument, First quarter 2011.

[8] Wireless Power Consortium, "*System Description Wireless Power Transfer*," vol. I, Mar. 2012.

[9] www.pikeresearch.com.

[10] A. W. S. Putra, M. Tanizawa and T. Maruyama. “Optical Wireless Power Transmission Using Si Photovoltaic Through Air, Water and Skin.” *IEEE Phot. Technol. Lett.*, vol. 31, no. 2, pp. 157-160, Jan. 2019.

[11] S.O. Kasap, “*Optoelectronics and Photonics: Principles and Practices Second Edition*,” Pearson, 2013.

[12] Q. Yu, D. N. Spergel and J. P. Ostriker, “Rayleigh Scattering and Microwave Background Fluctuations,” *Astrophys. J.*, vol. 558, pp. 23-28, Jan. 2001.

[13] J.I. Agbinya, “Investigation of Near Field Inductive Communication System Models, Channels and Experiments,” *Prog. Electromagn. Res. B*, vol. 49, pp. 129–153, Feb. 2013.

[14] P. J. Abatti, S.F. Pichorim and C. M. de Miranda, “Maximum Power Transfer versus Efficiency in Mid-Range Wireless Power Transfer Systems.” *J. Microw. Optoelectron. Electromagn. Appl.*, vol. 14, no. 1, pp. Aop157-Aop169, Jun. 2015.

[15] C. Nataraj, S. Khan, M. H. Habaebi and A.G.A. Muthalif, “Analysis of Mutual Inductance And Coupling Factor Of Inductively Coupled Coils For Wireless Electricity,” *ARPN J. Eng. Appl. Sci.*, vol. 12, no. 13, Jul. 2017.

[16] J. Jadidian and D. Katabi, “Magnetic MIMO: How to Charge Your Phone in Your Pocket,” in Proc. of the annual Inter. Conf. on Mobile Computing and Networking, Maui, Hawaii, Sept. 2014.

[17] S. L. Ho, J. Wang, W. N. Fu, and M. Sun, “A Comparative Study Between Novel Witricity and Traditional Inductive Magnetic Coupling in Wireless Charging,” *IEEE Trans. Magn.*, vol. 47, no. 5, pp. 1522-1525, May 2011.

[18] A. Kurs, A. Karalis, R. Moffatt, J. D. Joannopoulos, P. Fisher, and M. Soljacic, “Wireless Power Transfer via Strongly Coupled Magnetic Resonances,” *Science*, vol. 317, no. 5834, pp. 83-86, June 2007.

[19] M. Kline, I. Izyumin, B. Boser, and S. Sanders, “Capacitive Power Transfer for Contactless Charging,” in Proc. IEEE Appl. Power Electron. Conf. Expo., pp. 1398-1404, Fort Worth, TX, Mar. 2011.

[20] www.witricity.com.

[21] A. Kurs, R. Moffatt, and M. Soljacic, “Simultaneous Mid-range Power Transfer to Multiple Devices,” *Appl. Phys. Lett.*, vol. 96, pp. 0441021044102-3, Jan. 2010.

[22] A. K. RamRakhyani, S. Mirabbasi, and C. Mu, “Design and Optimization of Resonance-Based Efficient Wireless Power Delivery Systems for Biomedical Implants,” *IEEE Trans. Biomed. Circuits Syst.*, vol. 5, no. 1, pp. 48-63, Feb. 2011.

[23] R. Xue, K. Cheng and M. Je, "High-Efficiency Wireless Power Transfer for Biomedical Implants by Optimal Resonant Load Transformation," *IEEE Trans. Circuits Syst. I, Reg. Papers*, vol. 60, no. 4, pp. 867-874, Apr. 2013.

[24] D. Ahn, and S. Hong, “Wireless Power Transmission with Self-Regulated Output Voltage for Biomedical Implant,” *IEEE Trans. Ind. Electron.*, vol. 61, no. 5, pp. 2225-2235, May 2014.

[25] A. Kawamura, K. Ishioka, and J. Hirai, “Wireless Transmission of Power and Information Through One High-frequency Resonant AC Link Inverter for Robot Manipulator Applications,” *IEEE Trans. Ind. Appl.*, vol. 32, no. 3, pp. 503-508, Jun. 1996.

[26] J. Gao, “Traveling Magnetic Field for Homogeneous Wireless Power Transmission,” *IEEE Trans. Power Del.*, vol. 22, no. 1, pp. 507-514, Jan. 2007.

[27] T. McGinnis, C. P. Henze, and K. Conroy, “Inductive Power System for Autonomous Underwater Vehicles,” in Proc. of IEEE OCEANS, Vancouver, BC, Oct. 2007.

[28] Z. Cheng, Y. Lei, K. Song and C. Zhu, "Design and Loss Analysis of Loosely Coupled Transformer for an Underwater High-Power Inductive Power Transfer System," *IEEE Trans. Magn.*, vol. 51, no. 7, pp. 1-10, Jul. 2015.

[29] F. Tang, K. Zhang, W. Yan, and B. Song, “Circuit Design of Compensation for Contactless Power System of AUV,” in Proc. of China Inter. Conf. on Electric. Dis., Shanghai, China, Sept. 2012.

[30] S. Raabe, J. T. Boys, and G. A. Covic, “A High Power Coaxial Inductive PowerTransferPickup,” in Proc of IEEE Pow. Electron. Spec. Conf., Rhodes, Greek, Jun. 2008.

[31] G. A. J. Elliott, G. A. Covic, D. Kacprzak, and J. T. Boys, “A New Concept: Asymmetrical Pick-ups for Inductively Coupled Power Transfer Monorail Systems,” *IEEE Trans. Magn.*, vol. 42, no. 10, pp. 3389-3391, Oct. 2006.

[32] N. A. Keeling, G. A. Covic, and J. T. Boys, “A Unity-Power-Factor IPT Pickup for High-Power Applications,” IEEE Trans. Ind. Electron., vol. 57, no. 2, pp. 744-751, Feb. 2010.

[33] H. H. Wu, A. Gilchrist, K. Sealy, P. Israelsen, and J. Muhs, “A Review on Inductive Charging for Electric Vehicles,” In Proc. of IEEE Inter. Electric Machines & Drives Conf., Niagara Falls, May 2011.

[34] H. Kim, C. Song, J. Kim, D. H. Jung, E. Song, S. Kim, and J. Kim, “Design of Magnetic Shielding for Reduction of Magnetic Near Field from Wireless Power Transfer System for Electric Vehicle,” In Proc. of Inter. Sym. on Electromagn. Compatibility, Gothenburg, Sweden, Sept. 2014.

[35] W. Khan-ngern, and H. Zenkner, “Wireless Power Charging on Electric Vehicles,” In Proc. of Inter. Electric. Eng. Cong., Chonburi, Thailand, Mar. 2014.

[36] A. O. Di Tommaso, F. Genduso, and R. Miceli, “A Small Power Transmission Prototype for Electric Vehicle Wireless Battery Charge Applications,” in Proc. of Inter. Conf. on Renew. Energy Res. and Apps., Nagasaki, Japan, Nov. 2012.

[37] D. S. Komm, R. T. Benton, H. C. Limburg, W. L. Menninger and Xiaoling Zhai, "Advances in space TWT efficiencies," *IEEE Trans. Electron. Dev.*, vol. 48, no. 1, pp. 174-176, Jan. 2001.

[38] R. M. Dickinson. “Wireless Power Transmission Technology State of Art: The First Bill Brown Lecture.” *Act. Astronaut.*, vol. 53, pp. 561-570, Aug. 2003.

[39] G.A. Landis, “Solar Power Satellites,” in *Comprehensive Renewable Energy*, Elsevier, 2012.

[40] W. Brown, “Electronic and Mechanical Improvement of the Receiving Terminal of a Free-Space Microwave Power Transmission System,” NASA Report No. CR- 135 194, NASA Contract No. NAS 3-19722, pp. 66, Aug. 1977.

[41] J.O. McSpadden, L. Fan and K. Chang, ”A High Conversion Efficiency 5.8GHz Rectenna,” in Proc. 1997 IEEE MTT-S Inter. Microw. Sym. Dig., Denver, USA, vol. 2, pp. 547-550, 1997.

[42] V. A. Vanke, H. Matsumoto, N. Shinohara and A. Kita, “High Power Converter of Microwaves into DC,” *J. Radioelectron.*, no. 9, 1999.

[43] W. Brown, “Power Without Wires,” *IRE Student Quarterly*, Sept. 1961.

[44] S. Silver, “*Microwave Antenna Theory and Design*,” IET Electromagnetics Wave Series, 1984.

[45] C.A. Balanis, “*Antenna Theory: Analysis and Design 4th Edition*,” Wiley, 2016.

[46] Q. Chen, X. Chen and X. Duan.” Investigation on Beam Collection Efficiency in Microwave Wireless Power Transmission,” *J. Electromagn. Wave.*, Vol. 32, No. 9, pp. 1136-1151, Jan. 2018.

[47] J. M. Osepchuk, “Health and safety issues for microwave power transmission,” *Solar Energy*, vol. 56, no. 1, pp. 53-60, Jan. 1996.

[48] International Telecommunication Union. “ITU Recommendation P. 676-11: Attenuation by atmospheric gases,” Aug. 2019. https://www.itu.int/rec/R-REC-P.676-11-201609-I/en.

[49] H. A. Hyatt, “Emission, Reflection, and Absorption of Microwaves at a Smooth Air-Water Interface,” *J. Quant. Spectrosc. Radiat. Transf.*, vol. 10, pp. 217-247, Apr. 1970.

[50] V. R. Gowda, O. Yurduseven, G. Lipworth, T. Zupan, M. S. Reynolds and D. R. Smith, "Wireless Power Transfer in the Radiative Near Field," *IEEE Antennas Wireless Propag. Let*., vol. 15, pp. 1865-1868, Mar. 2016.

[51] G. Goubau, "Microwawe Power Transmission from an Orbiting Solar Power Station," *J. Microw. Pow.*, vol. 5, no. 4, pp. 224-231, 1970.

[52] W.C. Brown, "The History of Power Transmission by Radio Waves", *IEEE Trans. MTT*, vol. 32, no. 9, pp.1230-1242, 1984.

[53] W.C. Brown, "Adapting Microwave Techniques to Help Solve Future Energy Problems", in Proc. 1973 G- MTT Inter. Microw. Sym. Dig. of Technical Papers, vol. 73, no.1, pp.189- 191, 1973.

[54] P.E. Glaser, "Power from the Sun," *Science*, vol.162, pp. 857-886, 1968.

[55] P.E. Glaser, "Power from the Sun: its future," *Science*, vol.162, pp. 857–861, 1968.

[56] S. Sasaki, K. Tanaka, K. Higuchi, N. Okuizumi, S. Kawasaki, N. Shinohara, et al., "A New Concept of Solar Power Satellite: Tethered-SPS", *Acta Astronaut.*, vol. 60, pp. 153–165, 2006.

[57] X.B. Hou, L. Wang, X.H. Zhang, L. Zhou, "Concept Design on Multi-rotary Joints SPS," *J. Astronaut.*, vol. 36, no. 11, pp. 1332–1338, 2015.

[58] X. Li, B. Duan, L. Song, Y. Yang, Y. Zhang and D. Wang, "A New Concept of Space Solar Power Satellite," *Acta Astronaut.*, vol. 136, pp. 182-189, 2017.

[59] S. Sasaki, K. Tanaka and K. Maki, "Microwave Power Transmission Technologies for Solar Power Satellites," in Proc. of the IEEE, vol. 101, no. 6, pp. 1438-1447, Jun. 2013.

[60] Kaya, N., S. Ida, Y. Fujino, and M. Fujita, "Transmitting Antenna System for Airship Demonstration (ETHER)," *Space Energy and Transport.*, vol.1, no.4, pp.237-245, 1996.

[61] N. Shinohara, "Beam Efficiency of Wireless Power Transmission via Radio Waves from Short Range to Long Range," *J. Electromagn. Eng. Sci.*, vol. 10, no. 4, Dec. 2010.

[62] A.W.S. Putra, H. Kato, H. Adinanta, T. Maruyama, "Optical wireless power transmission to moving object using Galvano mirror," in Proc. Free-Space Laser Communications XXXII 11272, Photonics West 2020, no. 112721E, Feb.2020.

[63] M. Yamada, "*Theory of Semiconductor Laser*," Springer, 2012.

[64] M. Bertolotti, "*The History of Laser*," CRC Press, 2014.

[65] L.A. Coldren and S.W. Corzine, "*Diode Lasers and Photonic Integrated Circuits*," Wiley Series in Microwave and Optical Engineering, 1995.

[66] A. L. Bloom, "Gas Lasers," *Appl. Opt.,* vol. 5, pp. 1500-1514, 1966.

[67] C.G.B. Garrett, "*Gas Lasers*," McGraw-Hill, 1967,

[68] M. Razeghi, "*Technology of Quantum Devices*," Springer, 2009.

[69] J. T. Kringlebotn, P. R. Morkel, L. Reekie, J. -. Archambault and D. N. Payne, "Efficient Diode-pumped Single-frequency Erbium:Ytterbium Fiber Laser," in IEEE Photon. Technol. Lett., vol. 5, no. 10, pp. 1162-1164, Oct. 1993.

[70] F. Kong, G. Gu, T.W. Hawkins, M. Jones, J. Parsons, M. T. Kalichevsky-Dong, S. P. Palese, E. Cheung and L. Dong. "Efficient 240w Single-Mode 1018nm Laser from An Ytterbium-doped 50/400μm All-Solid Photonic Bandgap Fiber," *Opt. Exp.*, Vol. 26, No. 3, pp. 3138 – 3144, 2017.

[71] W. Koechner, "*Solid-State Laser Engineering*," Springer, 2006.

[72] D. Liang and J. Almeida, "Highly Efficient Solar-pumped Nd:YAG Laser," *Opt. Exp.,* vol. 19, no. 27, pp. 26399-26405, 2011.

[73] J. Almeida, D. Liang, C. R. Vistas, and E. Guillot, "Highly Efficient End-side-pumped Nd:YAG Solar Laser by A Heliostat–Parabolic Mirror System," *Appl. Opt.,* vol. 54, no.8, pp. 1970-1977, 2015.

[74] B. V. Zhdanov, J. Sell and R. J. Knize. "Multiple Laser Diode Array Pumped Cs Laser with 48W Output Power," *Electron. Lett.*, vol. 44, no. 9, pp. 582-583, Apr. 2008.

[75] https://investors.nlight.net/news-releases/news-details/2006/NLIGHT-Demonstrates-73-Wall-Plug-Efficiency/default.aspx.

[76] http://www.nlightphotonics.com/nlight-files/file/technical_papers/PW10/Jan%2030%20Reliability%20of%20High%20Performance%209x x-nm%20Single%20Emitter%20Laser%20Diodes.pdf .

[77] M. Kanskar, T. Earles, T.J. Goodnough, E. Stiers, D. Botez and L. J. Mawst. "73% CW Power Conversion Efficiency at 50 W from 970 nm Diode Laser Bars." *Electron. Lett.*, vol. 41. no. 5, pp. 245-247, Mar. 2005.

[78] M. Hirota, S. Iio, Y. Ohta, Y. Niwa, and T. Miyamoto, "Wireless Power Transmission between A NIR VCSEL Array and Silicon Solar Cells," in Proc. Microoptics Conf., presentation no. H86, 2015.

[79] Y. Suda and T. Miyamoto, "Simultaneous Utilization of Spontaneous Emission and Laser Emission in VCSEL Array for High-Efficiency Optical Wireless Power Transmission," in Proc. The 24th Congress of Inter. Comiss. Opt., presentation no. Tu1J-07, 2017.

[80] Y. Katsuta and T. Miyamoto, "Efficiency Improvement by Serial-Connection of VCSEL Array for Optical Wireless Power Transmission," in Proc Microoptics Conf., presentation no. P-81, 2017.

[81] Y. Suda and T. Miyamoto, "Simultaneous Utilization of Spontaneous Emission and Laser Emission in VCSEL for Efficiency Improvement of Optical Wireless Power Transmission," in Proc. Microoptics Conf., presentation no. P-13, 2017.

[82] Tomoyuki Miyamoto, Optical wireless power transmission using VCSELs, Proceedings Volume 10682, Semiconductor Lasers and Laser Dynamics VIII; 1068204 (2018) (2018-01)

[83] S. Tsuboyama, K. Hiwada and M. Arai, "Optical Wireless Power Transmission Experiments Using 2-D LED Array and Photovoltaics," in Proc. Microoptics Conf., presentation no. P-28, 2018.

[84] H. Hirukawa, T. Yamaguchi, Y. Ushida, T. Onuma, and T. Honda, "Prototype Optical Wireless Power Transmission System Using Blue LD as Light Source and LED as Photovoltaic Receiver," in Proc. The 1st Optical Wireless and Fiber Power Transmission Conf. 2019, presentation no. OWPT-P-12, 2019.

[85] H. Yamada, C. Liu, and N. Uchiyama, "Wireless Power Transmission with Near-Infrared LEDs," in Proc. 1st Optical Wireless Power Transmission Conf. 2019, presentation no. OWPT-P-05, 2019.

[86] Y. Zhou and T. Miyamoto, "LED-based High Power Optical Wireless Power Transmission for Compact IoT," in Proc. Optical Wireless Power Transmission Conf. 2019, presentation no. OWPT-5-06, 2019.

[87] Y. Zhou and T. Miyamoto, "200mW-class LED Based Optical Wireless Power Transmission for Compact IoT," *Jpn. J. Appl. Phys.*, vol. 58, no. SJ, Aug 2019.

[88] O. Bouchet, H. Sizun, C. Boisrobert, F. de Fornel and P. N. Favennec, "*Free Space Optics: Propagation and Communication*," U.K., London: ISTE Ltd, 2006.

[89] K. Wakamori, K. Kazaura and I. Oka. "Experiment on Regional Broadband Network Using Free-Space-Optical Communication System." *J. Lightw. Technol.*, vol. 25, no. 11, pp. 3265-3273, Nov. 2007.

[90] S. A. Sullivan, "Experimental study of the absorption in distilled water, artificial sea water, and heavy water in the visible region of the spectrum," *Opt. Soc. Am. J.,* 53, 962--968, 1963.

[91] G. M. Hale and M. R. Querry, "Optical Constants of Water in 200nm to 200micrometer Wavelength Region," *Appl. Opt.*, Vol. 12, pp. 555-563, Mar. 1973.

[92] H. Buiteveld and J. M. H. Hakvoort and M. Donze, "The Optical Properties of Pure Water," in SPIE Proc. On Ocean Optics XII, Vol. 2258, pp. 174 – 183, 1994.

[93] S. L. Jacques and S. A. Prahl, Available: http://omlc.org/spectra/water/abs/index.html.

[94] X. Zhang, L. Hu and M. He, "Scattering by Pure Seawater: Effect of Salinity," *Opt. Express*, Vol. 17, No. 7, pp. 5698 – 5710, Mar. 2009.

[95] I. V. Meglinski and S. J. Matcher, "Quantitative Assessment of Skin Layers Absorption and Skin Reflectance Spectra Simulation in The Visible and Near Infrared Spectral Region," *Physiol. Meas.*, Vol. 23, No. 4, pp. 741-753, Oct. 2002.

[96] S. L. Jacques, "Origins of Tissue Optical Properties in UVA, Visible and NIR Regions," in *Advances Optical Imaging and Photon Migration vol 2 ed* , R R Alfano and J G Fujimoto (Washington DC: Optical Society of America) pp 364-371.

[97] S. L. Jacques, "Optical Properties of Biological Tissues: A Review," *Phys. Med. Biol.*, vol. 58, no. 11, pp. R37-R61, May 2013.

[98] S. A. Prahl, "Optical Absorption of Hemoglobin." http://omlc.ogi.edu/spectra/hemoglobin/.

[99] K. Imai, "Pocket Creation in Prepectoral Subfascial Position for Implantation of a Cardiac Implantable Electrical Device," *J. Arrhythmia*, Vol. 30, No. 2, pp. 92-94, Apr. 2014.

[100] O. Akkus, A. Oguz, M. Uzunlulu and M. Kizilgul, "Evaluation of Skin and Subcutaneous Adipose Tissue Thickness for Optimal Insulin Injection," *J. Diabet Metab.*, vol. 3, no. 8, Sept. 2012.

[101] W. F. Cheong, S.A. Prahl and A.J. Welch, "A Review of Optical Properties of Biological Tissues," *IEEE J. Quantum Elec.*, vol. 26, no. 12, pp. 2166-2185, Dec. 1990.

[102] H. Ding, J. Q. Lu, W.A. Wooden, P.J. Kragel and X.H. Hu, "Refractive Indices of Human Skin Tissues at Eight Wavelengths and Estimated Dispersion Relations Between 300 nm and 1600 nm," *Phys. Med. Biol.*, vol. 51, no. 6, Mar. 2006.

[103] Z. Gajinov, M. Matic, S. Prcic and V. Duran, "Optical Properties of Human Skin," *Serbian J. Dermat. Venereology*, vol. 2, no. 4, pp. 131-136, Jan. 2010.

[104] https://www.pveducation.org/pvcdrom/materials/optical-properties-of-silicon.

[105] https://www.pveducation.org/pvcdrom/design-of-silicon-cells/silicon-solar-cell-parameters.

[106] G.A. Landis, "Photovoltaic Receivers for Laser Beamed Power in Space," in Proc. The Conf. Rec. of the 22nd IEEE Photovoltaic Specialists Conf., 1991.

[107] S. Jarvis, J. Mukherjee, M. Perren and S. J. Sweeney, "On the Fundamental Efficiency Limits of Photovoltaic Converters for Optical Power Transfer Applications," in Proc. 2013 IEEE 39th Photovoltaic Specialists Conf., 2013.

[108] J. Mukherjee, S. Jarvis, M. Perren, and S. J. Sweeney, "Efficiency Limits of Laser Power Converters for Optical Power Transfer Applications," *J. of Phys. D: Appl. Phys.*, vol. 46, no. 26 , Jun. 2013.

[109] S. D. Farvis, J. Mukherjee, M. Perren, S. J. Sweeney, "Development and Characterisation of Laser Power Converters for Optical Power Transfer Applications," *IET Optoelectron.*, vol. 8, no. 2, pp. 64–70, Apr. 2014.

[110] M. Perales, "Laser-powered devices: high-concentration PV cell enables high-wattage laser power transmission," Laser Focus World, Feb. 2015.

[111] S. Fafard, "Ultrahigh Efficiency Optical Power Converters Based on The Vertical Epitaxial Hetero-Structure Architecture (VEHSA) Design," in Proc. The 1st Optical Wireless and Fiber Power Transmission Conf. 2019, presentation no. OWPT-3-01, 2019.

[112] M. Perales, M.-H. Yang, and J. Wu, "GoPower Company Limited, Low Cost Laser Power Beaming and Power Over fiber systems," in Proc. The 1st Optical Wireless and Fiber Power Transmission Conf. 2019, presentation no. OWPT-7-01, 2019.

[113] H. W. Brandhorst and D. R. Forester, "Effects of The Atmosphere on Laser Transmission to GaAs Solar Cells," In Proc. 54th International Astronaut. Cong. of the Intern. Astronaut. Fed., pp. R-3, 2003.

[114] E. Oliva, F. Dimroth, and A. W. Bett, "GaAs Converters for High Power Densities of Laser Illumination," *Prog. Photovolt.*, vol. 16, no. 4, pp. 289-295, Jan. 2008.

[115] Y. C. Yuan, C. W. Wu, and G. N. Chen, "Responses of Thin Film Photovoltaic Cell to Irradiation Under Double Laser Beams of Different Wavelength," *Mater. Sci. Forum*, vol. 743-744, pp. 937-942, 2013.

[116] C. De Santi, M. Meneghini, A. Caria, E. Dogmus, M. Zegaoui, F. Medjdoub, B. Kalinic, T. Cesca, G. Meneghesso and E. Zanoni, "GaN-based Laser Wireless Power Transfer System," *Materials*, vol. 11, no. 1, pp. no. 153, Jan. 2018.

[117] R. Jomen, F. Tanaka, T. Akiba, M. Ikeda, K. Kiryu, M. Matsushita, H. Maenaka, P. Dai, S. Lu and S. Uchida, "Conversion Efficiencies of Single-junction III–V Solar Cells Based on InGaP, GaAs, InGaAsP, and InGaAs for Laser Wireless Power Transmission," Jpn. J. Appl. Phys., vol. 57, no. 8S3, 2018.

[118] K. Hiwada, S. Tsuboyama, R. Wakaki, K. Maeda, M. Arai, "InAlGaP Growth on GaAs (311)B for Short Wavelength Range Optical Wireless Power Conversion Devices," in Proc. Mincrooptics Conf. 2018, presentation no. G-4, 2018.

[119] S. Miyajima and T. Nishimura, "Device Simulation of CsPbBr3 Photovoltaic Power Converter," in Proc. The 1st Optical Wireless and Fiber Power Transmission Conf. 2019, presentation no. OWPT-P-06, 2019.

[120] M. M. Wilkins, M. N. Beattie, D. Xia, M. C. Tam, M. Zamiri, C. E. Valdivia, S. Fafard, D. P. Masson, J. J. Krich, Z. R. Wasilewski, and K. Hinzer, "Progress towards Vertically Stacked InAlGaAs Photovoltaic Power Converters for Fiber Power Transmission at 1310 nm," in Proc. The 1st Optical Wireless and Fiber Power Transmission Conf. 2019, presentation no. OWPT-2-05, 2019.

[121] M. Taki, S. Okamoto, N. Aso, and T. Okamoto, "CdS/ZnTe and ZnS/ZnTe Photodiodes Fabricated by Close-spaced Sublimation for Receiver of Optical Wireless Power Transfer," in Proc. The 1st Optical Wireless and Fiber Power Transmission Conf. 2019, presentation no. OWPT-P-08, 2019.

[122] T. Nakamoto, K. Makita, T. Tayagaki, Y. Okano and T. Sugaya, "Photovoltaic Properties of Triple-junction GaAs Solar Cells and Their Application to Laser Power Converters," in Proc. The 1st Optical Wireless and Fiber Power Transmission Conf. 2019, presentation no. OWPT-3-02, 2019.

[123] Murata, T. Nishimura, and S. Miyajima, "CsPbBr3 Photovoltaic Devices for Blue Laser Power Converter," in Proc. The 1st Optical Wireless and Fiber Power Transmission Conf. 2019, presentation no. OWPT-P-03, 2019.

[124] G. Keller, D. Fuhrmann, T. Wierzkowski, A.-K. Volk, C. Wächter, and V. Khorenko, "AZUR SPACE Solar Power GmbH, GaAs multi-junction Photovoltaic Power Converters at AZUR SPACE: Current Status and Development Activities," in Proc. The 1st Optical Wireless and Fiber Power Transmission Conf. 2019, presentation no. OWPT-2-02, 2019.

[125] M. Arai, S. Tsuboyama, K. Hiwada, D. Horita, R. Wakaki, and K. Maeda, "MOVPE Growth of InAlGaP Based Materials for Short Wavelength Range Optical Wireless Power Receiving Devices," in Proc. The 1st Optical Wireless and Fiber Power Transmission Conf. 2019, presentation no. OWPT-3-03, 2019.

[126] N. A. Kalyuzhnyya, V. M. Emelyanov, V. V. Evstropov, S. A. Mintairov, M. A. Mintairov, M. V. Nahimovich, R. A. Salii and M. Z. Shvarts, "Thermal and Resistive Losses in InGaAs Metamorphic Laser (λ=1064nm) Power Converters with Over 50% Efficiency," in Proc. AIP Conf. Proc., vol. 2149, pp. no. 050006, 2019.

[127] Y. Takeda, "Light trapping for photovoltaic cells used for optical power transmission," *Appl. Phys. Exp.*, vol. 13, no. 5, pp. no. 054001, Apr. 2020.

[128] Y. Katsuta and T. Miyamoto, "Design and Measurement of Fly-eye Lens System for Optical Wireless Power Transmission," in Proc. Microoptics Conf. 2018, presentation no. P-20, 2018.

[129] N. Mori, "Design of Projection System for Optical Wireless Power Transmission Using Multiple Laser Light Sources, Fly-eye Lenses, and Zoom Lens," in Proc. The 1st Optical Wireless and Fiber Power Transmission Conf. 2019, presentation no. OWPT-4-02, 2019.

[130] Y. Katsuta and T. Miyamoto, "Experimental Characterization of Uniform Beam Irradiation Using Fly-eye Lens for High Efficiency Optical Wireless Power Transmission," in Proc. The 1st Optical Wireless and Fiber Power Transmission Conf. 2019, presentation no. OWPT-5-05, 2019.

[131] Y. Katsuta and T. Miyamoto, "Design, Simulation, and Characterization of Fly-eye Lens System for Optical Wireless Power Transmission", *Jpn. J. Appl. Phys.*, vol. 58, no. SJ, pp. no. SJJE02, Aug. 2019.

[132] Y. Toyama and T. Miyamoto, "Beam Control Using Liquid Lens for Optical Wireless Power Transmission System," in Proc. The 1st Optical Wireless and Fiber Power Transmission Conf. 2019, presentation no. OWPT-P-10, 2019.

[133] K. Goto, T. Nakagawa, O. Nakamura and S. Kawata, "An Implantable Power Supply with an Optically Rechargeable Lithium Battery," *IEEE Trans. Biomed. Eng.*, vol. 48, no. 7, pp. 830-833, Jul. 2001.

[134] W. J. Robinson, Jr., "The Feasibility of Wireless Power Transmission for An Orbiting Astronomical Station," *NASA Technical Memorandum X-53701*, Feb. 1968.

[135] M. D. Williams and E. J. Conway, “Space Laser Power Transmission System Studies,” *NASA Conf. Publication 2214*, Jan. 1982.

[136] R. J. De Young, J. H. Lee, M. D. Williams, G. Schuster, and E. J. Conway, “Comparison of Electrically Driven Lasers for Space Power Transmission,” *NASA Technical Memorandum 4045*, Jun. 1988.

[137] M. D. Williams, J. H. Kwon, G. H. Walker and D. H. Humes, “Diode Laser Satellite Systems for Beamed Power Transmission,” *NASA Technical Paper 2992*, Jul. 1990.

[138] G. A. Landis, “Photovoltaic receivers of laser beamed power in space,” *J. Propul. Power*, vol. 9, no. 1, pp. 105-112, Jan.-Feb. 1993.

[139] K. Arthur, “Propulsion to Orbit by Ground-based Lasers,” *AIAA J.*, vol. 10, no. 5, pp. 74-75, May 1972.

[140] G. A. Landis, “Space Power by Ground-based Laser Illumination,” *IEEE AES Systems Magazine*, Nov. 1991.

[141] G. Landis, M. Stavnes, S. Oleson, and J. Bozek, “Space Transfer with Ground-based Laser/Electric Propulsion,” *NASA Technical Memorandum TM-106060*, 1992.

[142] H. E. Bennett, “DOD and Navy Applications for Laser Power Beaming,” in Proc. SPIE Laser Power Beaming II, 1995.

[143] G. A. Landis, “Satellite Eclipse Power by Laser Illumination,” *Acta Astronaut.*, vol. 25, no. 4, pp. 229-233, Apr. 1991.

[144] G. A. Landis, “Moonbase Night Power by Laser Illumination,” *J. Propul. Power*, vol. 8, no. 1, pp. 251-254, Jan. 1992.

[145] M. D. Williams, R. J. Deyoung, G. L. Schuster, S. H. Choi, J. E. Dagle, E. P. Coomes, Z. I. Antoniak, J. A. Bamberger, J. M. Bates and M. A. Chiu, ”Power Transmission by Laser Beam from Lunar-synchronous Satellite,” https://ntrs.nasa.gov/search.jsp?R=19940015629.

[146] N. Kawashima, “The Importance of The Development of A Rover for The Direct Confirmation of The Existence of Ice on The Moon,” *Trans. Jpn. Soc. for Aeronaut. Space Sci.*, vol. 43, no. 139, pp. 34-35, Jan. 2001.

[147] B. C. Edwards and H. E. Bennett, “Wireless Power Transmission Experiment As An Early Contribution to Planetary Exploration Missions,” in Proc. SPIE - The Inter. Soc. for Optical Engineering Laser and Beam Control Technol., vol. 4632, pp. 141-147, 2002.

[148] K. Takeda, M. Tanaka, S. Miura, K. Hashimoto, and N. Kawashima, “Laser Power Transmission for The Energy Supply to The Rover Exploring Ice on The Bottom of The Crater in The Lunar Polar Region,” in Proc. SPIE, vol. 4632, pp. 223-227, 2002.

[149] K. Takeda and N. Kawashima, “100 m LD Laser Energy Transportation Experiment to A Model Rover to Explore the Ice on The Moon,” J. *Jpn. Soc. for Aeronaut. Space Sci.*, vol. 594, pp. 393-396, 2003.

[150] N. Kawashima and K. Takeda, “1.2 km Laser Energy Transmission for The Development of A Lunar Rover Confirming The Presence of Ice on The Moon,” In Proc. Inter. Lunar Conf., pp. 291, 2003.

[151] F. Steinsiek, W. P. Foth, K. H. Weber, C. Schafer, and H. J. Foth, “Wireless Power Transmission Experiment Using An Airship As Relay System and A Moveable Rover As Ground Target for Later Planetary Mission,” In Proc. Inter. Astronaut. Cong., Oct. 2003.

[152] D. Bushman, “Aircraft Demonstration of Laser Power Beaming,” In Proc. Inter. Workshop on The Laser Energy Transmission for Space Exploration and Ground Applications, pp. 20, 2004.

[153] C. Cougnet, E. Sein, A. Celeste and L. Summerer, “Solar Power Satellites for Space Exploration and Applications,” *J. Br. Interplanet. Soc*., vol. 59, no. 8, pp. 290–296, 2006.

[154] L. Summerer and O. Purcell, “Concepts for Wireless Energy Transmission via Laser,” *Proc. Eur. Space Agency*, 2009.

[155] R. Gray, “Lasers to Beam Energy to Earth from Space,” *The Telegraph*, 23 January 2010, https://www.telegraph.co.uk/news/earth/energy/solarpower/7060015/Lasers-to-beam-energy-to-Earth-from-space.html.

[156]R. Pena and Carlos Algora, “One-watt Fiber-based Power-by-light System for Satellite Applications,” *Prog. Photovolt.*, vol. 20, pp. 117-123, Jul. 2011.

[157] D. Goto, H. Yoshida, H. Suzuki, K. Kisara, K. Ohashi, and Y. Arimoto, “The Overview of JAXA Laser Energy Transmission R&D Activities and The Orbital Experiments Concept on ISS-JEM,” in Proc. International Conference on Space Optical Systems and Applications, presentation no. S5-2, , 2014.

[158] D. Shi, L. Zhang, H. Ma, Z. Wang, Y. Wang, and Z. Cui, “Research on Wireless Power Transmission System between Satellites,” in Proc. IEEE Wireless Power Transfer Conf., 2016.

[159] N. Kawashima, K. Takeda, and K. Yabe, “Application of The Laser Energy Transmission Technology to Drive A Small Airplane,” *Chin. Opt. Lett.*, vol. 5, pp. 109-110, 2007.

[160] R. Mason, “Feasibility of Laser Power Transmission to A High-Altitude Unmanned Aerial Vehicle,” Technical Report Rand Project Air Force Santa Monica CA, RAND, UG1242.D7.M35, 2011.

[161] T. J. Nugent and J. T. Kare, “Laser power for UAVs,” Laser Motive White Paper, 2010.

[162] M. C. Achtelik, J. Stumpf, D. Gurdan, and K. M. Doth, “Design of A Flexible High Performance Quadcopter Platform Breaking The MAV Endurance Record With Laser Power Beaming,” in Proc. IEEE / RSJ International Conf. on Intelligent Robots and Systems, pp. 5166–5172, 2011.

[163] NASA Armstrong Fact Sheet, “Beamed laser power for UAVs,” https://www.nasa.gov/centers/armstrong/news/FactSheets/FS-087-DFRC.html.

[164]P. Anand, R. Pandiarajan, and P. Raju, “Wireless Power Transmission to UAV Using Laser Beaming,” *Int. J. Mech. Eng Res.*, vol. 5, no. 1, pp. 137-142, 2015.

[165] J. Ouyang, Y. Che, J. Xu and K. Wu, “Throughput Maximization for Laser-powered UAV Wireless Communication Systems,” in Proc.2018 IEEE Inter. Conf. on Communications Workshops, 2018.

[166] M. Lu, M. Bagher, A. P. James and T. Phung, “Wireless Charging Techniques for UAVs: A Review, Reconceptualization and Extension,” *IEEE Access*, vol. 6, pp. 29865-29884, 2018.

[167] Y. Huo, X. Dong, T. Lu, W. Xu and M. Yuen, "Distributed and Multilayer UAV Networks for Next-Generation Wireless Communication and Power Transfer: A Feasibility Study," *IEEE Internet of Things Journal*, vol. 6, no. 4, pp. 7103-7115, Aug. 2019.

[168] N. Kawashima, K. Takeda, H. Matsuoka, Y. Fujii and M. Yamamoto, “Laser Energy Transmission for A Wireless Energy Supply to Robots,” in Proc. 22nd Inter. Sym. on Automation and Robotics in Construction, 2005.

[169]N. Kawashima and K. Takeda, “Laser Energy Transmission for A Wireless Energy Supply to Robots,” in *Robotics and Automation in Construction*, Carlos Balaguer and Mohamed Abderrahim (Ed.), IntechOpen, 2008.

[170] J. James, V. Iyer, Y. Chukewad, S. Gollakota and S. B. Fuller, “Liftoff of a 190 mg Laser-Powered Aerial Vehicle: The Lightest Wireless Robot to Fly,” in Proc. 2018 IEEE Inter. Conf. on Robotics and Automation, 2018.

[171] J. Fakidis, M. Ijaz, S. Kucera, H. Claussen and H. Haas, “On The Design of An Optical Wireless Link for Small Cell Backhaul Communication and Energy Harvesting,” in Proc. 2014 IEEE 25th Annual Inter. Sym. on Personal, Indoor, and Mobile Radio Communication, 2014.

[172] J. Fakidis, S. Videv, S. Kucera, H. Claussen and H. Haas, “Indoor Optical Wireless Power Transfer to Small Cells at Nighttime,” *J. Lightw. Technol.*, vol. 34, no. 13, pp. 3236-3258, Jul. 2016.

[173] J. Fakidis, “Optical Wireless Energy Transfer for Self-Sufficient Small Cells,” https://www.researchgate.net/publication/324132810_Optical_Wireless_Energy_Transfer_for_Self-Sufficient_Small_Cells.

[174] K. Murakawa, M. Kobayashi, O. Nakamura and S. Kawata, “A Wireless Near-Infrared Energy System for Medical Implants,” *IEEE Eng. Med. Biol.*, vol. 18, no. 6, pp. 70-72, Nov/Dec. 1999.

[175] M. Mujeeb-U-Rahman, D. Adalian, C. Chang and A. Scherer, “Optical Power Transfer and Communication Methods for Wireless Implantable Sensing Platforms,” *J. Biomed. Opt.*, vol. 20, no. 9, pp. no. 095012, pp. 1-9, Sept. 2015.

[176] Saha, S. Iqbal, M. Karmaker, S. F. Zinnat, and M. T. Ali, “A Wireless Optical Power System for Medical Implants Using Low Power Near-IR Laser,” in Proc. 39th Annual Inter. Conf. of the IEEE Engineering in Medicine and Biology Society, pp. 1978-1981, 2017.

[177] W. Nattakarn, T. Ishizu, M. Haruta, T. Noda1, K. Sasagawa, T. Tokuda, M. Sawan and J. Ohta, “CMOS-based Optical Energy Harvesting Circuit for Biomedical and Internet of Things Devices,” *Jpn. J. Appl. Phys.*, vol. 57, no. 4S, Mar. 2018.

[178] F. H. Fan, S, Ishibashi, "Underwater Applications of Light Emitting Diodes," in Proc. 2015 IEEE Underwater Technology 2015, pp. 1-5, 2015.

[179] S. M. Kim, J. Choi and H. Jung, “Experimental Demonstration of Underwater Optical Wireless Power Transfer Using A Laser Diode,” *Chin. Opt. Lett.*, vol. 16, no. 8, pp. no. 080101, Aug. 2018.

[180] A. W. S. Putra, T. Yoshida, H. Adinanta, H. Kato, and T. Maruyama, “Optical Wireless Power Transmission Through Water,” in Proc. The 1st Optical Wireless and Fiber Power Transmission Conf. 2019, presentation no. OWPT-8-03, 2019.

[181] J. Li and T. Miyamoto, “Investigation of Optical Wireless Power Transmission from Air to Underwater Considering Influence of Waves,” in Proc. The 1st Optical Wireless and Fiber Power Transmission Conf. 2019, presentation no. OWPT-P-17, 2019.

[182] Y. Kozawa, R. Kimoto and Y. Umeda, “Inverse Pulse Position Modulation Scheme for Underwater Visible Light Simultaneous Wireless Information and Power Transfer,” in Proc. The 1st Optical Wireless and Fiber Power Transmission Conf. 2019, presentation no. OWPT-8-05,2019.

[183] T. Nugent, “Efficiency Measurements & Comparisons in Power Beaming,” in Proc. The 1st Optical Wireless and Fiber Power Transmission Conf. 2019, presentation no. OWPT-P-19, 2019.

[184] https://www.nasa.gov/directorates/spacetech/centennial_challenges/beaming_tether/index.html.

[185] https://powerlighttech.com/.

[186] Alpert, “Long-Range Wireless Power Delivery by Infrared Light Beam - New Applications for Homes, Offices, Factories and Public Spaces,” in Proc. The 1st Optical Wireless and Fiber Power Transmission Conf. 2019, presentation no. OWPT-1-02, 2019.

[187] www.wi-charge.com.

[188] M. H. Smith, R. L. Fork and S. T. Cole, "Safe Delivery of Optical Power from Space," *Opt. Exp.,* vol. 8, no. 10, pp. 537-546, 2001.

[189] Ministry of Defence United Kingdom, “*Military Laser Safety*,” UK Ministry of Defence Publishing, 2005. https://assets.publishing.service.gov.uk/government/uploads/system/uploads/attachment_data/file/49543/jsp390_military_laser_safety_2005edition.pdf.

[190] K. J. Duncan, “Laser Based Power Transmission: Component Selection and Laser Hazard Analysis,” in Proc. IEEE PELS Workshop on Emerging Technologies: Wireless Power Transfer, pp. 100-103, 2016.

[191] A. Sahai and D. Graham, “Optical Wireless Power Transmission at Long Wavelengths,” in Proc. Inter. Conf. on Space Optical Systems and Applications, pp. 164-170, 2011.

[192] J. Mukherjee, W. Wulfken, H. Hartje, F. Steinsiek, M. Perren, and S. J. Sweeney, “Demonstration of Eye-Safe (1550nm) Terrestrial Laser Power Beaming at 30m and Subsequent Conversion Into

Electrical Power Using Dedicated Photovoltaics," in Proc. IEEE 39th Photovoltaic Specialists Conference, pp. 1074–1076, 2013.

[193] S. J. Sweeney, S. D. Jarvis, and J. Mukherjee, "Laser Power Converters for Eye-safe Optical Power Delivery at 1550nm: Physical Characteristics and Thermal Behavior," in Proc. The 1st Optical Wireless and Fiber Power Transmission Conf. 2019, presentation no. OWPT-2-04, 2019.

[194] T. Nugent, T. Arends, T. Griebling, A. Hay, and T. J. Sayles, "Automatic Active Safety Subsystem for Laser Power Beaming," in Proc. The 1st Optical Wireless and Fiber Power Transmission Conf. 2019, presentation no. OWPT-5-03, 2019.

[195] V. Iyer, E. Bayati, R. Nandakumar, A. Majumdar and S. Gollakota, "Charging A Smartphone Across A Room Using Lasers," in Proc. the ACM on Interactive, Mobile, Wearable and Ubiquitous Technologies, vol. 1, no. 4, pp. 143:1-21, 2017.

[196] Y. Kaymak, R. Rojas-Cessa, J. Feng, N. Ansari, M. Zhou and T. Zhang, "A Survey on Acquisition, Tracking, and Pointing Mechanisms for Mobile Free-Space Optical Communications," *IEEE Comm. Sur. Tut.*, vol. 20, no. 2, pp. 1104-1123, Second quarter 2018.

[197] H. Adinanta, K. Hirotaka and T. Maruyama, "Laser Tracking using Computer Vision for Optical Wireless Power Transmission," in Proc. The 78th JSAP Autumn Meeting 2017, Presentation no. 6p-C14-3, 2017.

[198] M. Hiruta, M. Nakagawa, S. Haruyama, and S. Ishikawa, "A Study on Optical Wireless Train Communication System Using Mobile Object Tracking Technique," in Proc. The 11th Inter. Conf. Advanced Communication Technology, pp. 35-40, 2009.

[199] S. Haruyama, H. Urabe, T. Shogenji, S. Ishikawa, M. Hiruta, F. Teraoka, T. Arita, H. Matsubara, and S. Nakagawa, "New Ground-to-train High-speed Free-space Optical Communication System with Fast Handover Mechanism," in Proc. Optical Fiber Communication Conf., presentation no. p. OWX4, 2011.

[200] H. Urabe, S. Haruyama, T. Shogenji, S. Ishikawa, M. Hiruta, F. Teraoka, T. Arita, H. Matsubara, and S. Nakagawa, "High Data Rate Ground-to-train Free-space Optical Communication System," *Opt. Eng.*, vol. 51, no. 3, pp. 031204–1, 2012.

[201] J. T. Kare, F. Mitlitsky, and A. Weisberg, "Preliminary Demonstration Of Power Beaming With Non-Coherent Laser Diode Arrays," in Proc. Space Technology and Applications International Forum, 1999.

[202] T. Blackwell, “Recent Demonstrations of Laser Power Beaming at DFRC and MSFC,” in Proc. 3rd Inter. Sym. on Beamed Energy Propulsion, vol. 766, pp. 73-85, 2005.

[203] P. Sprangle, B. Hafizi, A. Ting and R. Fischer, “High-Power Lasers for Directed-Energy Applications,” *Appl. Opt.*, vol. 54, no. 31, pp. F201-F209, Nov. 2015.

[204] J. Zhang and T. J. Kane, "Acquisition, Tracking, and Pointing for Reconfigurable Free Space Optical Communication Systems in RF Challenged Environments," in Proc. SPIE 11272, Free-Space Laser Communications XXXII, Photonics West 2020, presentation no. 112721L, 2020.

[205] Y. Toyama and T. Miyamoto, “Beam control using liquid lens for optical wireless power transmission”, in Proc. The 79th JSAP Autumn Meeting, presentation no. 18p-232-16, 2018.

[206] C. Schafer, O. Matoba and N. Kaya, “Optical Retrodirective Tracking System Approach Using an Array of Phase Conjugators for Communication and Power Transmission,” *Appl. Opt.*, vol. 46, no. 21, pp. 4633-4641, Jul. 2007.

[207] Q. Liu, J. Wu, P. Xia, S. Zhao, Y. Yang, W. Chen and L. Hanzo, “Charging Unplugged / Will Distributed Laser Charging for Mobile Wireless Power Transfer Work?,” *IEEE Vehicular Technol. Mag.*, vol. 11, no. 4, pp. 36-45, Dec. 2016.

[208] Q. Zhang, X. Shi, Q. Liu, J. Wu, P. Xia and Y. Liao, “Adaptive Distributed Laser Charging for Efficient Wireless Power Transfer,” in Proc. IEEE 86th Vehicular Technology Conf., 2017.

[209] S. M. Kim and S. M. Kim, "Wireless Optical Energy Transmission Using Optical Beamforming," *Opt. Eng.*, vol. 52, no. 4, pp. no. 043205, Apr. 2013.

[210] www.opencv.org.

[211] https://www.thorlabs.com/drawings/e4ed4a71b026e55e-BB3B31B2-EFDE-BC86-E3A223A85858A295/GVS002-Manual.pdf.

[212] H. Kato, H. Adinanta, A. W. S. Putra, and T Maruyama, “Object Recognition and Beam Steering System for Optical Wireless Power Transmission to Moving Object,” in Proc. The 1st Optical Wireless and Fiber Power Transmission Conf. 2019, presentation no. OWPT-6-03, 2019.

[213] A. W. S. Putra, H. Kato and T. Maruyama, "Infrared LED Marker for Target Recognition in Optical Wireless Power Transmission to Moving Object at Dark Environment Condition," in Proc. 24th Microoptics Conf., pp. 290-291, 2019.

[214] A.W.S. Putra, H. Kato, and T. Maruyama, “Infrared LED Marker for Target Recognition in Indoor and Outdoor Applications of Optical Wireless Power Transmission System,” Jpn. Appl. Phys., Vol. 59, No. SOOD06, Aug. 2020.

[215] K. Takahashi and T. Miyamoto, “Active Recognition of Position and Size of Solar Cell for OWPT,” in Proc. The 1st Optical Wireless and Fiber Power Transmission Conf. 2019, presentation no. OWPT-P-11, 2019.

[216] V. Bana, M. Kerber, G. Anderson, J. D. Rockway and A. Phipps, "Underwater Wireless Power Transfer for Maritime Applications," in Proc. 2015 IEEE Wireless Power Transfer Conf., 2015.

[217] T. M. Hayslett, T. Orekan and P. Zhang, "Underwater Wireless Power Transfer for Ocean System Applications," in Proc. OCEANS 2016 MTS/IEEE Monterey, pp. 1-6, 2016.

[218] Y. Wang, B. Song and Z. Mao, “Application of Shielding Coils in Underwater Wireless Power Transfer Systems,” *J. Mar. Sci. Eng.,* vol. 7, pp. no. 267, 2019.

[219] A. Dochhan, J. Poliak, J. Surof, M. Richerzhagen, H. F. Kelemu and R. M. Calvo, "13.16 Tbit/s Free-space Optical Transmission over 10.45 km for Geostationary Satellite Feeder-links," in Proc Photonic Networks; 20th ITG-Symposium, Leipzig, Germany, 2019, pp. 1-3.

[220] M. B. van der Mark, A. van Dusschoten and M. Pekar, "All-Optical Power and Data Transfer in Catheters Using An Efficient LED," in Proc. SPIE 9317, Optical Fibers and Sensors for Medical Diagnostics and Treatment Applications XV, pp. no. 93170E, 2015.